

**RL-TR-96-152**  
**Final Technical Report**  
**July 1996**



# **BRAGG FILTERS USING HIGH SCATTERING EFFICIENCY VOLUME HOLOGRAPHIC GLASSES**

**Radiation Monitoring Devices, Inc.**

**L. Pierre de Rochemont**

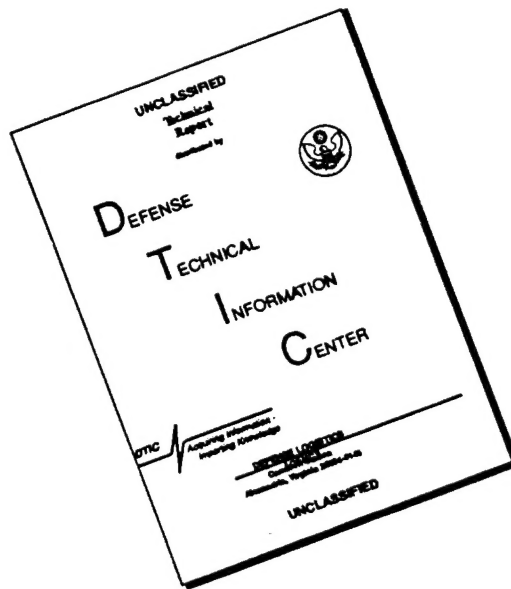
*APPROVED FOR PUBLIC RELEASE; DISTRIBUTION UNLIMITED.*

**19960924 059**

**DTIC QUALITY INSPECTED 3**

**Rome Laboratory  
Air Force Materiel Command  
Rome, New York**

# DISCLAIMER NOTICE

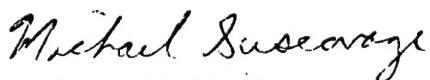


THIS DOCUMENT IS BEST QUALITY AVAILABLE. THE COPY FURNISHED TO DTIC CONTAINED A SIGNIFICANT NUMBER OF PAGES WHICH DO NOT REPRODUCE LEGIBLY.

This report has been reviewed by the Rome Laboratory Public Affairs Office (PA) and is releasable to the National Technical Information Service (NTIS). At NTIS it will be releasable to the general public, including foreign nations.

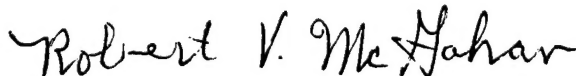
RL-TR-96-152 has been reviewed and is approved for publication.

APPROVED:



MICHAEL SUSCAVAGE  
Project Engineer

FOR THE COMMANDER:



ROBERT V. MCGAHAN, Acting Director  
Electromagnetics & Reliability Directorate

If your address has changed or if you wish to be removed from the Rome Laboratory mailing list, or if the addressee is no longer employed by your organization, please notify RL ( ERXO ) Hanscom AFB MA 01731. This will assist us in maintaining a current mailing list.

Do not return copies of this report unless contractual obligations or notices on a specific document require that it be returned.

# REPORT DOCUMENTATION PAGE

Form Approved  
OMB No. 0704-0188

Public reporting burden for this collection of information is estimated to average 1 hour per response, including the time for reviewing instructions, searching existing data sources, gathering and maintaining the data needed, and completing and reviewing the collection of information. Send comments regarding this burden estimate or any other aspect of this collection of information, including suggestions for reducing this burden, to Washington Headquarters Services, Directorate for Information Operations and Reports, 1215 Jefferson Davis Highway, Suite 1204, Arlington, VA 22202-4302, and to the Office of Management and Budget, Paperwork Reduction Project (0704-0188), Washington, DC 20503.

1. AGENCY USE ONLY (Leave Blank)		2. REPORT DATE July 1996		3. REPORT TYPE AND DATES COVERED Final	
4. TITLE AND SUBTITLE BRAGG FILTERS USING HIGH SCATTERING EFFICIENCY VOLUME HOLOGRAPHIC GLASSES				5. FUNDING NUMBERS C - F19628-93-C-0089 PE - 65502F PR - 3005 TA - RC WU - 82	
6. AUTHOR(S) L. Pierre de Rochemont					
7. PERFORMING ORGANIZATION NAME(S) AND ADDRESS(ES) Radiation Monitoring Devices, Inc. 44 Hunt St Watertown MA 02172				8. PERFORMING ORGANIZATION REPORT NUMBER N/A	
9. SPONSORING/MONITORING AGENCY NAME(S) AND ADDRESS(ES) Rome Laboratory/ERXO 80 Scott Dr Hanscom AFB MA 01731-2909				10. SPONSORING/MONITORING AGENCY REPORT NUMBER RL-TR-96-152	
11. SUPPLEMENTARY NOTES Rome Laboratory Project Engineer: Michael Suscavage/ERXO/(617)377-5252					
12a. DISTRIBUTION/AVAILABILITY STATEMENT Approved for public release; distribution unlimited.				12b. DISTRIBUTION CODE	
13. ABSTRACT (Maximum 200 words) The objective of this contract was to develop fiber-optic Bragg filters with improved scattering efficiencies for application in optical telecommunications and multiport fiber optic data transfer links. To achieve this objective, a basis of understanding for the physical mechanisms that drive grating formation in oxide glass was developed to identify glass compositions with improved scattering efficiencies.					
14. SUBJECT TERMS Volume holographic glass, Bragg filters, Three-wave mixing, Four-wave mixing				15. NUMBER OF PAGES 88	
				16. PRICE CODE	
17. SECURITY CLASSIFICATION OF REPORT UNCLASSIFIED	18. SECURITY CLASSIFICATION OF THIS PAGE UNCLASSIFIED	19. SECURITY CLASSIFICATION OF ABSTRACT UNCLASSIFIED	20. LIMITATION OF ABSTRACT UL		



## TABLE of CONTENTS

<i>Acknowledgments</i> .....	ii
I. PROGRAM SUMMARY .....	1
II. TECHNICAL OBJECTIVES: .....	3
IIIA. BACKGROUND ON THE FUNCTIONAL CHARACTERISTICS OF BRAGG-FILTERS .....	4
IIIB. BACKGROUND TO THE PHENOMENOLOGY OF NONLINEAR OPTICAL GRATING STRUCTURES IN GLASS .....	5
IV. EXPERIMENTAL ORGANIZATION AND LABORATORY PROCEDURES .....	8
IVA. EMPIRICAL RESULTS OF PHASE I RESEARCH.....	8
IVB. PHASE II COMPOSITIONAL VARIATION AND ANALYSIS .....	12
IVC. PHASE II MATERIALS PREPARATION METHODS .....	21
<i>Glass Melting and Sample Preparation:</i> .....	21
IVD. PHASE II MATERIALS CHARACTERIZATION.....	24
<i>Three-Wave Mixing Measurements</i> .....	30
<i>Raman Scattering Measurements</i> .....	31
<i>Brillouin Scattering Measurements</i> .....	31
<i>Fiber-optic Optical Properties</i> .....	31
V. RESEARCH RESULTS .....	32
<i>Glass Transition Temperature</i> .....	32
<i>Thermal Diffusivity Measurements</i> .....	37
<i>Bulk Glass Optical Properties</i> .....	39
<i>Four-wave Mixing Measurements</i> .....	43
<i>Three-Wave Mixing Measurements</i> .....	61
<i>Raman Scattering Measurements</i> .....	62
<i>Brillouin Scattering Measurements</i> .....	71
<i>Fiber-optic Optical Properties</i> .....	71
VI. CONCLUSIONS AND SUGGESTIONS FOR FUTURE RESEARCH .....	74
<i>References</i> .....	78

## **Acknowledgments**

L. Pierre de Rochemont would like to acknowledge the efforts Yelena Klugerman, RMD, has made in preparing the glass samples. Professor James P. Wicksted, Cindy Porter, Abdul Y. Hamad, and Patricia Watson, with the Oklahoma State University, Center for Laser Research, are credited for characterizing the glasses prepared under the contract and a large measure of the success this research project has experienced. Professor George Dixon is recognized for his generous offer to perform thermal diffusivity measurements on the glass samples without financial support. Prof. George Sigel, Jr., Chairman, with Brian Cole and David Auw, Rutgers University, Fiber-optic Materials Research Program, Piscataway, NJ are gratefully acknowledged for preparing the doped fiber-optic preforms and optical fiber submitted as deliverables in this research.

Michael J. Suscavage and Robert J. Andrews, with Rome Laboratory are acknowledged for their support and assistance in the laboratory. Finally, Dr. Osama el-Bayoumi, AFOSR, is acknowledged and thanked, for without his firm belief and persistent support this project would not have been possible.

## ***I. Program Summary***

This Phase II research studied phenomena associated with optically-prepared gratings in glass. Optically-prepared gratings were recorded in rare earth-doped oxide glass using write-beams tuned to an excited-state transition of the rare earth ion that has a strong decay branch through non-radiative multiphonon emission processes. The properties of superimposed transient and permanent were evaluated. The lifetime of transient gratings (2.2 ms) in europium-doped glass was found to be independent of write beam power, and to be identical to the fluorescence lifetime of the excited state of the rare earth ion. This suggests that transient gratings are related to the hyperpolarizability of ligands in the immediate vicinity of the rare earth ion. Permanent gratings were found to depend on glass composition and to be strongly dependent on the vibrational characteristics of the glass. Since the fluorescence (and transient grating) lifetime(s) was (were) not observed to change as a result of the write-process, permanent gratings are attributed to a structural change in the glass network close to, but not in the nearest neighbor environment of, the rare earth ions.

Resonant and nearly-resonant Raman spectroscopy was used to probe the frequency-dependence in the density of states profiles of optical phonons localized to the rare earth ions and optical phonons localized to the network lattice away from the rare earth ion. Thermal diffusivity measurements were used to examine the strength of low-frequency extended-range phonons that can be used to couple the photostimulated vibrational energy generated at a rare earth ion site to vibrational modes resonant with the rest of the network. Empirical results suggest that is necessary to use a host glass in which there is a strong frequency overlap between the lattice-localized modes and the write-beam-excited modes at rare earth ion sites to record laser-induced gratings. It is equally important that the host glass contain extended-range phonons to couple these two types of localized modes in the glass.

The program specifically examined the compositional basis for preparing photosensitive glass with improved scattering efficiencies and faster recording times. This was accomplished by performing doping studies on a suitable magnesium-soda-aluminosilicate base-host composition. The absolute scattering efficiency of the base host composition was compared versus changes in rare earth ion concentration, changes in average alkali-modifier mass, changes in average alkaline earth-modifier mass, changes in network former content, and changes alkali-modifier content. The strongest scattering intensities were observed in systems that contained the highest concentrations of network formers and rare earth ions ( $\eta_{\text{peak}} = 1.55 \times 10^{-3} \text{ cm}^{-2}$ ). However, increasing the network former ( $\text{SiO}_2$ ) concentration by a mere 2% increased the absolute scattering efficiency to a greater degree (120% increase in scattering efficiency per percentage increase

in silica mol%) than increasing the rare earth ion concentration by 100% (7.8% increase in scattering efficiency per percentage increase in europium oxide mol%). Increasing the alkali-modifier concentration decreased the absolute scattering efficiency. The results suggest that it is more important to engineer a host that has an ordered network, than it is to increase the glass's sensitivity to the write beam.

The program evaluated europium ( $\text{Eu}^{3+}$ ) and praseodymium ( $\text{Pr}^{3+}$ ) as rare earth ion photosensitizers for the network. Both ions can be pumped by the 465.8 nm line of an argon laser. Despite the fact that praseodymium is more strongly absorbing than europium at 465.8 nm, gratings were recorded at much faster rates in the base host glass when it was doped with  $\text{Eu}^{3+}$ . This research suggests that even stronger scattering efficiencies, and faster recording rates, should be possible in  $\text{Pr}^{3+}$ -doped glasses when write-beams at 488 nm are used to record the grating.

The program also evaluated transition-metal-doping as a means to increase absolute scattering efficiency. Transition-metal doped glasses were found to be suitable photosensitive glasses; however, the strong absorption of the transition-metal interfered with write-beam power needed to record a grating. More conclusive results will probably be derived using transition-metal-doped thin film glasses containing  $\text{Pr}^{3+}$  ions, and 488 nm write-beams to record the grating.

The program evaluated 38 different glass compositions. 31 different glass compositions were submitted as deliverables. The program also developed a novel manufacturing technique to fabricate optical fiber that is coincidentally doped with transition-metal and rare earth ions. 3 different preforms and 3 spools of fiber drawn from these preforms have been submitted as contract deliverables. An infrared laser diode was also submitted as a deliverable.

## II. Technical Objectives:

A variety of optical signal processing applications can be enhanced using holographic recording media as optical signal-transfer and memory elements. Optical thin films and single crystals constitute the most commonly used holographic recording media. While these materials aptly demonstrate the feasibility for a variety of potential optical technologies, they cannot always be easily configured in large scale systems, nor can they be simply manufactured in scaled volumes.

Glass is a unique material medium in that it is rugged, durable and can be easily manufactured in bulk. It can be molded into a variety of shapes and forms, including optical fiber, and mass produced at low cost. These considerations alone enhance the commercial potential of products developed using glass systems over products prepared from crystalline materials.

It has recently been discovered that certain glass compositions can be used as holographic recording media using write-beams at appropriate wavelengths. Nonlinear optical grating structures have been recorded in glass and observed to have effective  $\chi^{(2)}$  properties (second harmonic generation (SHG) and parametric oscillation), as well as effective  $\chi^{(3)}$  properties (four-wave mixing) when probed under conditions of optical phase matching. These "permanent" grating structures can be erased by an uncrossed write-beam. This allows the potential to apply these glass systems as erasable/programmable read-only optical memory systems when configured as holographic recording media. These materials also have the potential to be applied as upconversion display components if three-wave mixing configurations are satisfied. While the scattering efficiencies for many of the glasses studied to date are not as intense as those observed in the better single crystal photorefractives, there is evidence that the scattering efficiencies of glass systems can be improved by compositional tailoring.

The engineering and scientific objectives of this contract are to investigate the compositional basis for nonlinear scattering in these systems, and to identify a theoretical basis for engineering glass networks with improved scattering efficiencies. The technological aim of this contract is to develop fiber-optic Bragg-filters with high scattering efficiencies for application in optical telecommunications and multiport fiber-optic data-transfer links. To achieve this objective a basis of understanding for the physical mechanisms that drive grating formation in oxide glass must be developed. This Phase II contract has been devoted to achieving this objective.

### IIIa. Background on the Functional Characteristics of Bragg-filters

It has recently been shown that amorphous solids can be utilized as volume holographic recording media using sufficiently intense write-beams at appropriate wavelength(s). The commercial potential for passive micro-optical components manufactured from the glassy state is significant. Laser-induced gratings recorded in optical fiber have already demonstrated feasibility for use as weak distributed-feedback optical filters. These same devices can also be incorporated into integrated optical networks if the photosensitive glass composition is deposited as a thin film on silicon in conjunction with integrated electronic circuitry. (See Figure 1).

#### Fiber-optic Bragg Filters

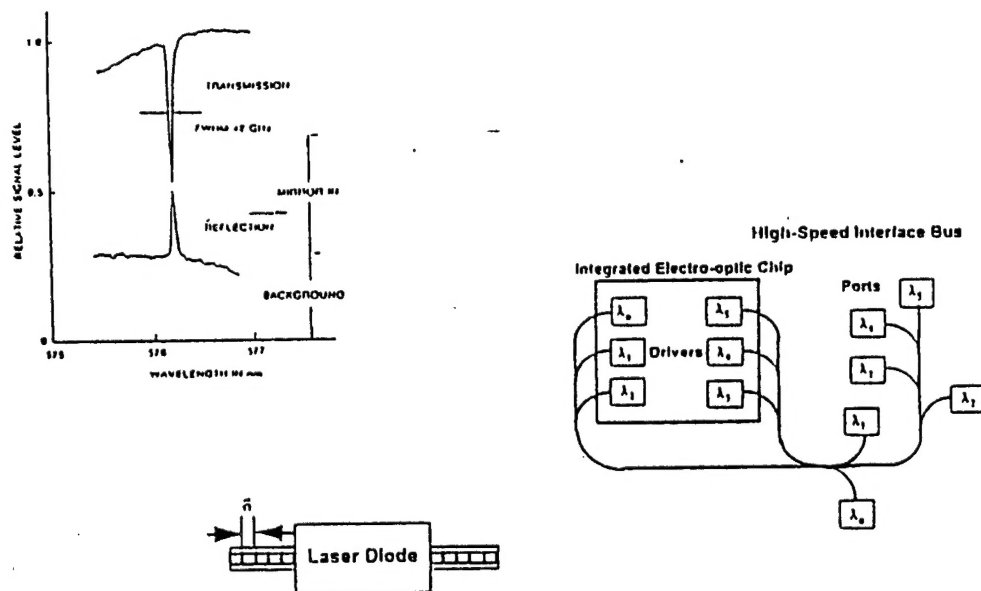


**Figure 1.** Transmission/Reflectance spectral characteristic of an optically-prepared fiber-optic Bragg-filter and conceptual uses for these electronic components. (Spectra is after Meltz, G., Morey, W.W., and Glenn, W.H., Opt. Lett., 14(15), 823 (1989).

The optical filtering characteristic of this device is generated by holographically recording a laser interference pattern in the fiber using write-beams at wavelengths to which the glass is photosensitive. The development of more powerful fiber-optic Bragg filters can potentially introduce new designs which could lower the cost of distributed-feedback diode lasers, impact the design of integrated optical circuitry and the architecture of fiber-optic bus interfaces.

### **IIIb. Background to the Phenomenology of Nonlinear Optical Grating Structures in Glass**

In telco (telecommunications grade) optical fiber holographic gratings can be recorded using a variety of write-beam wavelengths. However, the rate at which the gratings form, and their ultimate scattering intensity, is dependent upon the power of a particular write-beam wavelength. The most efficient method used to record these gratings in telco optical fiber uses 30 MW (peak power) write-beams at 244 nm from an excimer/dye laser [Metlz, *et al.*], by pumping (and bleaching) the (E') silicon-germanium oxygen vacancy defect that results in the fiber core after the draw process. Spectroscopic studies reveal that the E' defects are photoionized as a result of the write process. The grating is observed to be in phase with the optical interference pattern.

Holographic gratings have also been observed in rare earth doped glasses of significantly lower optical quality. In this instance, high write-beam powers and ultraviolet wavelengths do not have to be used. These gratings have been recorded in europium-doped ( $\text{Eu}^{3+}$ ) alkali silicates, alkali phosphates, alkali germanates and alkali borates, using the 465.8 nm emission line of an argon ion ( $\text{Ar}^{3+}$ ) laser. Write-beams with powers as low as 7 mW have been found to be effective in preparing these gratings [Durville *et al.*]. The 465.8 nm emission line of the  $\text{Ar}^{3+}$  laser is resonant with the  ${}^7\text{F}_0 \rightarrow {}^5\text{D}_2$  (ground state to excited state) absorptive transition. The decay of the  ${}^5\text{D}_2$  excited state is known to branch strongly through nonradiative decay mechanisms (multiphonon emissions) to the  ${}^5\text{D}_0$  excited state, which in turn undergoes a radiative decay, (fluorescing in the orange), to the ground state multiplets. These holographic gratings have also been found to be in phase with the optical interference pattern of the 465.8 nm write-beams. Powell et al. have proposed a Two-Level System (TLS) phenomenological model for the alkali modified glass systems. This model suggests that these gratings form through the optical phonon-assisted tunneling of alkali cations out of regions of constructive optical interference and into regions of destructive write-beam interference, where optical phonon densities are lower and the probabilities for phonon-assisted tunneling events are significantly reduced [Behrens *et al.*].

The physics of grating formation in both the telco grade optical fiber and alkali-modified oxide glass systems have distinct differences but exhibit sufficient commonality to suggest the underlying physics may be the same. State densities of microscopic dipoles related to color-center dynamics are believed to be responsible for the photorefractive effect in both cases. In the case of the telco fiber, color-center changes are related to the photoionization and subsequent electron charge-transfer from regions of constructive write-beam optical interference. In the case of the alkali modified glasses, empirical relationships between the mass of the positively charged alkali cation and the saturated scattering intensity suggest that ionic charge-transfer is the underlying mechanism behind



grating formation. The addition of alkali ions to borate, germanate, phosphate, and silicate networks are known to alter the density of ultraviolet color-centers in these glass networks. Gratings in both systems can be thermally erased, or optically erased using a single write-beam that does not have a sharp spatial intensity distribution profile.

Even though the two systems may have completely different network dynamics, the physical basis is indeed similar. State-defining charged particles, although oppositely charged, appear to be altering the equilibrium distribution of color-centers in the regions of constructive and destructive write-beam interference. This physical alteration in the distribution of color-centers in the network will locally alter the dispersion characteristics of the glass through the Kramers-Krönig relationship.

Studies on photo-induced gratings in fiber have demonstrated that intense electric fields ( $10^5$ - $10^6$  V/cm) develop as the grating forms. These electric fields are periodic and observed to be  $90^\circ$  out of phase with the grating. The induced periodic electric fields that develop produce an effective second-order polarization ( $\chi^{(2)} = E_{DC} \sin(\Lambda) \cdot \chi^{(3)}_{\text{photoinduced}}$ , where  $\Lambda$  represents the period of the grating vector). This effective photo-induced second-order susceptibility can be used to generate harmonic radiation scattered off of a probe that is optically phase-matched to the grating. The detection of photoinduced periodic electric fields and/or second harmonic generation (SHG) and other phenomena related to  $\chi^{(2)}$  optical nonlinearities have yet to be observed in the rare-earth doped alkali-modified glass networks. This is due, in large measure, to the fact that this phenomena has not yet been explored in sufficient detail.

The detection of the intense periodic electric fields and associated second-order optical nonlinearities have led many to suggest that photoconductive mechanisms are responsible for grating formation in optical fibers. Current theories emphasize a mythical conduction band into which electrons trapped in the  $E'$  defect are promoted by the interfering write-beams. This explanation is contradicted by the properties of radiation-induced polarization in glass. If a voltage is applied to a glass sample inserted between two electrodes and exposed to ionizing radiation fields, photocurrents are not observed in glass. If the ionizing particles are incident on the glass sample from a preferred direction, then increased capacitance is observed. The increased polarization is observed to be maximally aligned with the trajectory of the incident particle beam. If the ionizing radiation uniformly strikes the sample from all possible directions, then no changes in the sample's polarization are detected.

This suggests that, although ionizing radiation will displace electronic charge in glass, the electrons are not promoted into a conduction band that allows them to move freely in response to applied electric fields. Rather, the ionizing interaction imparts kinetic energy to the liberated electron which then travels in a direction that conserves the



momentum supplied to it during the ionizing field interaction. If the net transfer of electrons is along one direction, (as would be the case with a uniaxial ionizing particle beam), the resultant net charge separation results in a "net polarization". If electrons are isotropically scattered by an isotropic ionizing particle beam, no net charge-transfer is induced, and zero net changes in capacitance are observed.

In the case of telco fiber, write-beams with wavelengths in the ultraviolet do not have sufficient energy to impart ballistic energy to an electron that has been photoionized from an E' defect. Unassisted, the liberated electron is unlikely to move anywhere after the photoionization process. However, studies on laser isotope separation have revealed that intense vibrational resonances are generated during the photodissociation process. Photodissociation uses lasers, tuned to the bonding state/anti-bonding state transition of a molecular bond, to sufficiently weaken the bond and eventually break it. Once a bonding electron has been promoted to the anti-bonding state of the molecular bond, the atoms forming the bond prefer to separate, thus leaving one of the atoms in the pair with an excess electron and the other with a self-trapped hole. This process produces intense vibrational resonances within the former molecular components.

Optically-prepared nonlinear gratings can be recorded in glass oxide networks by pumping an excited state of a rare earth ion doped into the network, provided the excited state decays sharply through a nonradiative decay branch. The stimulated multiphonon emissions have a distribution profile that is virtually in phase with the pumping fields, because of the low mean free path for phonons in glass networks. The wavelengths and optical intensities of the write-beams are insufficient to photoionize the rare earth ion. Therefore, the imbalance in the rates of stimulated multiphonon emissions between the regions of constructive and destructive interference triggers the photoactivated diffusion of a state-defining charged carrier (alkali cation) that alters the equilibrium distribution of color-centers in each region of the glass network.

A DC electric field, that has yet to be observed in the alkali-modified glass systems, should be established between the regions in the glass where the write-beams were in states of destructive and constructive interference. During grating saturation, the migrating alkali cations have the greatest probability of being collected in regions of destructive interference where their phonon-assisted tunneling or hop frequency is less. Regions of constructive interference would be maximally depleted of charge-balancing alkali cations that are electrostatically tied to non-bridging points in the network at equilibrium. The static lattice charges remain fixed and unbalanced after the grating has been formed. This creates a situation where mobile positive charges are displaced 180° from the static lattice-charges they once balanced when the network was in a state of thermodynamic equilibrium. The DC electric field line-density is strongest at the mid-point that separates these two charge distributions, i.e., 90° out of phase with the write-beams.

The fact that intense vibrational resonances and strong stimulated Raman scattering is also observed during the write process of gratings in telco optical fiber indicates that the underlying physics between the two phenomena is probably similar, but with subtle distinctions. In the telco fiber system, the state-defining charge carrier is an electron, which is displaced through the network by small polaron tunneling mechanisms, (i.e., as an electron cloaked in a cloud of phonons). The static lattice-charge is a self-trapped hole at the site from which the electron was originally photoionized. In the case of the alkali-modified network, photostimulated multiphonon emissions are known to be solely responsible for grating evolution. The state-defining charged-particles are ions and carry a positive electric charge, whereas the static lattice-charges are negative. In either case, the state-defining charged-particle tunnels through the network via phonon-assisted mechanisms. In both cases, a condition of dynamic equilibrium would be established when the number of charged carriers in one region, multiplied by the hop frequency in that region (which is proportional to the phonon density in that region) is equal to the number of charged carriers in an adjacent region, multiplied by its hop frequency (phonon density).

The striking similarity in the physical mechanisms that are simultaneously present in the case of the telco fiber and rare-earth doped glass leads one to link the general phenomena in the two systems as fundamental to the overall dynamics that underlie the entire grating process. This picture proposes that these systems represent a different (or opposite) manifestation of the same physical principles. Greater understanding of the compositional dependencies that impact these mechanisms will lead to the discovery of glass compositions with improved scattering efficiencies and faster response times. This Phase II program plans to investigate the similarities of these two fundamentally different glass systems in an effort to identify relationships between the strength of the saturated grating, its rate of formation, and their relationship to the compositional character of the glass.

#### ***IV. Experimental Organization and Laboratory Procedures***

##### ***IVa. Empirical Results of Phase I Research***

Research performed in Phase I and Phase II has focused on experiments with the rare-earth doped ( $\text{Eu}^{3+}$ ) alkali modified oxide networks. Phase I research examined compositions within the borate, phosphate, and silicate glass forming systems. Phase II has focused on the experimentation with stable aluminosilicate glass phases. The preference for using aluminosilicates is to provide a host glass network that has sufficient flexibility to allow coincidental doping with  $\text{Eu}^{3+}$  and first-row transition-metal ions. Alumina ( $\text{Al}_2\text{O}_3$ ) concentrations have been batched at 3 mol%, with alkali concentrations running at 15 mol%. This 5:1 ratio of alkali to aluminum cations in the network allows a sufficient excess of alkali to participate in grating formation, allowing roughly 20% of the alkali cations to charge-balance alumina sites in the network.

Phase I research demonstrated the importance of engineering the host network to have suitable phonon properties. During the initial phase of this research, a variety of host glass compositions were examined. Distinct relationships between compositional selection, vibrational spectra, and grating formation were observed. The early results pointed to the need to impedance-match the vibrational frequency-dependence in the host network to the vibrational excitations during write-beam resonance. This is shown in **Figure 2**, which compares off-resonant (514.8 nm) Raman scattered spectra with nearly-resonant (457.9 nm) Raman spectra.

### Frequency Matching Write Resonant to Lattice Optical Phonons

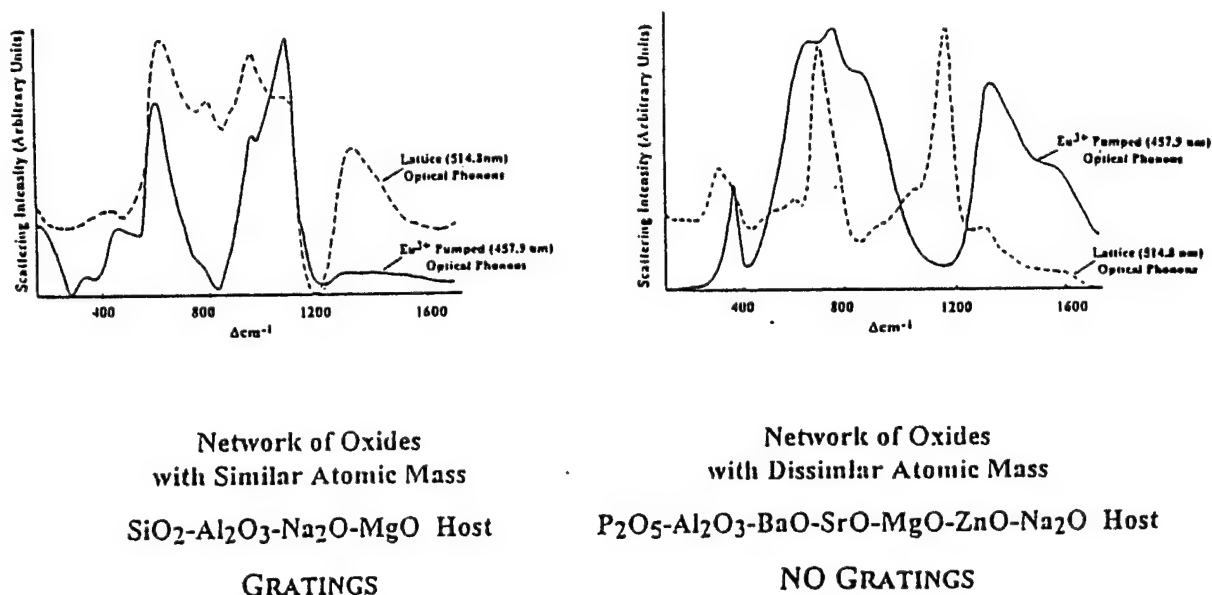


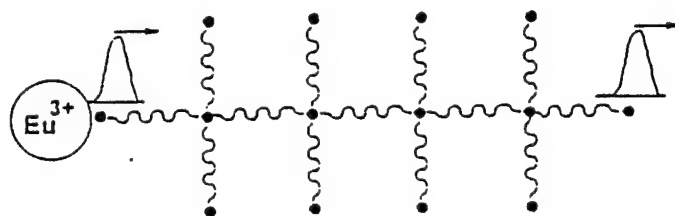
**Figure 2.** Optical phonon profiles of network lattice phonons and phonons generated in the vicinity of the  $\text{Eu}^{3+}$  ion measured with off-resonant (514.8 nm) and nearly-resonant (457.9 nm) Raman probes in glasses that produced gratings and those that did not.

Host glasses that were composed of metal oxide constituents, whose metals occupy positions on different rows of the periodic table were found to have "lattice" phonons at frequencies that did not overlap with the frequencies of the "write-resonant" optical phonons. These glasses did not produce nonlinear gratings using crossed laser beams tuned to the  ${}^7\text{F}_0 \rightarrow {}^5\text{D}_2$  transition. Host glasses that were composed of metal oxides with similar cationic atomic mass, (i.e., from consecutive columns in the same row of the periodic table), were susceptible to optically-prepared grating phenomena. Those glasses were observed to support network lattice optical phonons at frequencies that overlap the

frequencies of phonons generated during write-beam resonance. This has led to an analogy with network transmission-line theory. A vibrational "pulse" (or phonon) produced at an  $\text{Eu}^{3+}$  site will propagate more easily through a lumped circuit of mechanical oscillators that are resonant with the frequency of the pulse than it will through a circuit composed of elements that do not oscillate at its frequency. (See Figure 3).

### Network Model to Phonon Propagation/Charge Tunneling in Glass

#### Impedance Matched Network



#### Non-Impedance Matched Network

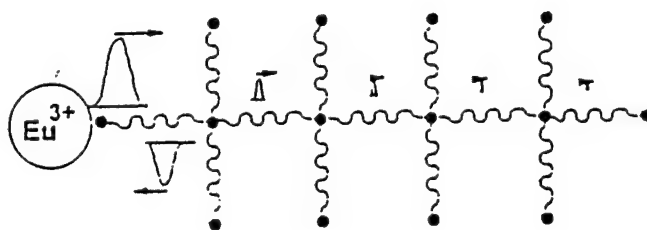


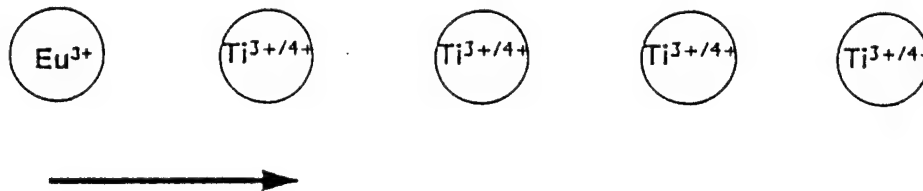
**Figure 3.** Network theory model for phonon propagation and charge tunneling in glass.

Grating formation in telco fiber and rare-earth doped alkali ions is dependent upon the diffusion of state-defining charged particles from regions of constructive interference to regions of destructive interference. Depending on the crossing angle of the write-beam, these regions could be separated by distances on the order of microns. While it may be possible that some of the state-defining charged particles do indeed migrate over these distances, it is more likely that the charge displacement is due to cooperative restructuring within the network. In either case, the efficiency of the grating process will ultimately be tied to the efficiency of the charged particle displacement. These charged particles tunnel or hop through the network within a cloud of phonons, either as a small polaron (in the case of an electron) or a hopping cation. The facility with which the particle moves is ultimately linked to the ease with which the phonons dressing the charged carrier can pull it through the network. Theoretical considerations impress the need to

identify glass hosts in which long phonon mean-free-paths consequently allow the state-defining charged particles to have the longest possible diffusion lengths. This is shown schematically in **Figure 4**.

## Engineering the Host Network

### Phonon Mean Free Paths



### Low Probability of Cooperative Self-Organization



### High Probability of Cooperative Self-Organization

**Figure 4.** Schematic representation of the relationship between phonon propagation lengths and the probability for cooperative self-organization of the optically-prepared grating. The  $\text{Ti}^{3+/4+}$  ion is used as the bistable color-center with an electron as the state defining charged carrier in this presentation.

The Phase II program was structured to evaluate these considerations. All host and doped-host glass compositions being prepared in this research are being examined with respect to their phonon structure and diffusive properties, as well as their ability to record gratings.

#### IVb. Phase II Compositional Variation and Analysis

A research objective is to determine the contribution of the different functional groups (network formers and modifiers) on grating formation. One of the more stable soda-lime-aluminosilicate glass phases was selected as a base glass composition. The effect of changes in a grating's optical scattering was then correlated with systematic compositional changes in a functional group of this glass phase. The base composition which is being varied is based on:

	SiO <sub>2</sub>	Al <sub>2</sub> O <sub>3</sub>	CaO	Na <sub>2</sub> O
mol%	70	3	12	15

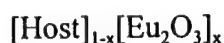
The initial glasses prepared substituted MgO for CaO to provide a network of metal oxides that all had comparable cationic atomic mass units, i.e.,

	SiO <sub>2</sub>	Al <sub>2</sub> O <sub>3</sub>	MgO	Na <sub>2</sub> O
mol%	70.00	3.00	12.00	15.00
metal cation mass (a.m.u.)	28.09	26.98	24.31	22.99

#### Variations to the Rare-earth Ion Content in the Glass

In certain rare-earth doped glasses gratings are formed by optically pumping excited states of these ions that decay strongly through a non-radiative relaxation process. Vibrational modes excited through the decay process then initiate the grating process. The amount of energy extracted from the optical pump and distributed as lattice excitations is thus proportional to the molar absorption coefficient of the rare earth ion at the write-beam wavelength, multiplied by the ion concentration per unit volume in the network. Higher concentrations of rare-earth ions would be expected to stimulate stronger lattice energies for a given write-beam intensity. Lower rare-earth ion concentrations would be expected to reduce the amount of stimulated lattice energy which drives the grating process.

To determine the effect the concentration of rare earth ions has on grating scattering efficiency, a series of glass compositions was prepared in which europium was gradually doped into the host composition as follows:



where,  $x = 0.001, 0.005, 0.01, 0.025, 0.05$ .

The following glass compositions were prepared in accordance with this compositional variation. In this series the Bragg-5 composition was used as the base host upon which all compositional variations were based. The Bragg-1 glass composition was prepared to replicate Phase I research results. All glass compositions are reported in mol%.

ID	Batch Composition				
	SiO <sub>2</sub>	Al <sub>2</sub> O <sub>3</sub>	MgO	Na <sub>2</sub> O	Eu <sub>2</sub> O <sub>3</sub>
Bragg-1	65.00	3.00	15.00	12.00	5.00
Bragg-5	70.00	3.00	12.00	15.00	---
Bragg-6	69.93	2.99	11.99	14.99	0.1
Bragg-7	69.65	2.985	11.94	14.925	0.5
Bragg-8	69.30	2.97	11.88	14.85	1.0
Bragg-9	68.25	2.925	11.70	14.625	2.5
Bragg-10	66.50	2.85	11.40	14.25	5.0

In addition to increasing the amount of lattice energy available for grating formation, higher europium concentrations may limit phonon propagation. These studies have been made to monitor the effect of europium additions on the optical and acoustic phonon structure, as well as the phonon mean-free-path. Europium plays a crucial role in these networks because it provides the source of the optical phonons that initiate grating formation. However, Eu<sup>3+</sup> is also a large and heavy ion that is incompatibly mated with the smaller and lighter cations that form the host network. While it is beneficial to have an abundant supply of oscillators to drive the write process, an over abundant supply of significantly larger and heavier cation (such as europium) in the lattice may have counterproductive effects by attenuating the mean-free-path of extended phonons in the network. If the propagation lengths of these phonons are seriously attenuated, it may be difficult to form stable gratings with the glass.

#### *Variations to the Alkali-mass in the Glass*

Electrical charge is transported in glass networks by alkali ions which diffuse through the network hopping and tunneling mechanisms. The theories proposed to account for grating formation in rare-earth doped glass assumes that lattice energies are highly excited in regions of constructive optical interference, and less so in regions of destructive optical interference. As a result of this energetic imbalance, alkali-ions diffuse out of the excited regions and into the regions with lower lattice energies, in turn, altering equilibrium bonding configurations and their microscopic optical properties in the two regions. Heavier alkali-ion mass increases the energy required for these ions to migrate.

It is, thus, expected that gratings formed in glasses with lower mass alkali-ion might form and relax more readily than glasses containing higher mass alkali-ions.

The effect of alkali mass and mixed alkali masses on the grating formation process are being studied using the following glass compositions:

ID	SiO <sub>2</sub>	Al <sub>2</sub> O <sub>3</sub>	MgO	Li <sub>2</sub> O	Na <sub>2</sub> O	Eu <sub>2</sub> O <sub>3</sub>
Bragg-11	70	3	12	7.5	7.5	---
Bragg-12	68.25	2.925	11.70	7.312	7.313	2.5

and:

ID	SiO <sub>2</sub>	Al <sub>2</sub> O <sub>3</sub>	MgO	Na <sub>2</sub> O	K <sub>2</sub> O	Eu <sub>2</sub> O <sub>3</sub>
Bragg-13	70.0	3.0	12.0	7.5	7.5	--
Bragg-14	68.25	2.925	11.70	7.312	7.313	2.5

The rare-earth-doped compositions follow the equation:

$$[\text{Alkali-modified Host}]_{1-0.025}[\text{Eu}_2\text{O}_3]_{0.025}$$

#### *Variations to the Alkaline Earth-mass in the Glass*

Alkaline earth ions (Group II series ions on the periodic table) play the role of network modifiers in a glass. Substituting one type of alkaline earth ion for another in a glass network will alter the mechanical properties (stiffness and crack propagation) in the glass. On the microscopic level, these changes will also alter phonon propagation and vibrational characteristics of the glass, which, according to theory, will alter the rates of grating formation in these networks.

The effect of the mass of the alkaline earth network modifier was examined by systematically substituting CaO, SrO, and BaO for MgO in a manner similar to the alkali-modified system. The following glasses were studied.

ID	SiO <sub>2</sub>	Al <sub>2</sub> O <sub>3</sub>	MgO	CaO	Na <sub>2</sub> O	Eu <sub>2</sub> O <sub>3</sub>
Bragg-15	70.0	3.0	6.0	6.0	15.0	--
Bragg-16	68.25	2.925	5.85	5.85	14.625	2.5

and,



ID	SiO <sub>2</sub>	Al <sub>2</sub> O <sub>3</sub>	MgO	SrO	Na <sub>2</sub> O	Eu <sub>2</sub> O <sub>3</sub>
Bragg-17	70.0	3.0	6.0	6.0	15.0	--
Bragg-18	68.25	2.925	5.85	5.85	14.625	2.5

and,

ID	SiO <sub>2</sub>	Al <sub>2</sub> O <sub>3</sub>	MgO	BaO	Na <sub>2</sub> O	Eu <sub>2</sub> O <sub>3</sub>
Bragg-19	70.0	3.0	6.0	6.0	15.0	--
Bragg-20	68.25	2.925	5.85	5.85	14.625	2.5

Samples 15 through 20 fractured easily and frequently during processing, so only pieces of limited size could be made. These glasses often had non-homogeneous optical properties. Given the strong affect that alkaline earth substitutions had on network properties and uniformity, a similar series of glass with much smaller substitutions was also prepared. The second series included glasses of the following batch compositions.

ID	SiO <sub>2</sub>	Al <sub>2</sub> O <sub>3</sub>	MgO	CaO	Na <sub>2</sub> O	Eu <sub>2</sub> O <sub>3</sub>
Bragg-21	70.0	3.0	10.8	1.2	15.0	--
Bragg-22	68.25	2.925	10.53	1.17	14.625	2.5

ID	SiO <sub>2</sub>	Al <sub>2</sub> O <sub>3</sub>	MgO	SrO	Na <sub>2</sub> O	Eu <sub>2</sub> O <sub>3</sub>
Bragg-23	70.0	3.0	10.8	1.2	15.0	--
Bragg-24	68.25	2.925	10.53	1.17	14.625	2.5

and,

ID	SiO <sub>2</sub>	Al <sub>2</sub> O <sub>3</sub>	MgO	BaO	Na <sub>2</sub> O	Eu <sub>2</sub> O <sub>3</sub>
Bragg-25	70.0	3.0	10.8	1.2	15.0	--
Bragg-26	68.25	2.925	10.53	1.17	14.625	2.5

The rare earth doped compositions follow the equation:

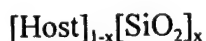


### *Variations to the Concentration of Network Formers in the Glass*

Network formers are the predominant constituent in the glass. These ions have the highest coordination numbers in the network and form bonds with their nearest neighbors that are essentially covalent. Alkali and alkaline earth ions are fully ionized in glass and locate themselves in electrostatic potential wells that balance the charge of non-bridging oxygen ions in the network. Network formers are also intrinsically flexible, in that the location of oxygen ions in their immediate coordination sphere may become considerably distorted.

According to theory, alkali ions driven out of regions of constructive optical interference will collect in regions of destructive optical interference. Once there, the alkalis will distort (stretch) oxygen bonds bridging network formers. Most frequently, an alkali ion that has migrated into the coordination sphere of a network former will break the bond between a bridging oxygen and one of the network formers to which it is attached. This creates a negatively charged non-bridging oxygen ion that balances the charge of the alkali, and a dangling bond (hole or electron vacancy) at the network former site.

Stretching a bond lowers its internal energy and shifts optical absorption to longer wavelengths. The dangling bonds which are created when a bond is broken also introduce microscopic absorption centers. The following series of glasses were prepared to ascertain the relative impact that a larger number of network formers have on grating formation. These glass compositions were prepared by first preparing a silica-enriched glass composition into which europium oxide is doped as follows:



where  $x = 0.025$  and  $x = 0.05$ , and,

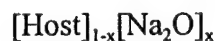


to yield the following glass compositions.

ID	SiO <sub>2</sub>	Al <sub>2</sub> O <sub>3</sub>	MgO	Na <sub>2</sub> O	Eu <sub>2</sub> O <sub>3</sub>
Bragg-27	68.98	2.85	11.41	14.26	2.5
Bragg-28	66.71	2.78	11.12	13.89	2.5

### *Variations to the Concentration of Alkali Ions in the Glass*

According to theory, it is expected that a larger number of diffusing alkali-ions would create more non-equilibrium microscopic color-centers (stretched bonds and dangling bonds) in regions of destructive optical interference in a saturated grating. To evaluate the effect that a larger number of alkali ions in the glass might have on grating scattering efficiency, the basic host composition was modified as:



where  $x = 0.05$  and  $x = 0.10$ , and,



These changes yielded the following batch compositions.

ID	SiO <sub>2</sub>	Al <sub>2</sub> O <sub>3</sub>	MgO	Na <sub>2</sub> O	Eu <sub>2</sub> O <sub>3</sub>
Bragg-29	64.84	2.78	11.11	18.77	2.50
Bragg-30	61.43	2.63	10.53	22.91	2.50

### *Variations to the Rare Earth Ion and Write-Beam Absorption in the Glass*

Exchanging europium oxide for a rare earth ion that is more strongly absorbing at the write-beam wavelength and decays strongly through a non-radiative relaxation branch will increase the amount of lattice energy available to the network during the write process. This was examined by substituting praseodymium oxide (Pr<sub>2</sub>O<sub>3</sub>) for europium oxide (Eu<sub>2</sub>O<sub>3</sub>) in the host glass. The following compositions were prepared and studied.

ID	SiO <sub>2</sub>	Al <sub>2</sub> O <sub>3</sub>	MgO	Na <sub>2</sub> O	Pr <sub>2</sub> O <sub>3</sub>
Bragg-31	69.65	2.985	11.94	14.925	0.5
Bragg-32	69.30	2.97	11.88	14.85	1.0
Bragg-33	68.25	2.925	11.70	14.625	2.5

These compositions are based on an equivalent doping equation to that used in the previous study on Eu<sub>2</sub>O<sub>3</sub> concentration, modified as:



where,  $x = 0.005, 0.01, 0.025$ .

## Transition-metal Ion Doping as a Means to Increase Scattering Efficiency in the Glass

In glass, transition-metal ions produce bi-stable or multi-stable color-center ions that are dependent on their valence state. The transition-metal was incorporated into the network as a way to improve the scattering efficiency of the grating. The varying valence states of these ions produce associated color-centers in the near-uv, visible, and near-infrared window of the glass, with the reduced valence states closer to the near-infrared region of the spectrum. If photo-activated small polaron conduction can be stimulated by pumping the  $\text{Eu}^{3+}$  ion, then a significant enhancement in the scattering efficiency will result since the dispersion will be shifted to longer wavelengths along with the color-centers. (See Figure 5).

### Increasing Scattering Efficiency in Glass

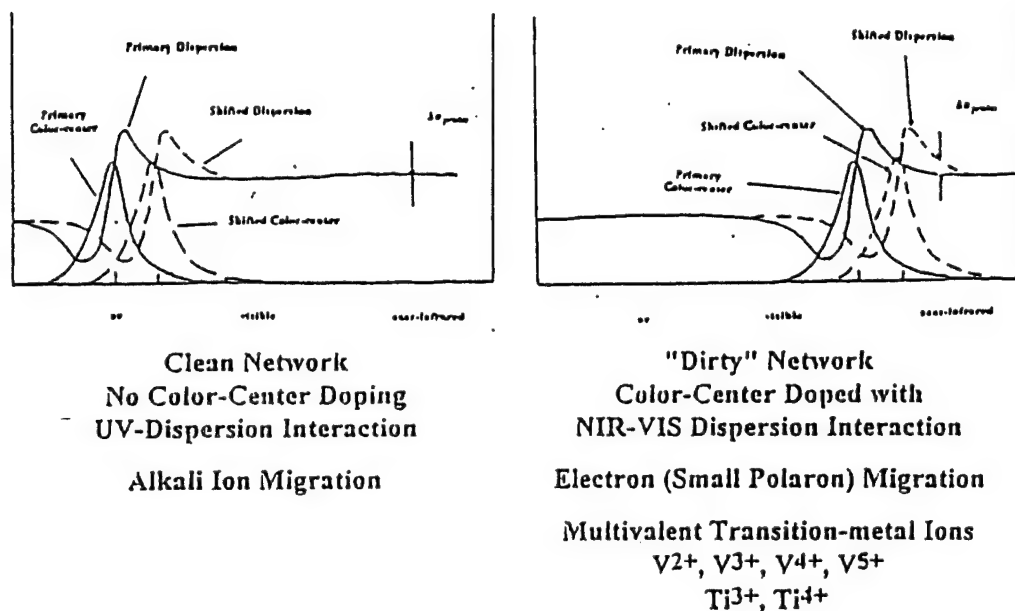


**Figure 5.** Schematic representation of the relationship between the spectral location of the bi-stable color-centers and the increased intensity in the scattering efficiency of the grating at longer wavelengths when the color-center are shifted to longer wavelength.

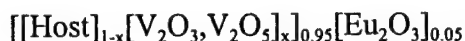
In Phase I, a glass containing  $\text{Eu}^{3+}$  and  $\text{V}^{(3+,4+,5+)}$  was prepared using a host composition that had previously demonstrated grating formation. Gratings could not be recorded in this glass then, and still cannot be recorded now. It is not known if this is due to the fact that the phonon propagation characteristics of the host glass were altered through the addition of the transition-metal ions to the network, or if some other mechanism, like

multi-phonon emission quenching by transition-metal ions in close proximity to the rare-earth, is responsible for the glass' failure to record a grating.

The following glass compositions were prepared in Phase II to further test this hypothesis.

ID	SiO <sub>2</sub>	Al <sub>2</sub> O <sub>3</sub>	MgO	Na <sub>2</sub> O	V <sub>2</sub> O <sub>3</sub>	V <sub>2</sub> O <sub>5</sub>	Eu <sub>2</sub> O <sub>3</sub>
Bragg-37	65.5	2.80	11.2	14.0	0.71	0.71	5.0
Bragg-38	66.2	2.98	11.3	14.2	0.24	0.24	5.0

The compositional equations used to prepare these glasses is based on



with  $x = 0.015$  and  $0.005$ .

The careful compositional analysis described above has been designed to allow project researchers to determine how compositional changes to the network alter grating functionality and what options might be available to engineer greater performance through compositional tailoring.

### ***Transition-metal Ion Doping in Optical Fiber***

The silicate optical fiber produced under the contract was produced from pure silica preforms. This glass did not contain alkali or alkaline earth network modifiers, and, as such, provided an excellent medium through which to test photo-activated small polaron migration between transition-metal ions. Prior research in transition-metal doped fiber utilized titanium doped in a germano-silicate network. Excimer lasers were used to record gratings by photo-bleaching an absorption band attributed to the silicon-germanium oxygen-vacancy defect. Some interpretations of the grating formation mechanism suggest photo-conductive models in which electrons trapped at the defect site are promoted to a conduction band and quickly trapped at some other nearby recombination center. These theories ignore the fact that conduction-band theory is predicted on the fact that Bloch electrons are free to move within a conduction band by virtue of the enormous symmetry consistent with a crystalline lattice. This level of symmetry is not present in a glass, therefore, the underlying basis for conduction-band theory is removed.

Electron migration in glass networks is known to occur through small polaron conduction mechanisms, in which an electron, dressed with phonons, moves through the network. In short, the lattice distortions caused by the vibrational modes sufficiently

perturb local electrostatic field potentials to allow the electron to slip through. The 244 nm laser beam has just enough energy to photo-dissociate the silicon-germanium oxygen vacancy defect. Photo-dissociation does generate considerable vibrational energies, which in turn can propel an electron out of the local area by small polaron conduction processes.

An objective of the research was to conclusively determine whether small polaron conduction is the transport mechanism underlying grating formation. Pumping excited states of a rare-earth ion that decays strongly through non-radiative relaxation mechanisms will produce lattice energy without promoting electrons to some hypothesized conduction band. Multivalent transition-metal ions, which are located close to the rare-earth ion, can shed and adopt hopping electrons.

Three doping schemes were prepared. Due to limitations in the synthesis method, (discussed below) chromium was used as the transition-metal dopant. It was doped into a germano-silicate fiber and coincidentally doped with praseodymium ( $\text{Pr}^{3+}$ ) and europium ( $\text{Eu}^{3+}$ ). These three different types of fiber were developed to contrast a proven photo-sensitive glass (germanium-doped) that uses an ultraviolet pump, with to the rare-earth ions which render glass photo-sensitive to the blue lines (465 nm) of an argon ion laser.

#### ***IVc. Phase II Materials Preparation Methods***

##### ***Glass Melting and Sample Preparation:***

Glass compositions are batched from europium carbonate, aluminum hydroxide, alkali carbonate, alkaline earth carbonate, and silica precursor powders. The use of non-oxide powders, wherever possible, is being advanced to improve precursor subdivision in the final melt. These powders are melted in a platinum crucible at 1650-1680 °C for 8-10 hours. Optical quality samples have been made by transferring the charged crucible (cooled to 1550 °C in the melting furnace) into an annealing oven (heated to 450-550 °C) and annealing both the crucible and its charge for 1 hour at 700-725 °C. A core drill is used to remove the annealed glass from the crucible. The blank is then cut into three 1" dia. pieces measuring approximately 1.0 cm, 0.5 cm, and 0.75 cm thick. These pieces are then ground and polished to a 1  $\mu$ m finish. The 0.75 cm blank is cut into a square rectangle (parallelepiped) and polished on all six sides for Raman scattering, Brillouin scattering, and three-wave mixing experiments.

##### ***Optical Fiber Preparation***

Transition-metal ions can be formed into volatile organometallic or halogen salts that can be used in the bubbler delivery systems of modified chemical vapor deposition ("MCVD") preform lathes. Unfortunately, transition-metal ions are exceedingly strong optical absorbers, and, as such, are serious contaminants to the bubblers in lathe delivery systems normally used to produce high transparency optical fiber. To complete fiber deliverables, the program developed a novel solution-doping process.

The solution-doping process ("SDP") is a modification of the standard industrial process for making optical fiber. This work was performed at the Rutgers University Fiber-optic Materials Research Program, ("FOMRP"), Piscataway, NJ, by Brian Cole, and David Au, under the direction of Dr. George Sigel, Jr. A silica glass soot is formed on the inside of a quartz tube by passing a carrier gas (normally hydrogen) through a bubbler containing a volatile metal oxide precursor. Silicon tetrachloride ( $\text{SiCl}_4$ ) and germanium tetrachloride ( $\text{GeCl}_4$ ) were the MCVD precursors used for the deposition of silica ( $\text{SiO}_2$ ) and germania ( $\text{GeO}_2$ ) soots. Aluminum trichloride ( $\text{AlCl}_3$ ) was used to make alumina soot which was added as a network former/modifier to accommodate the large rare-earth ions doped into the glass. The volatilized precursors were passed through the interior of a spinning quartz tube which was mounted on a lathe. An hydrogen-oxy torch repeatedly traversed the length of the spinning tube so as to locally heat the quartz under the flame. Volatile precursors that passed over the heated quartz pyrolyzed on the inner surface of the tube to form a porous glass soot.

Under normal processing, the quartz tube and glass soot are thermally collapsed into a solid preform once the desired thickness of soot has been deposited. The soot on the interior of the tube becomes the core of the optical waveguide while the tube becomes its cladding. The collapsed preform is mounted on a draw tower and is drawn down to the cross-sectional dimension of optical fiber. It is then coated with a polymer jacket to environmentally protect the glass from factors that promote microcrack formation and growth, i.e., (direct contact with abrasive surfaces and/or water) before it is spooled.

With solution-doping, the dopants are introduced into the preform core soot prior to its being collapsed into the solid preform by immersing the unfinished preform into a salt solution. In the past the solutions have been alcohol-based, typically chloride salts in ethanol. The unfinished preform is immersed in the salt solution for a prolonged period of time, ranging from hours to days, and is then removed and hung to dry. During the drying process, the alcohol solvent evaporates depositing salt crystals on the glass soot particles. The drying preform is flipped often to ensure a more even dopant distribution throughout the preform. The dry preform is then remounted on the lathe where the torch, initially set a low temperature burn (900 °C), is used to decompose the salts into their respective oxides before the final product is collapsed into the finished preform.

Alcohol-based solutions are fairly fluid and do not always result in uniform dopant distributions. The salts will frequently precipitate out of the drying solution in clusters, creating dopant-rich sites in the fiber core that have a higher tendency to nucleate crystallites during the collapse-and-draw processing steps. To overcome these processing deficiencies, this program initiated the first use of 2-ethylhexanoic acid-based salts solutions. This 2-ethylhexanoic acid is an excellent film forming solvent and, as such, is used extensively in chemical web processing. Metal-precursor salts are fairly easy to synthesize. The use of 2-ethylhexanoates was expected to provide more uniform dopant surface coverage over the soot particles and throughout the preform.

The 2-ethylhexanoates were applied by preparing individual dopant solutions for praseodymium, europium, and chromium, by exchange-reacting each of the metals as acetates with 2-ethylhexanoic acid to form their respective 2-ethylhexanoates. The europium 2-ethylhexanoate solution was remarkably stable and could be made to high concentration (1.1 M, 15.32 wt%). The praseodymium solution was much less stable and exhibited a strong tendency to precipitate waxy salts. It had to be diluted to 0.27 M (3.9 wt%) before a stable solution could be formed. The chromium solution was made to be relatively dilute (0.22 M, 1.2 wt%) because of the high optical density of chromium.

After drying the preforms, they were mounted on the lathe and torched at 900 °C to decompose the 2-ethylhexanoates for ½ hour prior to collapsing the preform. A series of runs was performed with individual dopants to roughly calibrate doping levels in fin-



ished fiber. The team at FOMRP noticed that this technique proved to be more reproducible than alcohol-based solution-doping processing and produced fiber and fiber preforms that contained more uniform distributions of rare earth and transition-metal ions. The group is continuing the work to develop a statistical basis for these findings.

#### IVd. Phase II Materials Characterization

##### Glass Transition Temperature

Glass transition temperature ( $T_g$ ) was measured using differential scanning calorimetry (DSC) and differential thermal analysis. The DSC apparatus could only scan up to 500 °C, which is generally well below the standard transition temperatures of most silicate glasses. The DTA apparatus was capable of measuring thermal properties up to temperatures of 1000 °C, but provides a far less certain measurement of  $T_g$ . All scans were made at a rate of 15 °C/min.

##### Thermal Diffusivity Measurements

Limited thermal diffusivity measurements were performed by Professor George Dixon, at Oklahoma State University. As is shown in **Figure 6**, these measurements can be used to collect information related to the activity and coupling of localized phonons and extended phonons in glass networks. An objective of this Phase II research was to develop glass hosts that strongly couple the localized phonons at optically stimulated  $\text{Eu}^{3+}$  sites to extended phonon modes that propagate the vibrational resonances across greater distances in the network. The more easily excitable network should transfer state-defining charge carriers over greater ranges and with greater ease.

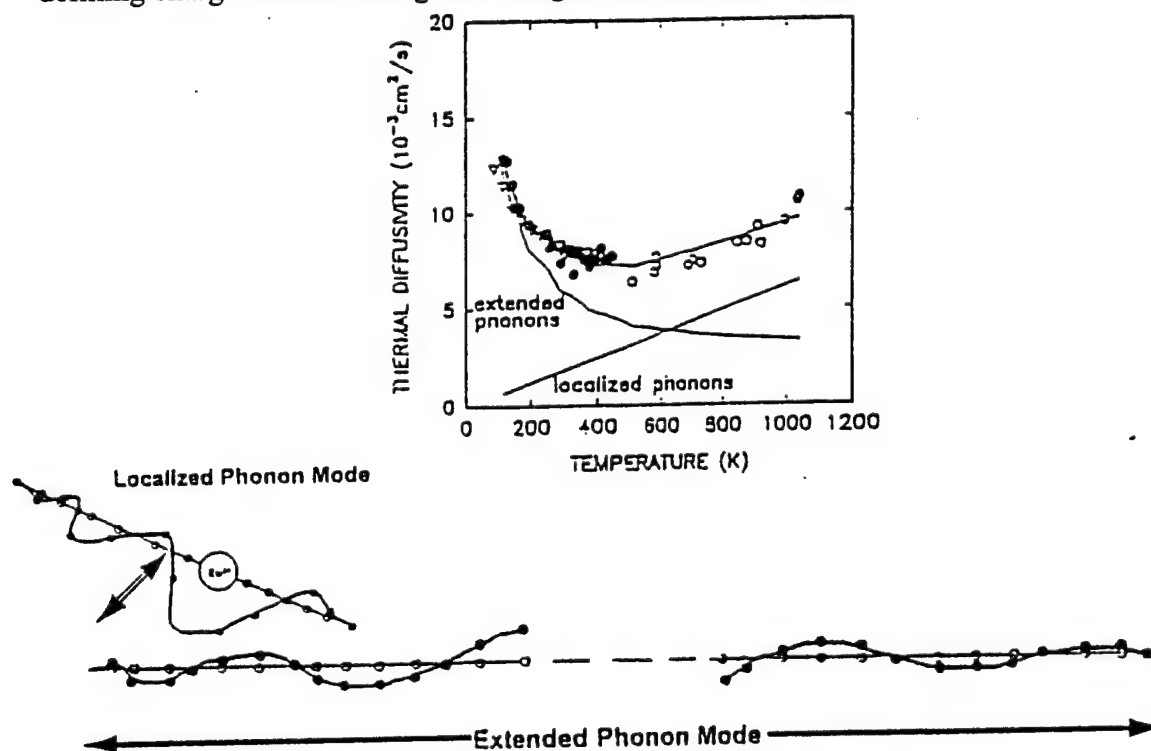


**Figure 6.** Using thermal diffusivity measurements to determine the concentration and coupling of localized phonon modes and extended phonon modes.

Amorphous solids (glass) have thermal properties with low-temperature characteristics that are not found in crystalline solids with equivalent chemical make-up. These "anomalous" low-temperature properties are universal to glass systems and are only weakly dependent on the specific chemical composition of the amorphous solid. They include: low-temperature specific heat, thermal conductivity, ultrasound propagation, dielectric loss, electric and acoustic echo, as well as some other properties governed by low-frequency modes (Buchanau *et al.* 1992). Below a temperature of 1 K, these anomalies are phenomenologically interpreted by the two-level system model (TLS) [Anderson *et al.*, and Phillips], in which an atom or group of atoms dynamically oscillate between two states of quasi-equilibrium confined in a double potential well. (See **Figure 7**). According to this model, the TLS associated with local tunneling states in double well potentials are characterized by an energy difference  $\Delta$  between the minima and a tunnel splitting  $\Delta_0 = \hbar \omega_c \exp(-\lambda)$ . Here,  $\omega_c$  is a crystal-like vibrational frequency and  $\lambda$  is a tunnel integral. The parameters  $\Delta$  and  $\lambda$  are random, but their distribution function  $P(\Delta, \lambda)$  is assumed to be constant. The tunneling model explains the main features of thermodynamics and kinetics in glasses at very low temperatures, i.e.,  $< 1$  K.

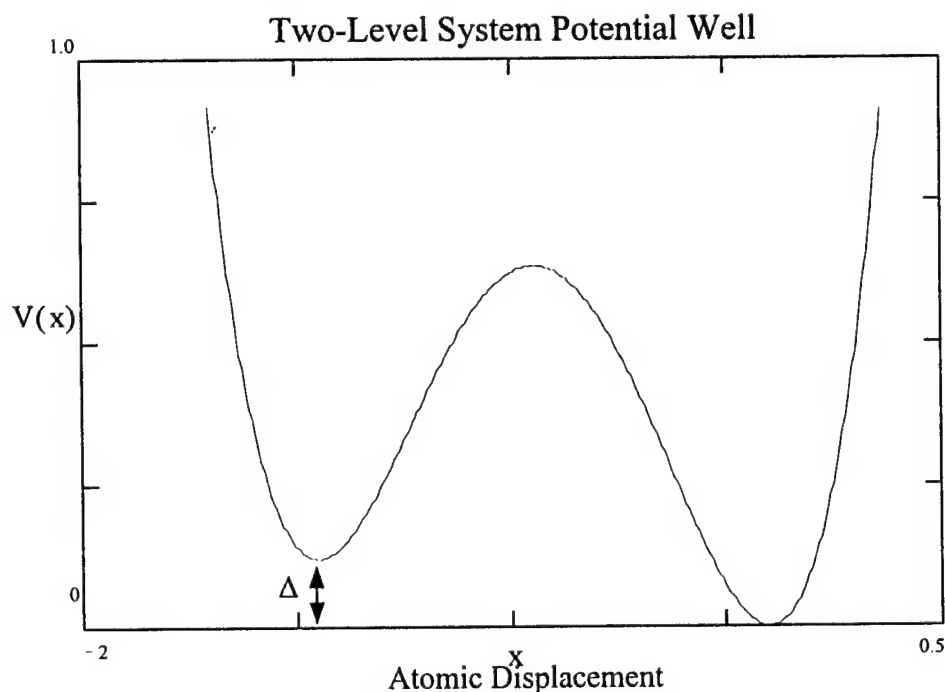


**Figure 7. TLS double potential well.**

At temperatures above 1 K, glass properties deviate from the tunneling model. Thermal conductivity plateaus around 5 K. This plateau cannot be explained in terms of a constant density of tunneling states, nor in terms of phonon scattering from static disorder. Furthermore, there is an additional increase in specific heat which indicates the ex-

istence of still another kind of low-frequency mode. Experimentally, one finds both TLS states and soft harmonic vibrations (Buchanau *et al.* 1986) coexisting with sound waves in glasses. Neutron measurements have shown these soft harmonic vibrations to cross-over to anharmonicity at the low-frequency end, i.e., at frequencies corresponding to several Kelvin (Buchanau *et al.* 1988). These findings support the soft-potential model (Karpov *et al.* and Galperin *et al.*), which is an extension of the TLS tunneling model. The soft-potential model describes both the tunneling and the soft vibrational motion as a localized soft mode in terms of soft anharmonic potentials with locally varying parameters. Buchanau estimates that these soft modes are localized to about 100 participating atoms. This description can be interpreted as *extended-range* phonons, whose existence phenomenologically accounts for thermal properties of glasses at temperatures below a plateau region.

At temperatures above the plateau, there is not yet consensus on the nature of phonons that provide the heat carriers, nor on the elastic properties of the glass that may be needed for effective thermal transport by these modes. The most successful models hypothesize that the phonons are weakly localized by the disordered structure of the glass and that the thermal process is one in which these localized phonons diffuse among neighboring sites by a random walk or hopping process. Cahill and Pohl have used such a random walk model in which the localized phonons have a strong, temperature-independent damping and tend to diffuse among equivalent sites to account for the thermal conductivities of a number of simple glasses. Their model predicts that the thermal transport coefficients will become independent of temperature once the glass is at a sufficiently high temperature that equipartition applies. Alexander *et al.* and Jagannathan *et al.* developed a model in which the localized phonons (fractons) execute thermally-activated hopping (TAH) among equivalent localization sites. The TAH model predicts that the thermal transport coefficients will be proportional to  $T$  at high temperatures.

Dixon *et al.* have shown how thermal diffusivity versus temperature measurements can be used to correlate the activation and participation of different types of extended-range and localized phonons at specific glass temperatures. Linear temperature dependence is suggestive of transport by thermal activation of localized phonons similar to that described by the TAH model. There are two basic ingredients to the TAH model. First, the existence of a phonon spectrum of the glass containing both low-frequency extended-range phonons and localized phonons above a minimum frequency  $\omega_c$ , which can be interpreted as a phonon-mobility edge. The second is the existence of significant anharmonic forces that thermally activate the localized phonons.

The photo-sensitive glass samples used in this research have backward scattered Brillouin spectra (see Section V) with well defined wave vectors at room temperature. This indicates the presence of longitudinal mode extended-range phonons in the acoustic

branch with well defined wave vectors at room temperature. Work done by Dixon *et al.* on other photo-sensitive glass compositions reveals a similar characteristic in the forward-scattered transverse acoustic mode phonons.

Raman scattering in glasses shows a broad low-frequency peak, known as the "boson-peak", starting at 10-30  $\text{cm}^{-1}$  and having its maxima typically in the 30 to 80  $\text{cm}^{-1}$  range. Wavevectors are no longer well defined above this frequency. Extended-range phonons with wavevector  $q$  is expected, on general theoretical grounds, to have a wavelength on the scale of  $\xi_c$ , the disorder in the network. Wavevectors with  $q^{-1}$  that are comparable or less than  $\xi_c$  would be expected to be strongly scattered by inhomogeneities in the density or elastic properties of the network. It is not possible to have a normal mode unless the mean-free-path  $\Lambda$  and wavevector  $q$  satisfies the Ioffe-Regel criterion,  $q\Lambda > 1$ . Hence, the condition  $q\xi_c \approx 1$  divides the low-frequency, extended states with reasonably well defined wavevectors from higher frequency localized modes for which the wavevector is no longer a good quantum number [Bell and Dean].

Localized phonons are believed to contribute to thermal transport through a three phonon anharmonic process. When a localized phonon decays, energy conservation requires that it reappear in some other mode, at a distance away ( $R$ ), elsewhere in the glass. This process will have a significant probability of occurring if there is a substantial overlap of the donor (decaying) and acceptor (activating) phonon wavefunctions. Extended-range phonons are likely to facilitate the energy "hopping" between localized donor and acceptor modes, since very few localized modes are likely to have exactly the same frequency. Because extended-range phonons have access to the entire sample, they are the most likely candidate for the low-frequency phonon that is emitted and absorbed in the energy transfer between localized donor and acceptor phonons.

The TAH process contributes to thermal diffusivity as

$$\alpha_{\text{loc}} = \langle R^2 \rangle \tau_{\text{loc}}$$

where  $\langle R^2 \rangle$  is a thermally averaged square hopping distance and  $\tau_{\text{loc}}$  is the mean lifetime of the localized phonon. Since this process is facilitated by extended-range phonons,  $\tau_{\text{loc}}$  will be inversely proportional to the population of extended-range phonons when  $k_B T \gg \hbar \omega$ , i.e.,

$$\tau_{\text{loc}} \propto 1/n(\omega) \approx \hbar \omega / k_B T.$$

$\langle R^2 \rangle$  does not depend on temperature when  $T$  is large enough for equipartition to apply. A linear dependence of the thermal diffusivity is a signature of significant transport due to thermally-activated hopping.

The extended-range phonons also contribute to the thermal transport with a conduction process described in the conventional phonon-gas picture. The net thermal conductivity ( $\sigma$ ) is the sum of the contributions from the extended-range and the localized phonons,

$$\sigma = (C_{\text{ext}}/3)v_s^2\tau_{\text{ext}} + C_{\text{loc}}(R^2)/\tau_{\text{loc}}$$

where  $C_{\text{ext}}$  and  $C_{\text{loc}}$  are the heat capacities per unit volume of the extended-range and localized phonons, respectively. The corresponding thermal diffusivity  $\alpha = \alpha_{\text{ext}} + \alpha_{\text{loc}}$  is

$$\alpha = (C_{\text{ext}}/3C)v_s^2\tau_{\text{ext}} + (1 - C_{\text{loc}}/C)(R^2)/\tau_{\text{loc}}$$

where  $C = C_{\text{ext}} + C_{\text{loc}}$ , and  $v_s^2$  is the velocity of sound in the glass. As discussed above, TAH contributes a linear temperature dependence. Using the assumption that phonon-phonon scattering is the dominant resistive process for the extended-range phonons, then  $\tau_{\text{ext}} \approx T^{-1}$ , and the thermal diffusivity can be fit to a function of the form:

$$\alpha = (C_{\text{ext}}/C)AT^{-1} + (1 - C_{\text{loc}}/C)BT$$

The apparent connection between optical grating formation in glass and underlying features of phonon mode coupling in suitable glass hosts motivated this research to include thermal diffusivity measurements. These measurements were performed by George S. Dixon, with the Department of Physics, Oklahoma State University, Stillwater, OK, without financial support from this contract. These measurements were made by cutting glass samples into 3x3x15 mm<sup>2</sup> rectangular parallelipeds. Shallow grooves were cut into the sample to hold three 0.025 mm diameter chromel-alumel thermocouples referenced to electronic ice points. The thermocouples were anchored to the sample with a small amount of thermally conducting paste (an alumina-filled silicone grease). This paste was also used to attach the sample base to a resistance heater which was used to obtain a transient temperature distribution of the sample. High-temperature measurements were made by mounting the samples in a small tube furnace that controlled the mean temperature of the sample. Low-temperature measurements were obtained by mounting the assembly on the cold finger of a liquid nitrogen cryostat.

A microcomputer was used to control the instruments over an IEEE-488 interface bus. Simultaneous readings of the three thermometers were obtained by sending a group trigger command to the digital voltmeters. Each of thermocouples was read with a Hewlett-Packard model 3478A digital multimeter having a sensitivity of 0.1  $\mu$ V. Under steady-state conditions, temperature readings were taken to establish a "baseline" measurement. Upon a computer command, a digital relay was closed to supply current to the transient heater. A constant current was maintained while simultaneous temperature measurements were taken by the three thermocouples at 0.5 sec intervals. Data was col-

lected over an elapsed time of 50 to 100 s, over which time the thermocouple closest to the heater typically recorded a temperature change of 3 to 7 K. The digital relay to the transient heater was opened at the end of a data collection interval to re-establish steady-state conditions in the sample.

Thermal diffusivity,  $\alpha$ , was obtained by applying a finite difference algorithm to the diffusion equation

$$(\partial T / \partial t) = \alpha \nabla^2 T.$$

## **Bulk Glass Optical Properties**

### ***Linear Optical Properties***

Optical transmission windows in all bulk glass samples were measured using a near-ultraviolet-visible-near-infrared (near-uv-vis-near-ir) spectrophotometer. On average, each glass sample was cut into a 1 cm<sup>2</sup> x 0.75 cm cube and polished to a 1  $\mu$ m finish and was then scanned. Each sample was then ground into a 1 cm<sup>2</sup> x 0.5 cm cube and again polished to a 1 micron finish before being scanned a second time. Spectral attenuation  $\alpha(\lambda)$  was measured as:

$$\alpha(\lambda) = \ln(T_1/T_2)/(t_2-t_1)$$

where  $T_1$  and  $T_2$  are the measured percent transmission coefficients, and  $t_1$  and  $t_2$  are the respective measured thicknesses.

### ***Four-wave Mixing Measurements***

The four-wave mixing (FWM) test apparatus utilizes two write-beams at 465 nm from a Spectra-Physics argon ion laser, and a HeNe probe at 632 nm. Data is collected using the photon counting technique (preamplifier/amplifier/discriminator (PAD) and rate meter) in order to determine FWM efficiency. The transient characteristics of permanent gratings are measured using write/block/erase sequences. In the writing mode, both beams are incident on the sample after the probe has been phase-matched to the interaction area. During the block sequence, both write-beams are blocked while the probe remains on. During the erase sequence, one of the probe beams is blocked and the other is left incident on the sample while the probe scans the interaction zone.

FWM scattering efficiencies were characterized as a function of crossing angle and write-beam power.

### Three-Wave Mixing Measurements

Three-wave mixing measurements have been attempted by recording a permanent grating in the parallelepiped shaped Bragg-1-4 sample that had been polished on all sides for Raman and Brillouin scattering measurements. Attempts to record the grating was made by dilating the beam spot from roughly 0.5 mm to 1.0 cm, and increasing the write-beam crossing angle from  $3.5^\circ$  to  $42^\circ$ . The wider crossing angle provides the minimum condition under which optical phase matching for three-wave mixing can be achieved. (See **Figure 8**). A Q-switched YAG laser was used as the probe for the three-wave mixing experiments. Unfortunately, the table optics that are available to the project do not allow the YAG laser (used to probe the sample) and the argon ion laser (used to record the grating) to be housed in the same room. To compensate for this discrepancy, the write-beam spots were expanded to achieve maximal coverage over the surface of the parallelepiped shaped sample to define as large an interaction zone as possible. This was attempted to allow the sample to be moved to the YAG table and probed through a polished face that was perpendicular to the face exposed to the write-beams.

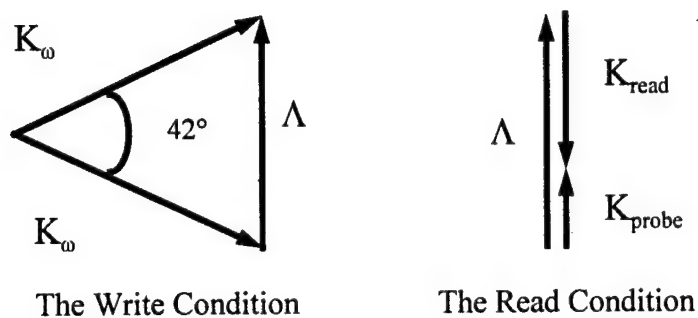


**Figure 8.** The conditions attempted for writing and reading SHG in alkali-modified rare earth-doped aluminosilicate glass.

No SHG signals were measured, nor could any FWM signals be detected during the write process. It is not known at this time whether or not it is possible to write gratings in rare earth-doped alkali-modified aluminosilicate glass at write-beam crossing angles of  $42^\circ$ , or if the optical amplitude in the interference pattern, and the associated differential in optical phonon population densities in regions of constructive and destructive interference was large enough to initiate grating formation. Future efforts will incorporate smaller sized samples so the write-beam spot sizes can be reduced to increase write-beam intensities at these extreme crossing angles.



### ***Raman Scattering Measurements***

Raman scattering is used to determine the frequency distribution profiles of optical phonons that are typically transported through the network, and those that are generated during the write-process. Parallelepiped samples, polished on all sides, are used for Raman scattering measurements performed with the Micro-Raman Facility at Oklahoma State University. Several excitation wavelengths from an argon-ion laser have been utilized. Off-resonance measurements are made using the 514.5 nm line. Near and at write-beam resonance are measured by probing the sample using beams with wavelengths at 457.9 nm, 472.7 nm, and 465.8 nm (on-resonance).

These optical phonon frequency distribution profiles will be correlated with FWM measurements to ascertain the underlying phonon structure(s) that is requisite to preparing high performance nonlinear optical grating structures in rare earth-doped glass.

### ***Brillouin Scattering Measurements***

As optical phonons are scattered within the amorphous network, their energy can be dispersed among acoustic mode phonons, which may also play a significant role in the grating formation process. Whereas Raman scattering is used to profile the frequency distribution profile of optical phonons, Brillouin scattering is used to derive information related to acoustic mode phonon structure. This research project is currently equipped to measure backward scattered Brillouin spectra, which reveals frequency information only on the longitudinal acoustic phonons present.

### ***Fiber-optic Optical Properties***

Refractive index profiles of fiber-optic preforms were measured using a profilometer. Optical transmission/absorption in the optical fiber drawn from these preforms was measured using an optical time-domain reflectometer (OTDR).

## V. Research Results

### Glass Transition Temperature

#### *The Effect of Rare Earth Lanthanide Doping on Glass Transition Temperature*

All reported glass transition temperatures ( $T_g$ ) were measured using DTA. The base host glass used in this research was a magnesium-soda-aluminosilicate composition:

	<b>SiO<sub>2</sub></b>	<b>Al<sub>2</sub>O<sub>3</sub></b>	<b>MgO</b>	<b>Na<sub>2</sub>O</b>
mol%	70.00	3.00	12.00	15.00

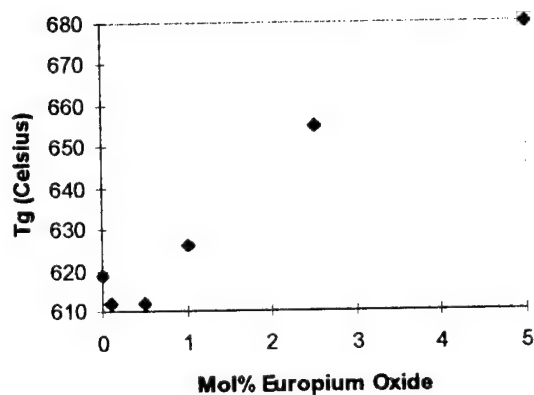
The host was doped using the standard doping scheme:

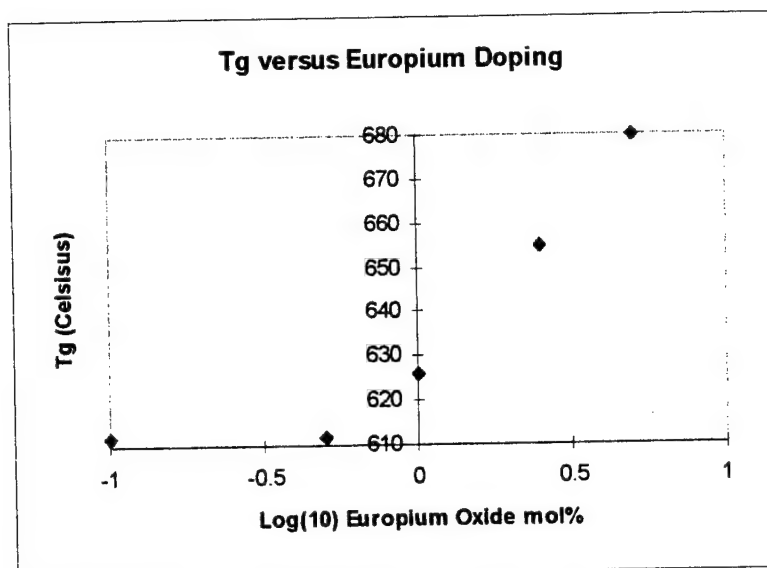


When this host composition was doped with europium its glass transition-temperature was found to increase as:

<b>Sample ID</b>	<b><math>T_g</math> (°C)</b>	<b>Eu<sub>2</sub>O<sub>3</sub> (mol%)</b>
Bragg-5	619	0.0
Bragg-6	612	0.1
Bragg-7	612	0.5
Bragg-8	626	1.0
Bragg-9	655	2.5
Bragg-10	680	5.0

**T<sub>g</sub> versus Europium Doping**





Similar relationships were not observed when the host was doped with praseodymium oxide.

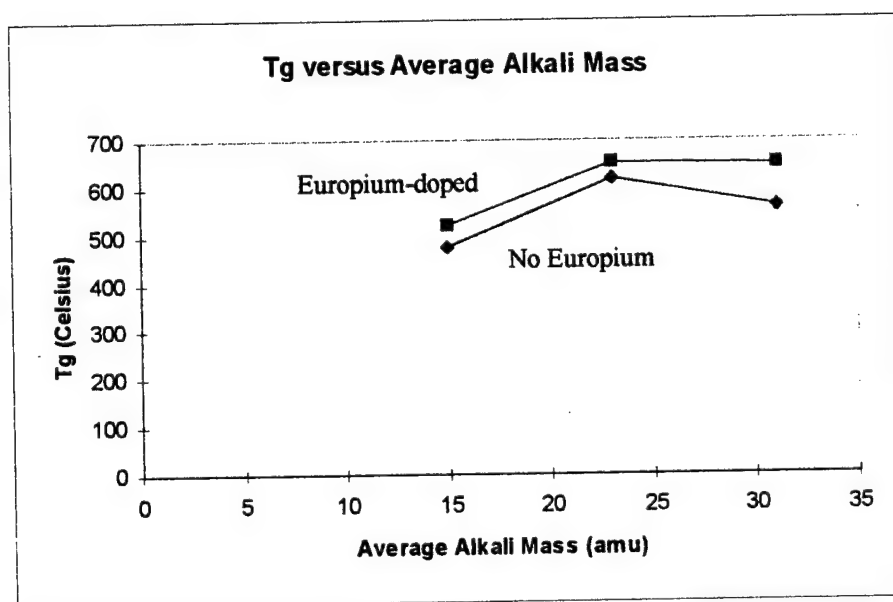
Sample ID	T <sub>g</sub> (°C)	Pr <sub>2</sub> O <sub>3</sub> (mol%)
Bragg-5	619	0.0
Bragg-31	643	0.5
Bragg-32	600	1.0
Bragg-33	609	2.5

### *The Effect of Alkali Substitution on Glass Transition Temperature*

The effect of alkali mass on grating formation was measured by partially substituting sodium ions (22.99 amu) with lighter mass lithium ions (14.97 amu) and heavier mass potassium (39.10 amu). Partial substitutions were made by preparing glasses in which 50% of the sodium ions in the base host composition were replaced with the other alkalis. These substitutions were made for undoped and base host compositions doped with europium at a level of 2.5 mol%. These substitutions impacted T<sub>g</sub> as delineated below. Samples Bragg-5, -11, -13 evaluate the effect of the substitutions on the host itself. Samples Bragg-9, -12, -14 evaluate the effect of the substitutions when the modified host is doped with europium. The following are based on 0.70 SiO<sub>2</sub>-0.03 Al<sub>2</sub>O<sub>3</sub>-0.12 MgO-0.15 A<sub>2</sub>O host compositions, where A represents the lithium (Li), sodium (Na), or potassium (K) alkali modifiers.

### Alkali-Modified Glass Compositions

Sample ID	$T_g$ (°C)	Na <sub>2</sub> O	mol%		Average Alkali Mass (amu)
			Li <sub>2</sub> O	K <sub>2</sub> O	
Bragg-5	619	15.0	0.0	0.0	22.99
Bragg-11	479	0.75	0.75	0.0	14.97
Bragg-13	560	0.75	0.0	0.75	31.04
Bragg-9	655	15.0	0.0	0.0	22.99
Bragg-12	522	0.75	0.75	0.0	14.97
Bragg-14	651	0.75	0.0	0.75	31.04

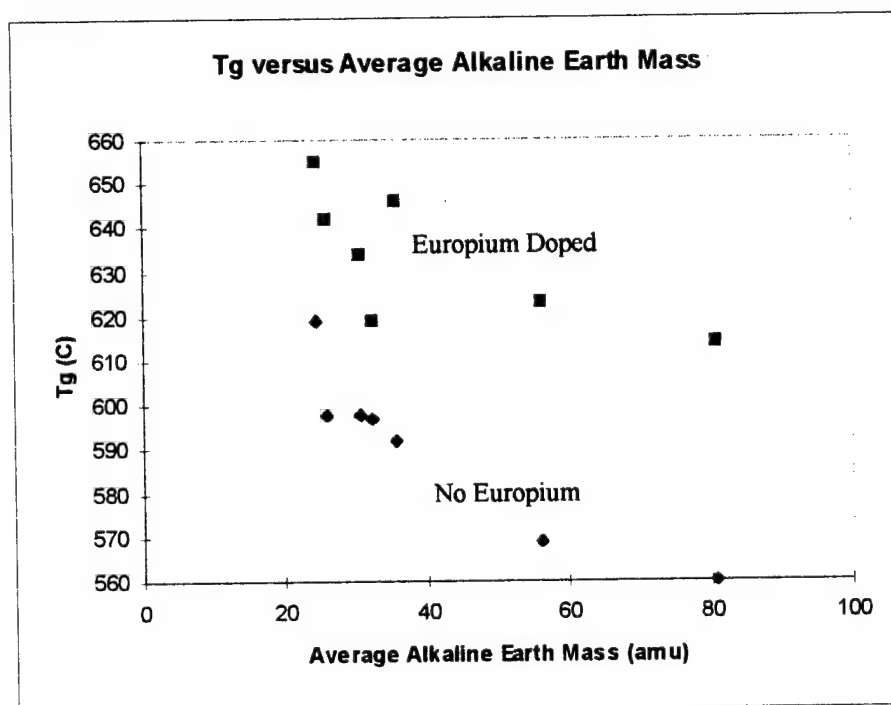


### *The Effect of Alkaline Earth Substitution on Glass Transition Temperature*

The effect of alkaline earth mass on grating formation was measured by partially substituting magnesium ions (24.3 amu) for heavier mass calcium ions (40.1 amu), strontium ions (87.6 amu), and barium ions (137.3 amu). Partial substitutions were made by preparing two series of glasses in which 10% and 50% of the sodium ions in the base host composition were replaced with the other alkaline earths. These substitutions were made for undoped and base host compositions doped with europium at a level of 2.5 mol%. These substitutions impacted  $T_g$  as delineated below. Samples Bragg-5, -15, -17, -19, and -21, -23, -25 evaluate the effect of the substitutions on the host itself. Samples Bragg-9, -16, -18, -20, -22, -24, and -26 evaluate the effect of the substitutions when the modified host is doped with europium. The following are based on 0.70 SiO<sub>2</sub>-0.03 Al<sub>2</sub>O<sub>3</sub>-0.12 AEO-0.15 Na<sub>2</sub>O host compositions, where AE represents the magnesium (Mg), calcium (Ca), strontium (Sr), or barium (Ba) alkaline earth modifiers.

### Alkaline Earth Modified Glass Compositions

Sample ID	T <sub>g</sub> (°C)	mol%				Average Alkaline Earth Mass (amu)
		MgO	CaO	SrO	BaO	
Bragg-5	619	12.0	0.0	0.0	0.0	24.3
Bragg-15	597	6.0	6.0	0.0	0.0	32.1
Bragg-17	569	6.0	0.0	6.0	0.0	56.0
Bragg-19	560	6.0	0.0	0.0	6.0	80.7
Bragg-21	598	10.8	1.2	0.0	0.0	25.9
Bragg-23	598	10.8	0.0	1.2	0.0	30.6
Bragg-25	592	10.8	0.0	0.0	1.2	35.6
Bragg-9	655	12.0	0.0	0.0	0.0	24.3
Bragg-16	619	6.0	6.0	0.0	0.0	32.1
Bragg-18	623	6.0	0.0	6.0	0.0	56.0
Bragg-20	614	6.0	0.0	0.0	6.0	80.7
Bragg-22	642	10.8	1.2	0.0	0.0	25.9
Bragg-24	634	10.8	0.0	1.2	0.0	30.6
Bragg-26	646	10.8	0.0	0.0	1.2	35.6



### ***The Effect of Silica Enrichment on Glass Transition Temperature***

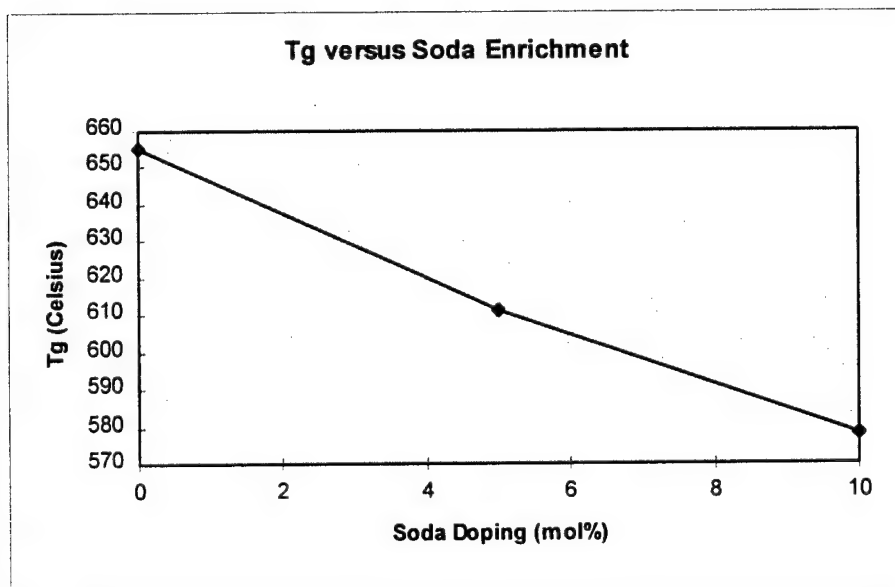
The effect of network formers on grating formation was evaluated by enriching the host composition with silica. This study prepared a modified host that was doped with silica at levels of 2.5 and 5.0 mol%. The modified host was in turn doped with 2.5 mol% of europium. Silica enrichment at these levels did not appear to increase  $T_g$ .

Sample ID	$T_g$ (°C)	SiO <sub>2</sub> -doping (mol%)
Bragg-9	655	0.0
Bragg-27	650	2.5
Bragg-28	651	5.0

### ***The Effect of Sodium (Alkali) Enrichment on Glass Transition Temperature***

Alkali ions are believed to be the state-defining charge carriers that actively participate in grating formation. The basic host glass was "soda-doped" at levels of 5.0 and 10.0 mol%. The soda-modified host was in turn doped with 2.5 mol% europium. Soda doping of the basic host did produce the expected decline in glass transition-temperature.

Sample ID	$T_g$ (°C)	SiO <sub>2</sub> -doping (mol%)
Bragg-9	655	0.0
Bragg-29	611	5.0
Bragg-30	578	10.0



### *The Effect of Transition-metal Doping on Glass Transition Temperature*

Transition-metals introduce multi-valent color-centers in the near-uv-vis-ir transmission window of the glass. Two vanadium oxides were introduced in equal proportions in to the base host:  $V^{(III)}_2O_3$  and  $V^{(V)}_2O_3$ . These dopants were introduced in total vanadium oxide levels of 1.5 and 0.5 mol%. The transition-metal doped host was in turn doped with 5.0 mol%  $Eu_2O_3$ . Transition-metal doping was observed to reduce glass transition-temperature.

Sample ID	$T_g$ (°C)	TM-doping (mol%)
Bragg-10	680	0.0
Bragg-37	622	1.5
Bragg-38	627	0.5

### **Thermal Diffusivity Measurements**

Thermal diffusivity measurements were used to determine coupling between localized phonon modes and extended-range mode phonons. It is considered important to have strong coupling between the localized modes and extended-range phonons in glass hosts to optimize their photo-sensitivity to optically-prepared holographic gratings. In rare-earth doped glass, the write process is known to occur by pumping excited states of the rare-earth ions that decay strongly through a non-radiative branch. Optical phonons stimulated during the write process provide the lattice energy that mediates the write process. The frequencies of these modes are well above the phonon mobility edge,  $\omega_c$ , and, as such, these phonons are highly localized to the  $Eu^{3+}$  ion sites. To prepare a grating, localized modes must be able to convey their lattice energy over distances in the glass that is at least some significant fraction of the period of the write-beam interference pattern. As discussed above, strong coupling to a low-frequency extended-range phonon would allow these localized phonons to "hop" over greater distances in the glass and to carry the state-defining charge carriers that alter microscopic optical properties along with them.

The contribution of extended-range phonons to thermal diffusivity is characterized by a  $1/T$  dependence in the thermal diffusivity versus temperature. The contribution of localized phonons to thermal diffusivity is directly proportional to temperature. Therefore, a suitable glass host would have a strong  $1/T$  dependence in its thermal diffusivity. **Figure 9** shows the measured thermal diffusivity in the base host glass used in this research. One sample (Bragg-5-2) was "fast-cooled" by removing from the melting furnace at 1550 °C and letting it stand at room temperature before annealing at 725 °C for one hour. Bragg-5-1 was "slow-cooled" by removing it from the 1550 °C melting furnace and placing it directly in the annealing oven heated to 550 °C prior to a one hour anneal

at 725 °C. The "slow-cooled" sample shows a dramatically enhanced  $1/T$  dependence in its thermal diffusivity.

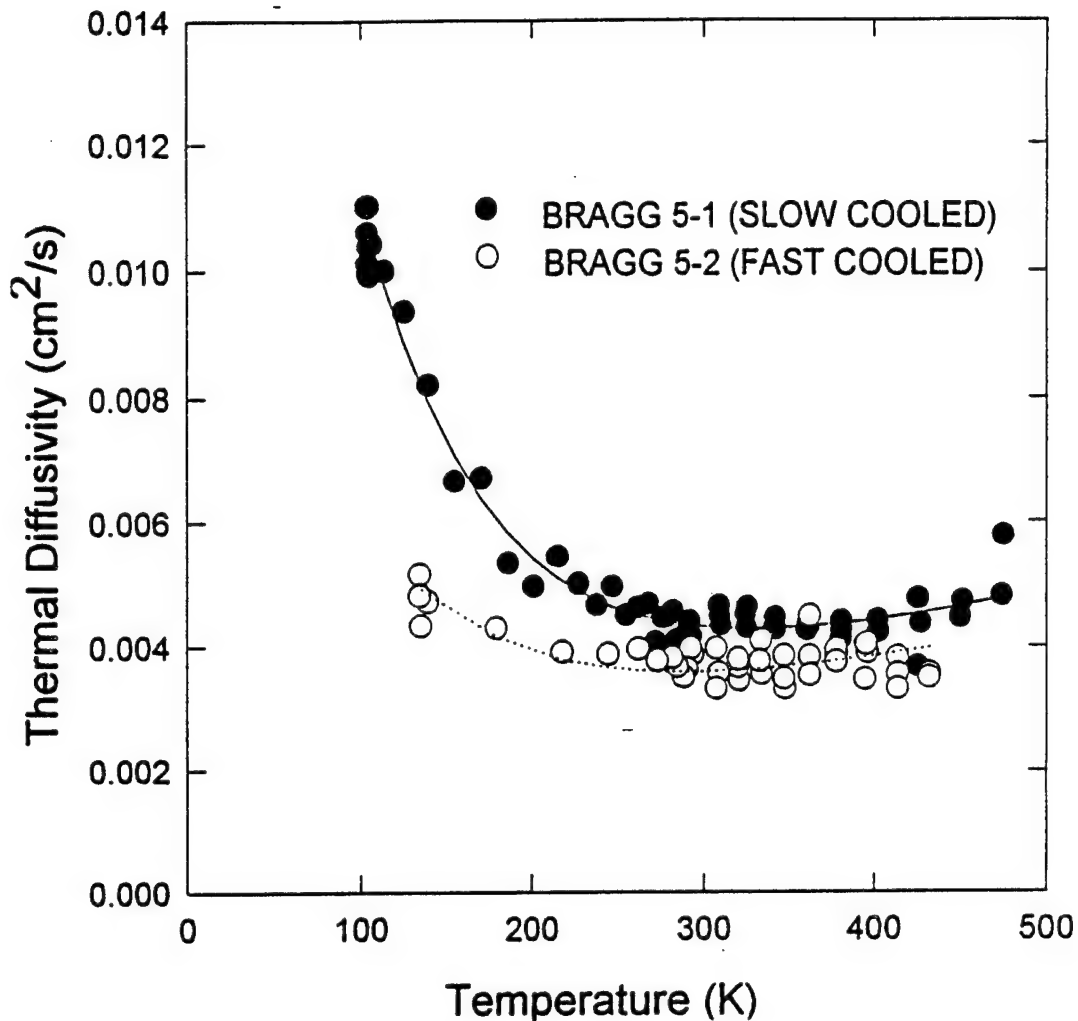


**Figure 9.** Thermal diffusivity curves of the magnesia-soda-aluminosilicate host glass composition. Both melts were identically processed in every respect except that one was "slow-cooled" and the other was "fast-cooled" prior to annealing.

The curves to the data in **Figure 9** are fits to the data using the model (described above) that treats both extended-range and localized phonons as important heat carriers. The extended-range phonons have two contributions to their mean-free-path. One varies as  $1/T$  for phonon-phonon scattering while the other remains constant and is related to disorder. Quenching from high temperature is expected to freeze greater disorder into the glass. This disorder provides a strong temperature-independent scattering mechanism for



extended-range phonons that, consequently, will disrupt their propagation. The constant factor measured in the  $1/T$  dependence increases by a factor of 3 in going from the "fast-cooled" to the "slow-cooled" specimens. Given this understanding, the "slow-cooled" samples were clearly preferred for preparing permanent-grating materials. All subsequent compositions examined in this research were prepared using the "slow-cooled" process.

The base host composition itself is near ideal as well. Even in the "fast-cooled" sample, the temperature-dependent mean-free-path is too long (as compared to the disorder) to make a good determination of its contribution to changes in thermal diffusivity. The contribution of the localized phonons to the thermal diffusivity is linear in temperature. Its coefficient decreases by 20% between the slow-cooled and fast-cooled material. However, almost all of this difference could be attributed to experimental uncertainty.

Specimens of every glass composition analyzed in this research were prepared for thermal diffusivity measurements. Given the unfunded status of this aspect of the research, only measurements on the Bragg-5 series were available at the time this report was drafted. Thermal diffusivity measurements on the other specimens are on-going and will be correlated with grating scattering efficiencies and reported in the open literature at some point in the future.

## **Bulk Glass Optical Properties**

### ***Linear Optical Properties***

#### ***The Effect of Rare-Earth Lanthanide Doping on Optical Transmission***

**Figure 10** illustrates the effect  $\text{Eu}_2\text{O}_3$  doping has on the optical transmission of the base host glass. The ultraviolet absorption edge is observed to move towards longer wavelengths and several narrow band peaks are introduced in the glass window. The  $^7\text{F}_0 \rightarrow \text{F}_0$  transition has its peak at 462 nm in these glasses. Therefore, an optical pump of 465 nm only penetrates the shoulder of the absorption band. **Figure 11** illustrates the effect  $\text{Pr}_2\text{O}_3$  doping has on the optical transmission window of the glass. Optical attenuation at 465 nm is greatly enhanced with this dopant.  $\text{Pr}_2\text{O}_3$ -doped glasses thereby allow more energy from the optical pump to be redirected into lattice energy during the write process.

Rare Earth Dopant	Attenuation ( $\text{cm}^{-1}$ )				Wavelength (nm)
	0.5 mol%	1.0 mol%	2.5 mol%	5.0 mol%	
$\text{Eu}_2\text{O}_3$	0.08	0.17	0.25	0.62	462
$\text{Pr}_2\text{O}_3$	0.51	0.81	1.69	---	465

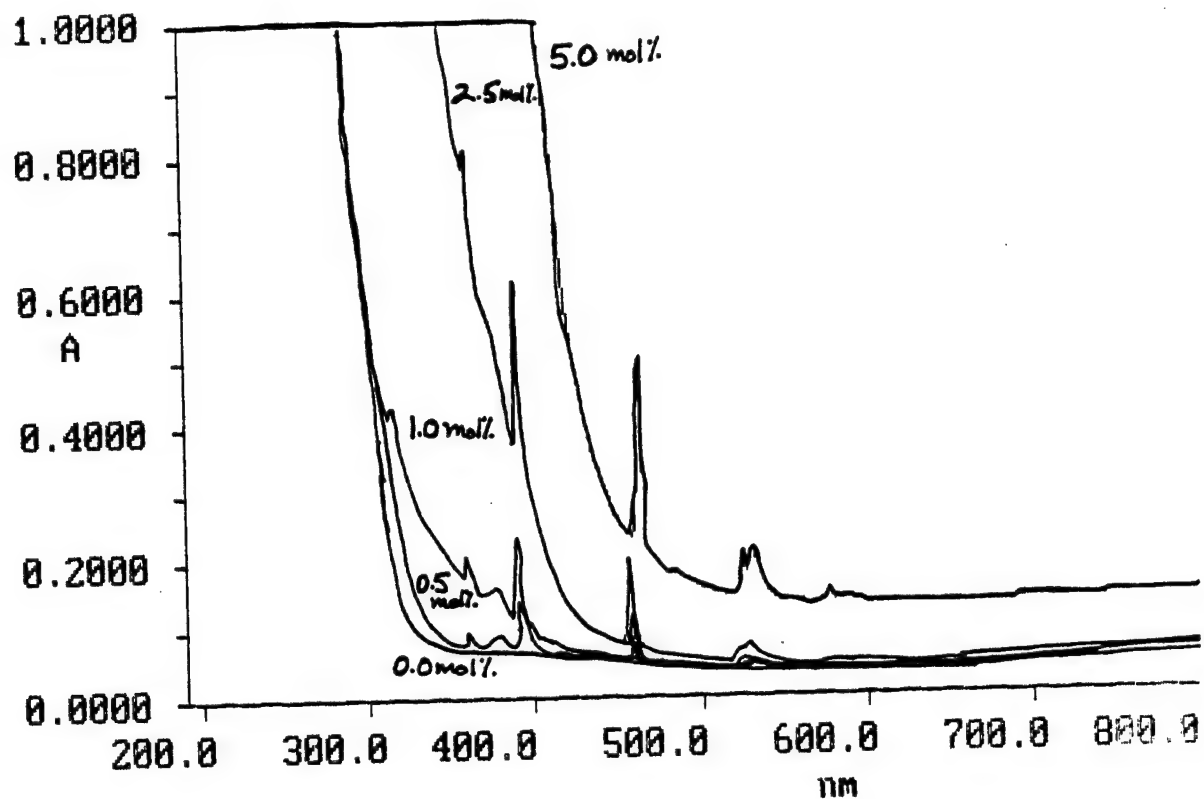


**Figure 10.** Optical transmission window in  $\text{Eu}_2\text{O}_3$ -doped glasses.

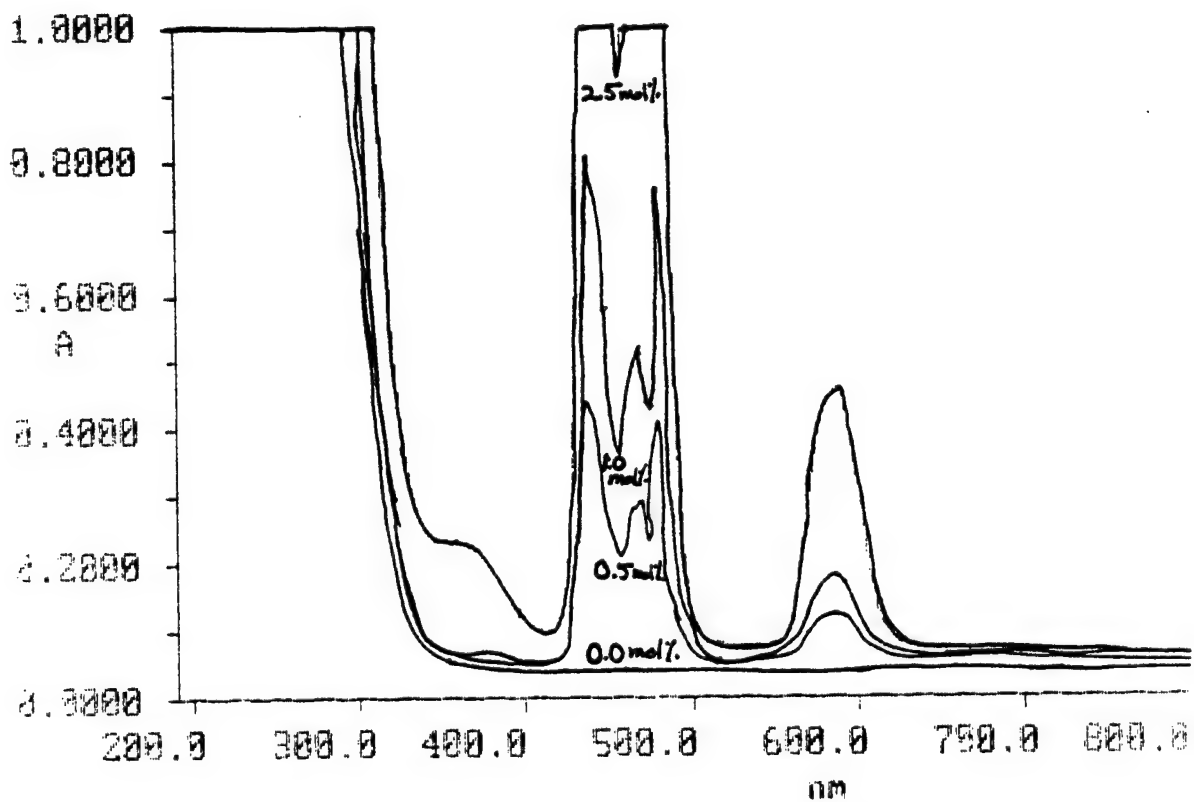


**Figure 11.** Optical transmission window in  $\text{Pr}_2\text{O}_3$ -doped glasses.

### ***The Effect of Alkali Substitutions on the Optical Transmission Window***

No noticeable effect was observed on the optical transmission window when 50% of the sodium oxide ( $\text{Na}_2\text{O}$ ) in the base host composition was substituted for lithium oxide ( $\text{Li}_2\text{O}$ ) or potassium oxide ( $\text{K}_2\text{O}$ ).

### ***The Effect of Alkaline Earth Substitutions on the Optical Transmission Window***

The ultraviolet edge was observed to move towards longer wavelengths when 50% of the magnesium oxide ( $\text{MgO}$ ) in the base host composition was substituted for calcium oxide ( $\text{CaO}$ ) and strontium oxide ( $\text{SrO}$ ). (See Figure 12).

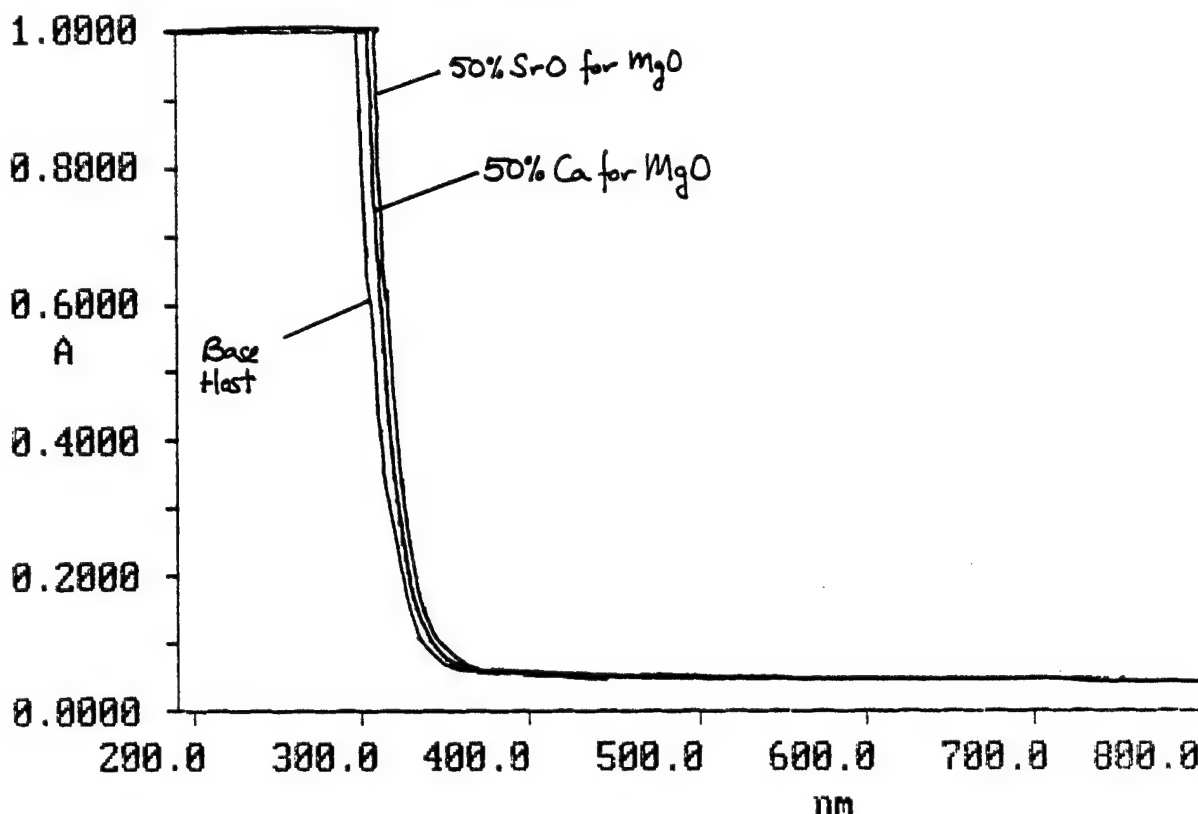


**Figure 12.** Optical transmission window in the base host glass and alkaline earth substituted glasses.

### ***The Effect of Silica-enrichment on the Optical Transmission Window***

No noticeable effect was observed on the optical transmission window when the base host composition was enriched with silica ( $\text{SiO}_2$ ) at levels of 2.5 mol% and 5.0 mol%..

### *The Effect of Soda-enrichment on the Optical Transmission Window*

The ultraviolet edge was observed to move towards significantly longer wavelengths when doped with 10% sodium oxide ( $\text{Na}_2\text{O}$ ). (See Figure 13).

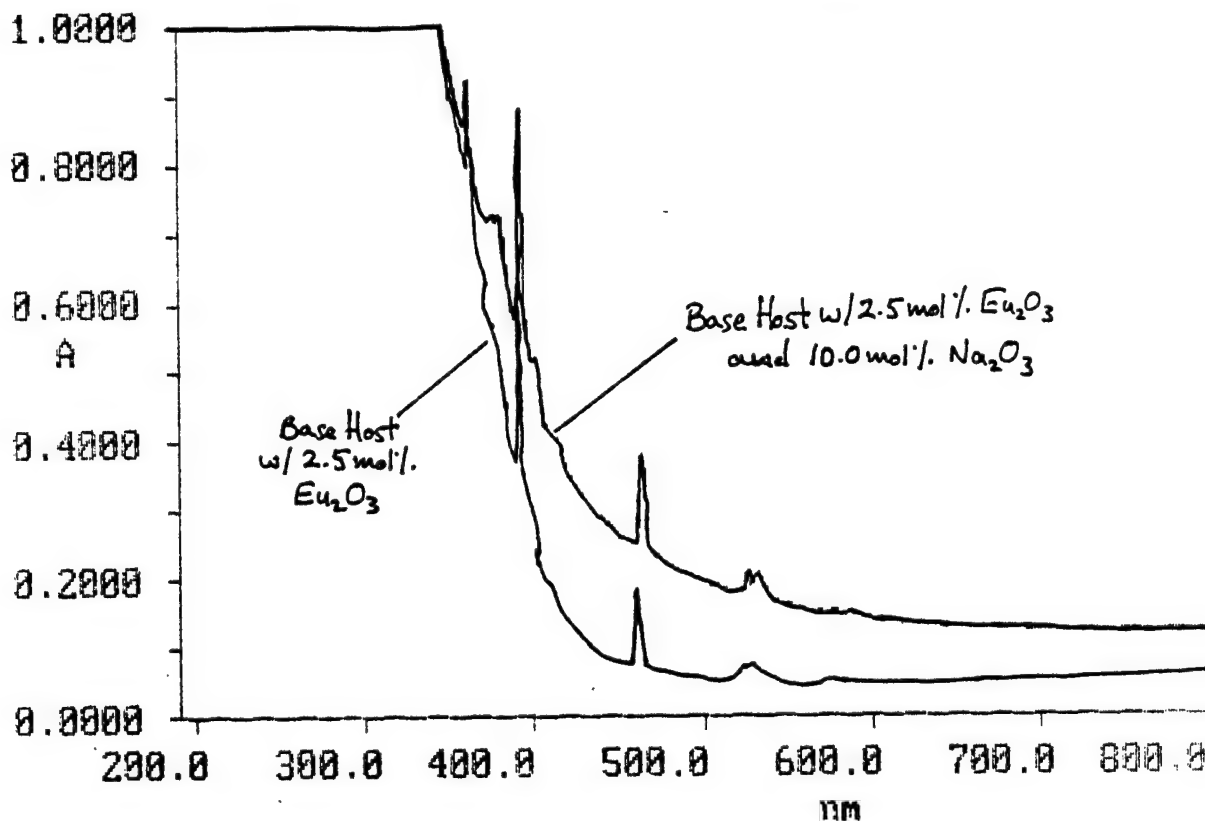


**Figure 13.** The effect of soda-enrichment on the optical transmission window in the base host glass doped with 2.5 mol%  $\text{Eu}_2\text{O}_3$ .

### *The Effect of Transition-metal doping on the Optical Transmission Window*

First-row transition-metal ions introduce strongly absorbing color-centers into the optical transmission window of glass. Vanadium (V) is a multi-valent transition-metal ion and will have color-centers at varying locations in the optical transmission window of silicate glasses that depend on its particular state of valence.  $\text{V}^{5+}$ , the valence state of vanadium pentoxide ( $\text{V}_2\text{O}_5$ ), produces a strongly absorbing near-ultraviolet color-center and leaves the rest of the window clear.  $\text{V}^{3+}$ , the valence state of vanadium trioxide ( $\text{V}_2\text{O}_3$ ), induces a brown color in the glass by producing broadly absorbing color centers at 460 nm, 630 nm, and 980 nm.

Because these color-centers are so strongly absorbing, vanadium could be doped into the silicates in only limited amounts without making the glass so opaque that read and write-beams could not pass through the sample without being fully attenuated. **Figure 14** shows the effect of vanadium color-centers on the optical transmission window of a

base host modified doped with 5.0 mol%  $\text{Eu}_2\text{O}_3$  that was modified to contain only 0.25 mol% of vanadium trioxide ( $\text{V}^{3+}$ ) and vanadium pentoxide ( $\text{V}^{5+}$ ), each.

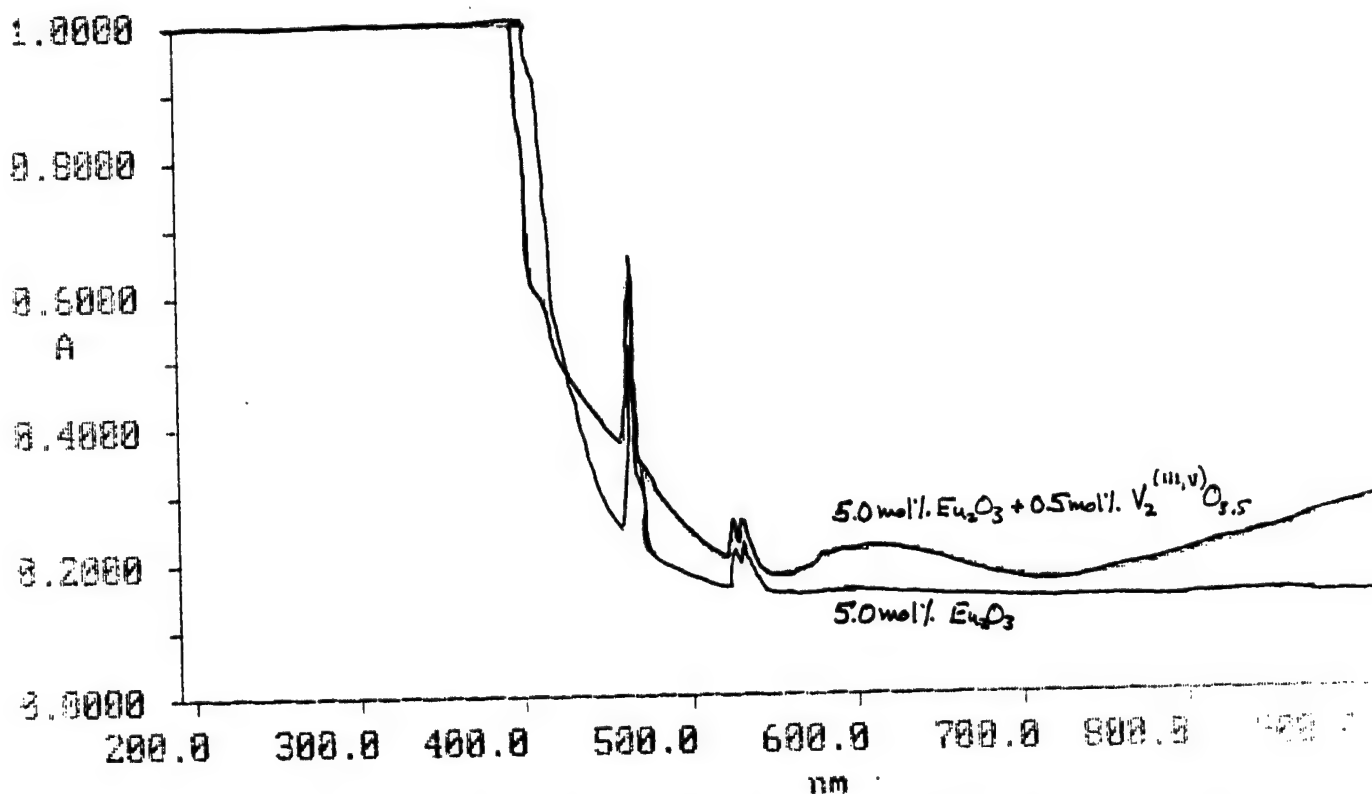


**Figure 14.** The effect of transition-metal doping (0.5 mol%  $\text{V}^{(\text{III,V})}\text{O}_{3.5}$ ) on the optical transmission window in the base host glass doped with 5.0 mol%  $\text{Eu}_2\text{O}_3$ .

#### Four-wave Mixing Measurements

The following data presents four-wave mixing (FWM) measurements in both qualitative and quantitative terms. Plots of the scattered signal intensity versus time are given to qualitatively display the temporal stability of the gratings versus various write conditions. These gratings were analyzed with respect to write-beam power and write-beam crossing angle. While spot-to-spot measurements within a given sample yielded consistent results, the gratings did not cycle back to their peak scattering efficiency. Initial write conditions frequently produced a peak signal within 5 minutes. However, signal strength would decay with prolonged writing to a stable value that was lower than the peak signal by a factor of 3, roughly. Grating signals were observed to have both transient and permanent signal components. Both components were observed under "Write" conditions. The transient signal was observed to decay when the write condition was turned off, leaving only the permanent signal component. A transient signal decay time of 2.2 ms was observed in several samples. This value appeared to be independent of write-beam power.

Qualitative measurements also examined permanent grating signal strengths when write-beam conditions were turned off and then re-established on the sample. The condition that exists when both write-beams on the sample are turned off is reported as "Blocked" write-beams. Grating recyclability was also evaluated by turning off one write-beam on the sample, thereby inducing conditions that "Erase" the grating, and then restoring the write beam that was turned off. These gratings were found to be permanent after the transient signal decayed since stable read beam signals were observed after both write-beams were turned off and kept off.

Quantitative analysis is based on peak signal intensities for a given sample, presented in terms of absolute FWM scattering efficiency. The FWM scattering efficiency is the Bragg diffraction intensity (as measured by the PMT), divided by the incident power of the HeNe read-beam ( $4.2 \pm 0.1$  mW). Absolute FWM scattering efficiencies are calculated on the assumption that these gratings are pure phase gratings. This has been done to provide a crude first-order approach for correlating signal intensities with sample composition. Absolute FWM scattering efficiencies are tabulated by dividing the measured FWM scattering efficiency by the square of the effective interaction length ( $L_{\text{eff}}$ ) of the grating and the read-beam in the sample. Certain assumptions were used in deriving these figures, the first having been that NeHe read-beam (632.8 nm) absorption was assumed to be small. Secondly, reflection losses were not been taken into account. Thirdly, the HeNe probe (which was unpolarized) was in an approximate counter-propagating direction to one of the write-beams when, actually, the HeNe beam made an angle of about  $4.7^\circ$  with the surface normal. The write-beam crossing angle ( $\theta$ , not  $2\theta$ ) was  $3.9^\circ$ . Finally, the beam waist of the crossed argon write-beams at 465.8 nm was about 100 microns while the beam waist of the HeNe probe at the crossed write-beams is about 125 microns.

This would be an accurate comparison if the gratings were pure phase gratings produced by plane-wave write-beams. It should be emphasized that the quantitative analysis is a crude first-order attempt at comparing the data. More accurate comparisons should consider that: (i) both write-beams are strongly absorbed within the samples at 465 nm, (ii) the HeNe read-beam at 632.8 nm undergoes some absorption, causing its efficiency to differ between samples of different thickness, and, (iii), all measurements used laser beams with  $\text{TEM}_{00}$  spatial profiles, not plane-wave beams.

### ***The Effect of Rare-Earth Ion Concentration on Absolute FWM Scattering Efficiency.***

Increasing the rare earth ion content had the effect of increasing the absolute scattering efficiency. (See **Figure 15**). An apparent quadratic dependence (versus rare-earth ion content) was observed in the peak scattering efficiency. (See **Figure 16**). Praseodymium ( $\text{Pr}^{3+}$ ) doping was not observed to increase the absolute scattering efficiency, as

calculated for this report, over an equivalent doping level of europium ( $\text{Eu}^{3+}$ ):  $\eta/L_{\text{eff}}^2 = 1.76 \text{ cm}^{-2}$  for the base host doped with 2.5 mol%  $\text{Eu}_2\text{O}_3$ ; and  $\eta/L_{\text{eff}}^2 = 2.01 \text{ cm}^{-2}$  for the base host doped with 2.5 mol%  $\text{Pr}_2\text{O}_3$ . Gratings were not observed in the base host glasses doped with 0.1 and 0.5 mol%  $\text{Eu}_2\text{O}_3$ .

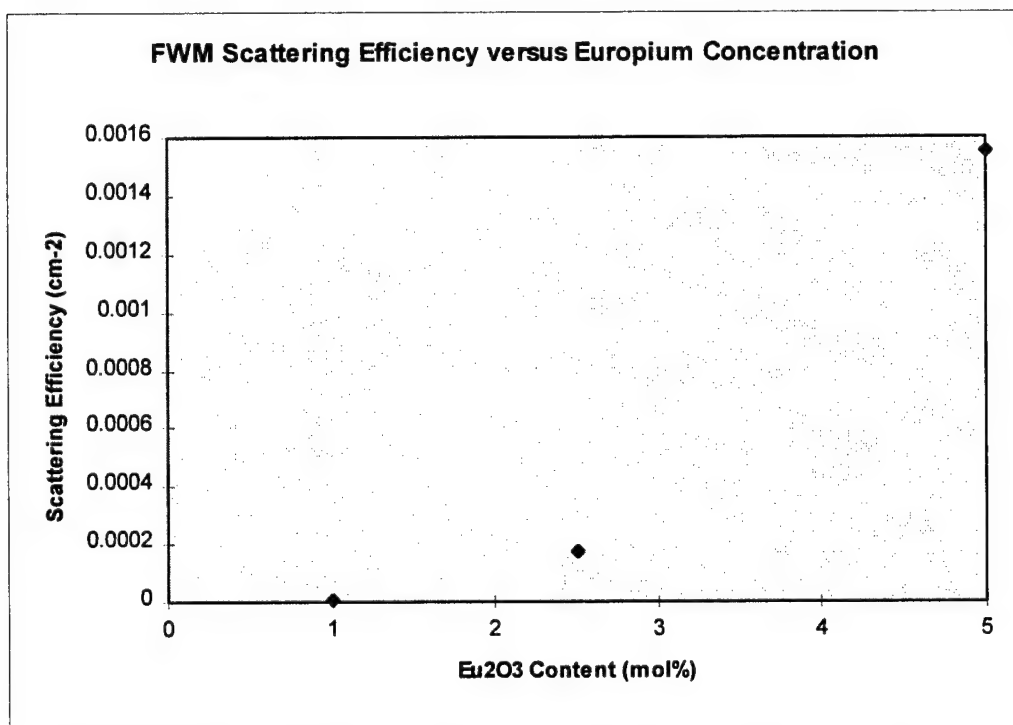


**Figure 15.** The effect of europium oxide doping concentration on absolute FWM scattering efficiency in the base host glass.

#### Absolute Scattering Efficiency Results

$\text{Eu}_2\text{O}_3$ (mol%)	$L_{\text{sample}}$ (mm)	$P_{\text{scattered}}$ (nW)	$P_{\text{input}}$ (mW)	$L_{\text{eff}}$ (mm)	$\eta/L_{\text{eff}}^2$ (cm <sup>-2</sup> )
1.0	4.00	4	4.2	4.00	$5.96 \times 10^{-6}$
2.5	4.20	130	4.2	4.20	$1.76 \times 10^{-4}$
5.0	6.15	2460	4.2	6.15	$1.55 \times 10^{-3}$

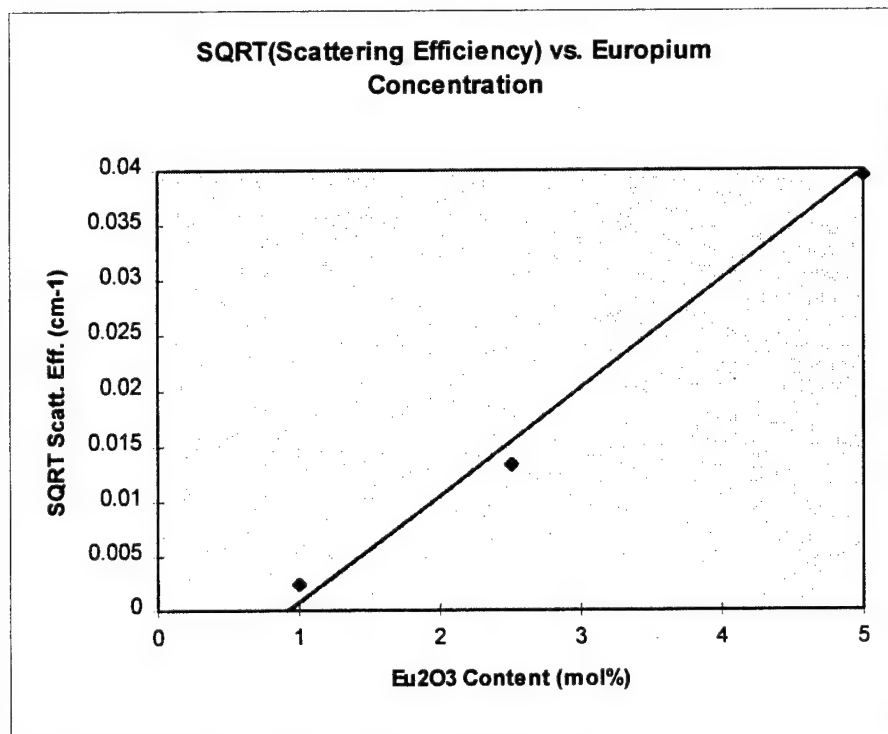


**Figure 16.** The apparent quadratic dependence in the absolute FWM scattering efficiency versus europium oxide concentration in the base host glass.

Some general relationships in the rates of grating formation, grating erasure, and grating stability that are expected to be important to interpreting the mechanism(s) underlying the process should be noted. In all studies using the base glass host composition doped with europium, prolonged writing led to a degradation in the grating's scattering efficiency. However, the rates at which these gratings formed and degraded was observed to be dependent upon the  $\text{Eu}_2\text{O}_3$  mol%. This is shown in **Figures 17** and **18**. **Figure 17** shows that gratings formed more quickly, degraded faster, and to a much greater degree in the sample doped with 5.0 mol%  $\text{Eu}_2\text{O}_3$  (Bragg-10), as compared to when the glass is doped with 2.5 mol%  $\text{Eu}_2\text{O}_3$  (Bragg-9). (See **Figure 18**).

Grating degradation appeared to proceed even when the write process was disrupted. **Figure 19** shows a sample doped with 5.0 mol%  $\text{Eu}_2\text{O}_3$  in which the write-beams are turned off and the grating is erased intermittently with write-beam exposures. Grating degradation proceeded towards a saturated value even after the specimen was allowed to "cool". This tendency towards reaching a degraded saturated scattering efficiency was not altered when the grating was erased. Re-establishing write conditions after an erasure caused the grating to move towards a state that produced roughly the same



saturated signal intensity (33-40% of peak signal) and at a rate that was roughly similar to the rate at which the signal decays during an uninterrupted write exposure.

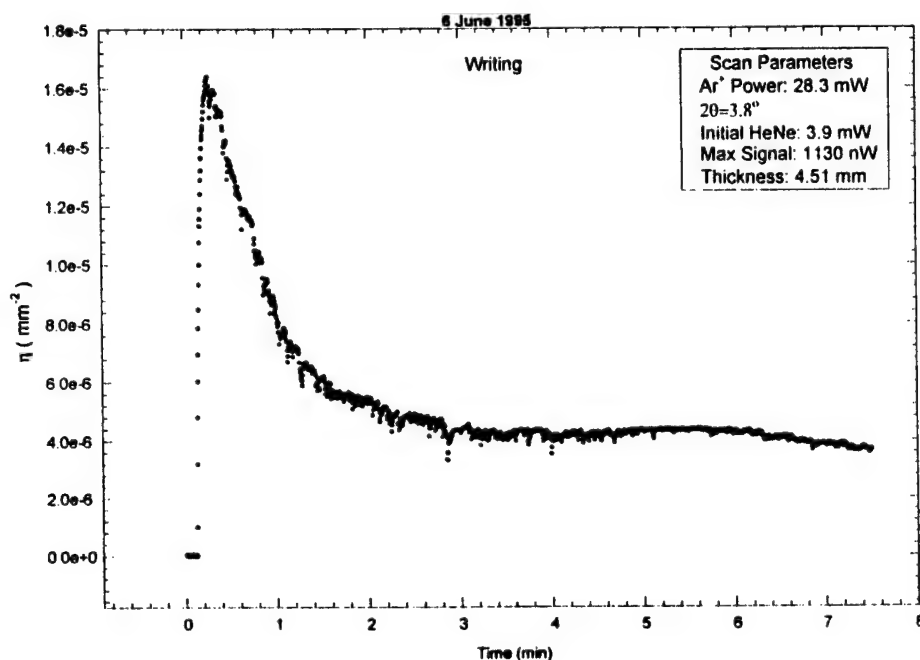


**Figure 17.** Temporal dependence in the grating signal intensity from a host glass doped with 5.0 mol%  $\text{Eu}_2\text{O}_3$  during an uninterrupted write-beam exposure.

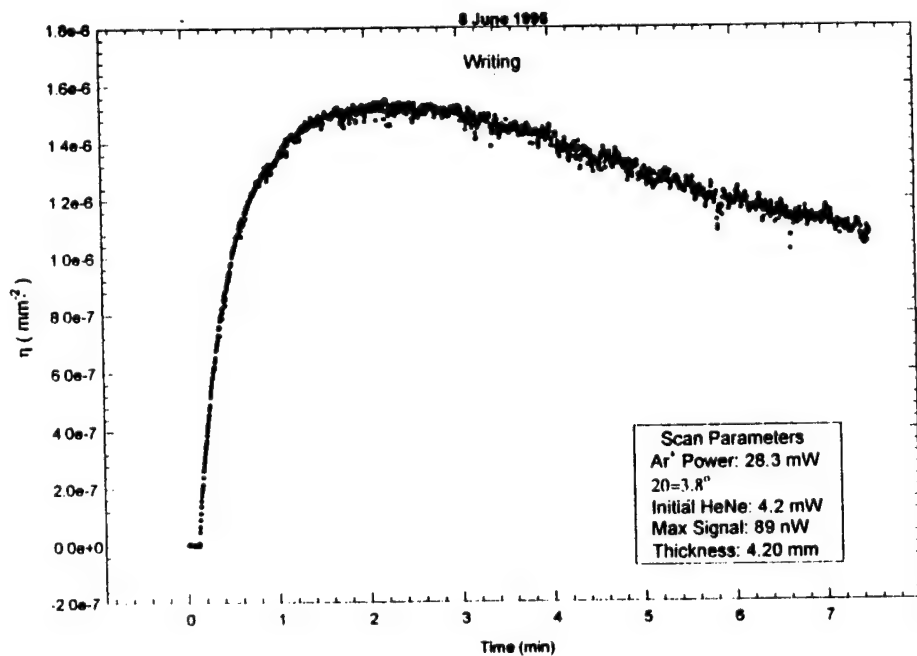


**Figure 18.** Temporal dependence in the grating signal intensity from a host glass doped with 2.5 mol%  $\text{Eu}_2\text{O}_3$  during an uninterrupted write-beam exposure.

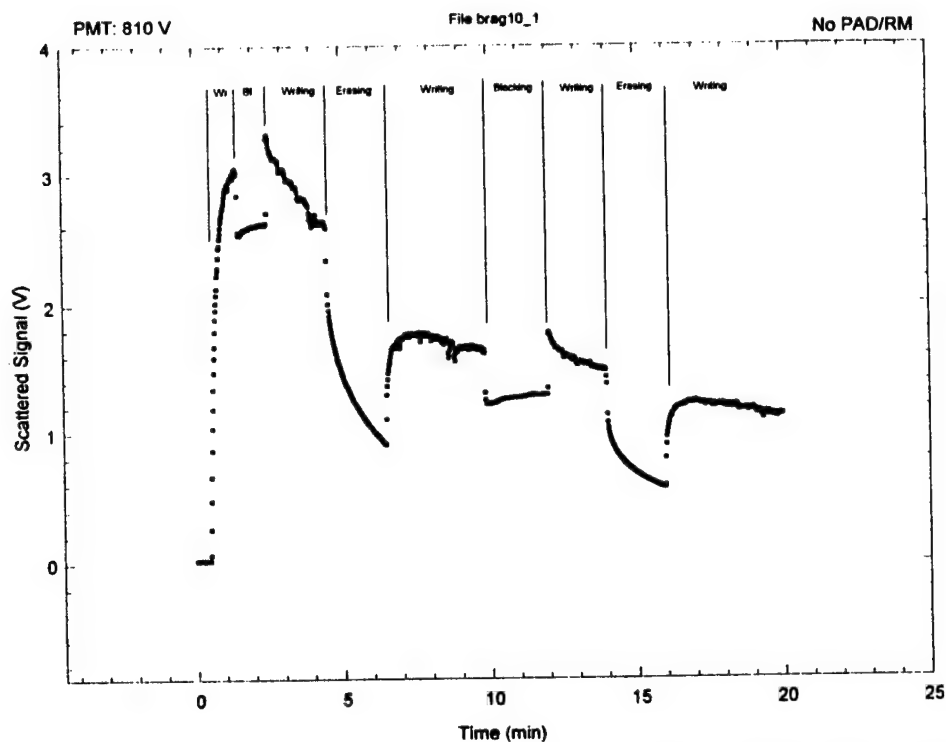


**Figure 19.** Temporal dependence in the grating signal intensity from a host glass doped with 5.0 mol%  $\text{Eu}_2\text{O}_3$  during interrupted write-beam exposures.

Samples doped with 2.5 mol%  $\text{Pr}_2\text{O}_3$  displayed much different temporal characteristics. Gratings in these samples were slower to form and degrade. (See **Figure 20**).

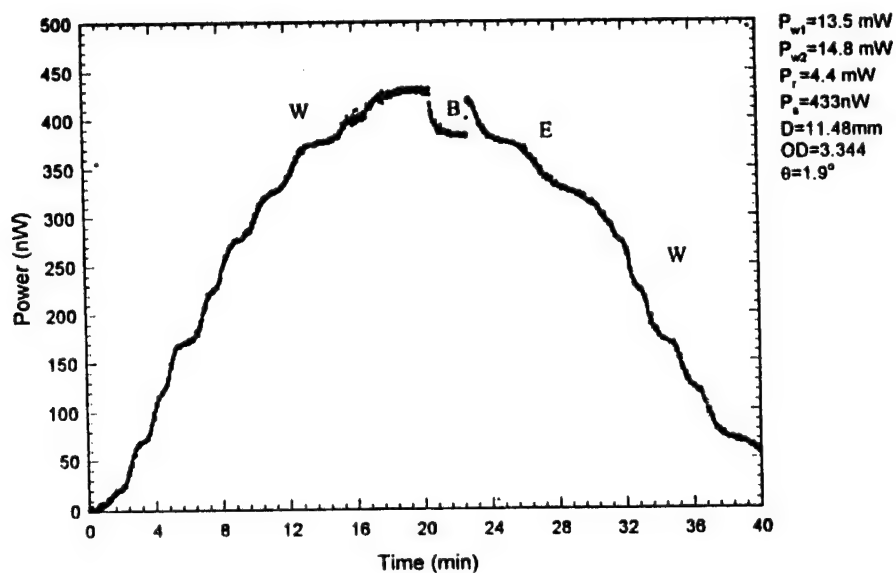


**Figure 20.** Temporal dependence in the grating signal intensity from a host glass doped with 2.5 mol%  $\text{Pr}_2\text{O}_3$  during interrupted write-beam exposures.

## The Effect Alkali Substitution on FWM Scattering Efficiencies

The effect of alkali substitution on FWM scattering efficiencies was evaluated by preparing mixed-alkali glasses and substituting 50% of the sodium oxide ( $\text{Na}_2\text{O}$ ) in the base host composition with lithium oxide ( $\text{Li}_2\text{O}$ ) and potassium oxide ( $\text{K}_2\text{O}$ ). These alkali-modified glasses were subsequently doped with 2.5 mol%  $\text{Eu}_2\text{O}_3$ .

Mixed-alkali glasses produced gratings with lower peak scattering efficiencies. The rates at which these gratings formed and degraded accelerated dramatically over the sodium-only composition doped with 2.5 mol%  $\text{Eu}_2\text{O}_3$ . (See **Figures 21** and **22**, note time scale in comparing **Figure 18** with **Figure 21**). The rate differences may be attributed to the fact that mixed-alkali glasses are reported to have faster ionic conductivities than single alkali glasses.

### Absolute Scattering Efficiency Results

Alkali Substitute	$L_{\text{sample}}$ (mm)	$P_{\text{scattered}}$ (nW)	$P_{\text{input}}$ (mW)	$L_{\text{eff}}$ (mm)	$\eta/L_{\text{eff}}^2 (\text{cm}^{-2})$
None	4.20	130	4.2	4.2	$1.76 \times 10^{-4}$
Li	6.15	114	4.0	9.30	$3.30 \times 10^{-5}$
K	9.60	43	4.4	4.85	$4.16 \times 10^{-5}$

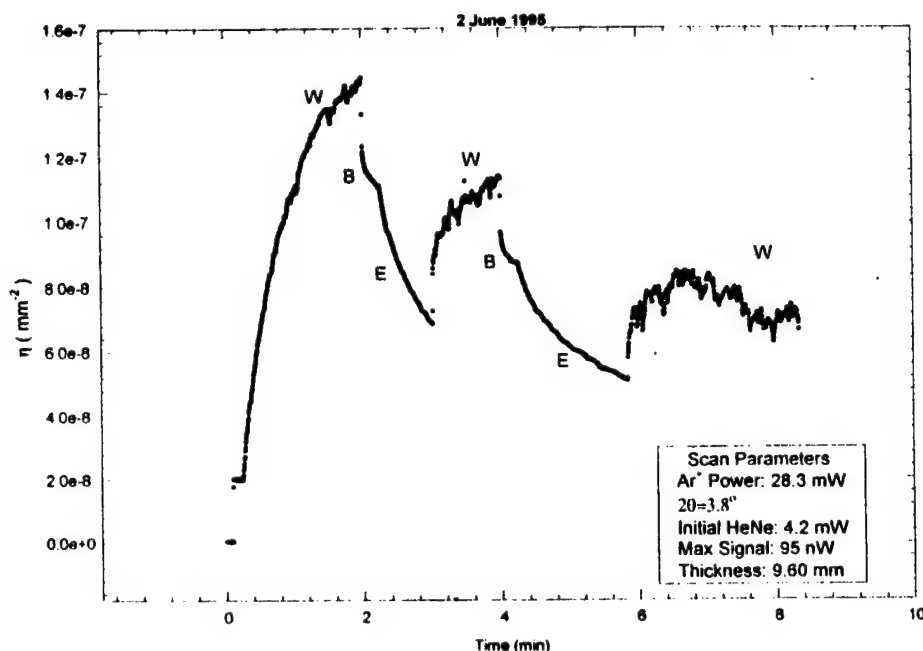


**Figure 21.** Temporal dependence in the grating signal intensity from a mixed-alkali (50%  $\text{K}^+$ , 50%  $\text{Na}^+$ ) host glass doped with 2.5 mol%  $\text{Eu}_2\text{O}_3$  during uninterrupted write-beam exposure.

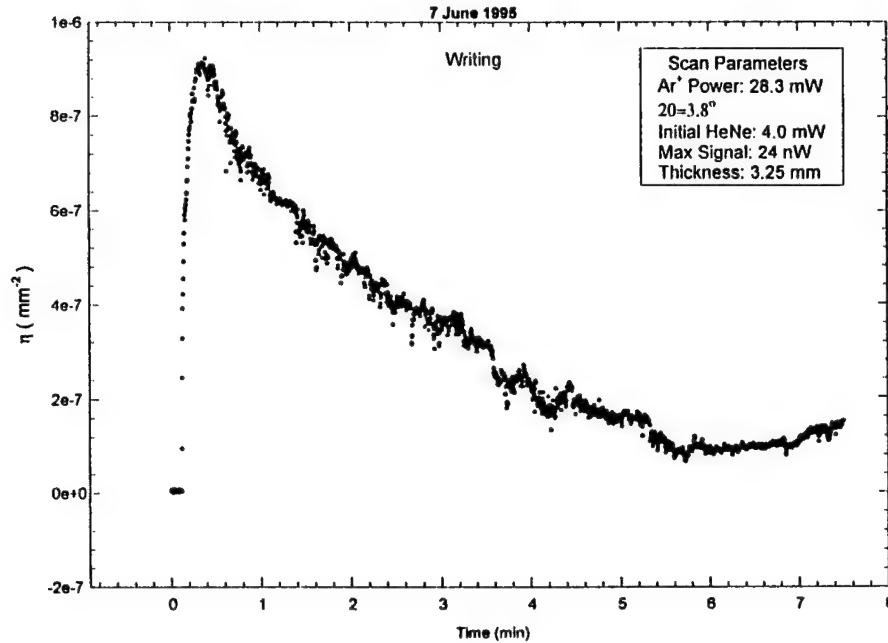


**Figure 22.** Temporal dependence in the grating signal intensity from a mixed-alkali (50%  $\text{Li}^+$ , 50%  $\text{Na}^+$ ) host glass doped with 2.5 mol%  $\text{Eu}_2\text{O}_3$  during interrupted write-beam exposures.

### *The Effect of Alkaline Earth Substitution on FWM Scattering Efficiencies*

No specific correlation between absolute FWM scattering efficiencies and the average alkaline earth mass could be identified. It can be generally stated that the absolute FWM scattering efficiency increased when heavier alkaline earth modifiers were substituted in small (10 mol%) concentrations for magnesium oxide (MgO). FWM scattering efficiencies decreased by an order of magnitude when larger substitutions (50 mol%) of heavier alkaline earth elements were made for MgO.

### **Absolute Scattering Efficiency Results**

AE Substitute	$L_{\text{sample}}$ (mm)	$P_{\text{scattered}}$ (nW)	$P_{\text{input}}$ (mW)	$L_{\text{eff}}$ (mm)	$\eta/L_{\text{eff}}^2 (\text{cm}^{-2})$
None	4.20	130	4.2	4.2	$1.76 \times 10^{-4}$
Ca (10%)	4.15	202	4.5	4.15	$2.61 \times 10^{-4}$
Ca(50%)	6.52	44	4.2	6.52	$2.47 \times 10^{-5}$
Sr(10%)	7.24	210	4.3	7.24	$9.32 \times 10^{-4}$
Sr(50%)	3.84	27	4.4	3.84	$4.16 \times 10^{-5}$
Ba(10%)	5.17	304	4.6	5.17	$2.47 \times 10^{-4}$

The temporal characteristics of the FWM scattering efficiencies in alkaline earth-modified glasses were also observed to change. The rates at which these gratings formed and degraded were much slower when larger concentrations (50 mol% as opposed to 10 mol%) of heavier alkaline earth-modifiers were incorporated in the glass. (Compare **Figure 23** to **Figure 24**). The rates at which gratings formed and degraded were equivalent, irrespective of alkaline earth mass, when heavier alkaline earth-modifiers were incorporated in similar concentrations. . (Compare **Figure 23** to **Figure 25**). Signals scattered from saturated gratings appeared to be far more stable in all of the mixed alkaline earth glasses. . (Compare **Figures 23-25** to **Figures 17 to 22**).

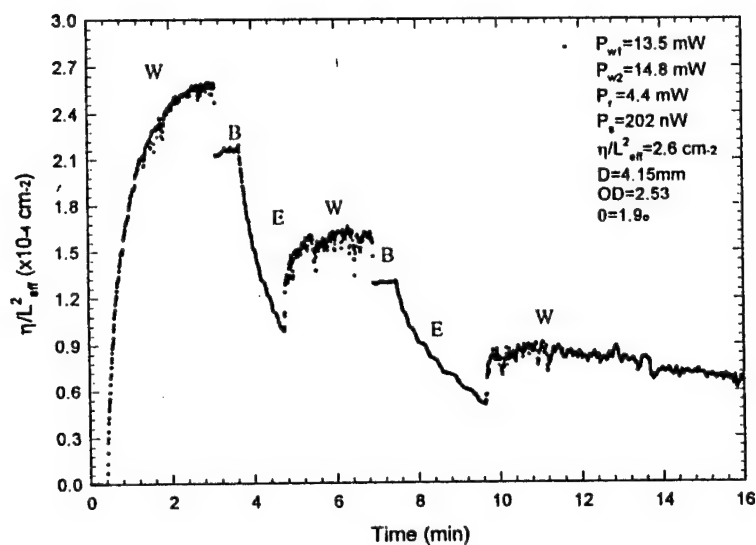


**Figure 23.** Temporal dependence in the grating signal intensity from a mixed-alkaline earth (10%  $\text{Ca}^{2+}$ , 90%  $\text{Mg}^{2+}$ ) host glass doped with 2.5 mol%  $\text{Eu}_2\text{O}_3$  during interrupted write-beam exposures.

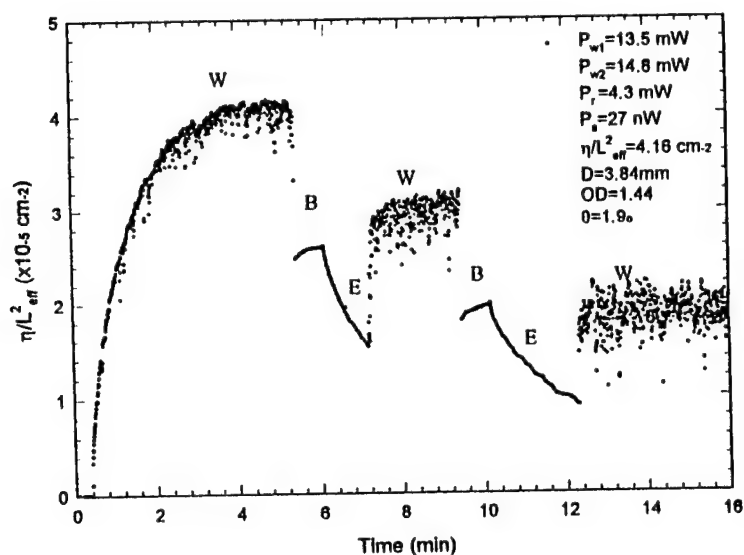


**Figure 24.** Temporal dependence in the grating signal intensity from a mixed-alkaline earth (50%  $\text{Sr}^{2+}$ , 50%  $\text{Mg}^{2+}$ ) host glass doped with 2.5 mol%  $\text{Eu}_2\text{O}_3$  during interrupted write-beam exposures.

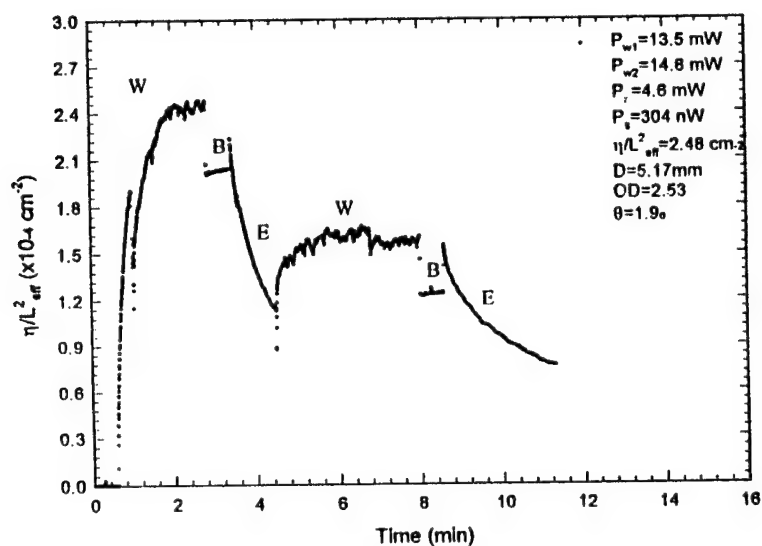


**Figure 25.** Temporal dependence in the grating signal intensity from a mixed-alkaline earth (10%  $\text{Ba}^{2+}$ , 90%  $\text{Mg}^{2+}$ ) host glass doped with 2.5 mol%  $\text{Eu}_2\text{O}_3$  during interrupted write-beam exposures.

### *The Effect of Silica-Enrichment on FWM Scattering Efficiencies*

FWM scattering efficiencies were observed to increase when the network was enriched with silica ( $\text{SiO}_2$ ). (See **Figure 26**). Measurements were made with the base host composition enriched with 2.5 and 5.0 mol%  $\text{SiO}_2$ . The silica-enriched compositions were then doped with 2.5 mol%  $\text{Eu}_2\text{O}_3$ . Although only a limited set of data was collected, a stronger correlation was obtained when the data was analyzed using a linear regression and a quadratic dependence in the absolute FWM scattering efficiency versus silica doping. (See **Figure 27**).

#### **Absolute Scattering Efficiency Results**

$\text{SiO}_2$ Doping	$L_{\text{sample}}(\text{mm})$	$P_{\text{scattered}}(\text{nW})$	$P_{\text{input}}(\text{mW})$	$L_{\text{eff}}(\text{mm})$	$\eta/L^2_{\text{eff}}(\text{cm}^{-2})$
None	4.20	130	4.2	4.2	$1.76 \times 10^{-4}$
2.5 mol%	4.26	240	4.0	4.26	$3.31 \times 10^{-4}$
5.0 mol%	4.68	589	4.5	4.68	$6.00 \times 10^{-4}$

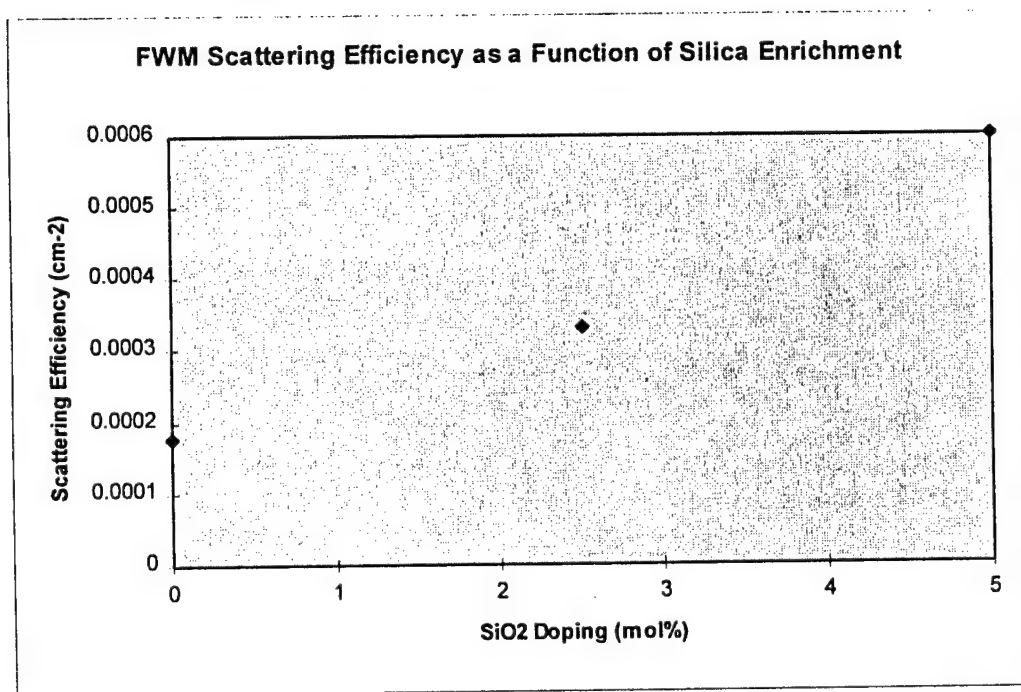


**Figure 26.** Variations in absolute FWM scattering efficiency measured versus silica doping in the base host composition.

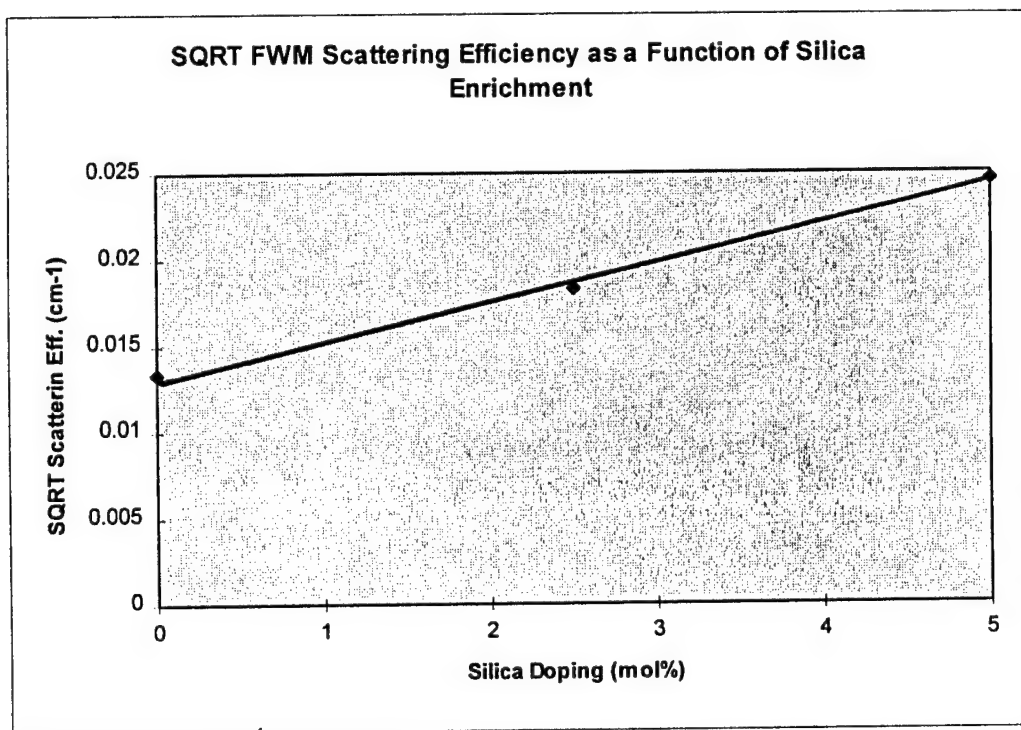


**Figure 27.** Linear regression of the square root of the absolute FWM scattering efficiency versus silica enrichment of the host compositions.

The rates of grating formation and degradation in the silica-enriched compositions was observed to be greater than in the base host under constant "on" write conditions, even though gratings in both systems were observed to decay to  $73\% \pm 1.5\%$  of their peak scattering efficiency after identical write-beam exposures. (Compare **Figure 28** to **Figure 18**).

Saturated grating signals appeared to stabilize under constant write-beam "on" conditions after multiple write/erase cycles in the silica-enriched samples (See **Figure 29** and compare to **Figures 19, 23, and 25**).



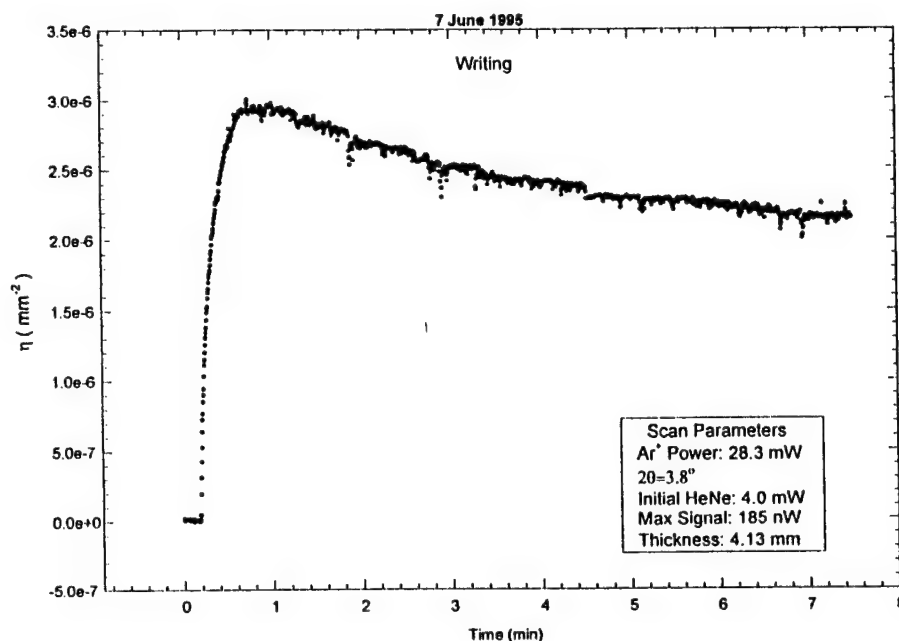


**Figure 28.** Temporal dependence in the grating signal intensity in a base host enriched with 2.5 mol% silica and doped with 2.5 mol%  $\text{Eu}_2\text{O}_3$  during uninterrupted write-beam exposure.

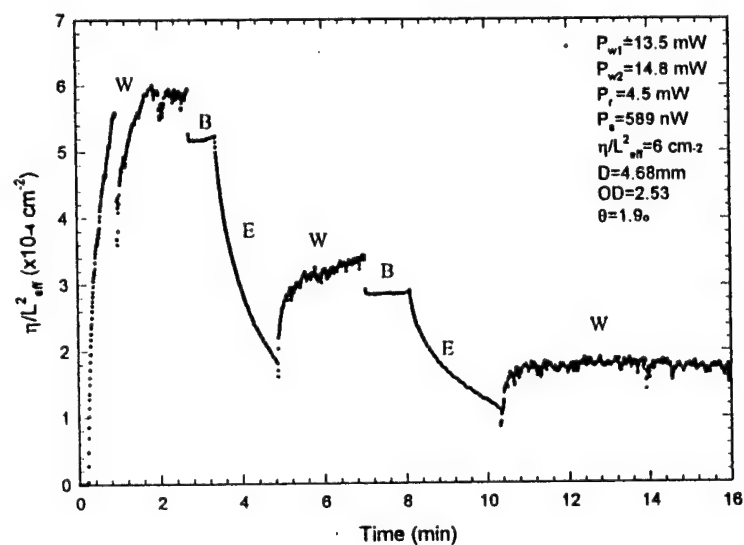


**Figure 29.** Temporal dependence in the grating signal intensity from a base host composition enriched with 5.0 mol% silica and doped with 2.5 mol%  $\text{Eu}_2\text{O}_3$  during cycled write/block/erase exposures.

### *The Effect of Soda-(Alkali)-Enrichment on FWM Scattering Efficiency*

FWM scattering efficiencies were observed to decrease when the base host network was enriched with soda ( $\text{Na}_2\text{O}$ ). (See **Figure 30**). It is believed that similar effects would be observed in lithia-enriched ( $\text{Li}_2\text{O}$ ) and potassia-enriched ( $\text{K}_2\text{O}$ ) in networks that contain only lithium oxide or potassium oxide, respectively, as the alkali-modifier. Measurements were made by enriching the base host glass with 5.0 and 10.0 mol%  $\text{Na}_2\text{O}$ . The soda-enriched host compositions were then doped with 2.5 mol%  $\text{Eu}_2\text{O}_3$ . No functional dependence in the FWM scattering efficiency with respect to soda-enrichment could be determined.

#### **Absolute Scattering Efficiency Results**

$\text{Na}_2\text{O}$ Doping	$L_{\text{sample}}$ (mm)	$P_{\text{scattered}}$ (nW)	$P_{\text{input}}$ (mW)	$L_{\text{eff}}$ (mm)	$\eta/L_{\text{eff}}^2 (\text{cm}^{-2})$
None	4.20	130	4.2	4.2	$1.76 \times 10^{-4}$
5.0 mol%	5.47	192	4.7	5.47	$1.37 \times 10^{-4}$
10.0 mol%	4.52	53	4.4	4.52	$5.90 \times 10^{-5}$

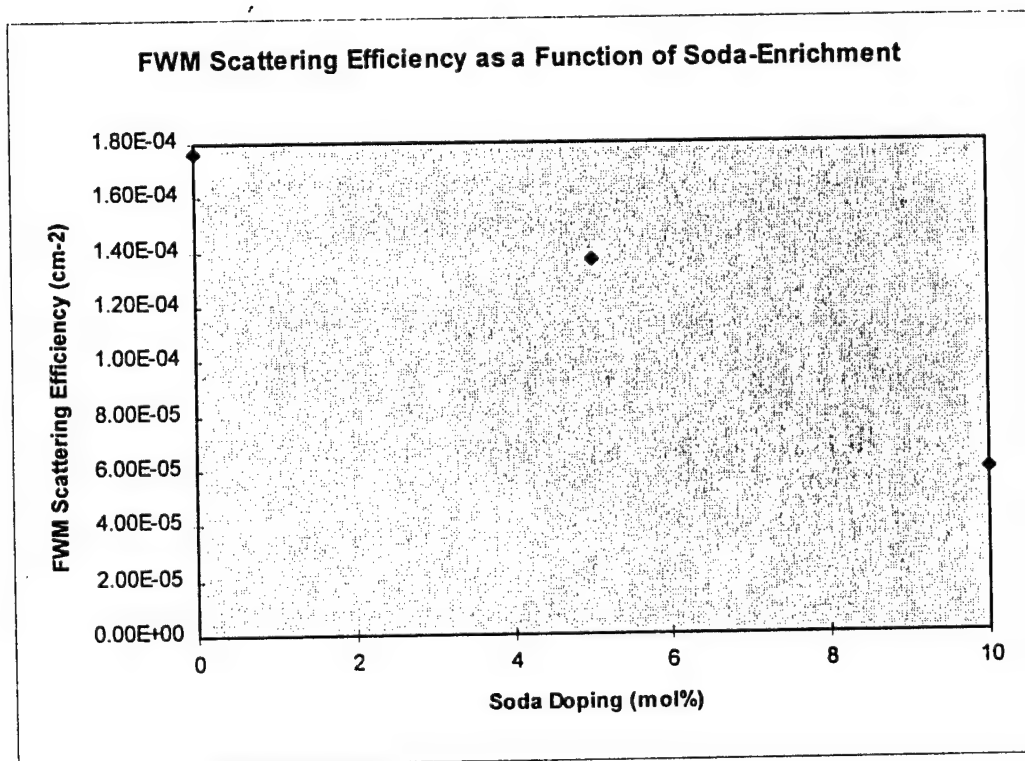


**Figure 30.** Variations in absolute FWM scattering efficiency measured versus soda doping in the base host composition.

The rates of grating formation and grating erasure were observed to decrease with soda enrichment. The grating's ability to recover to a previous saturated grating intensity after write/erase cycling was also reduced by soda enrichment. (See **Figures 31** and **32**).

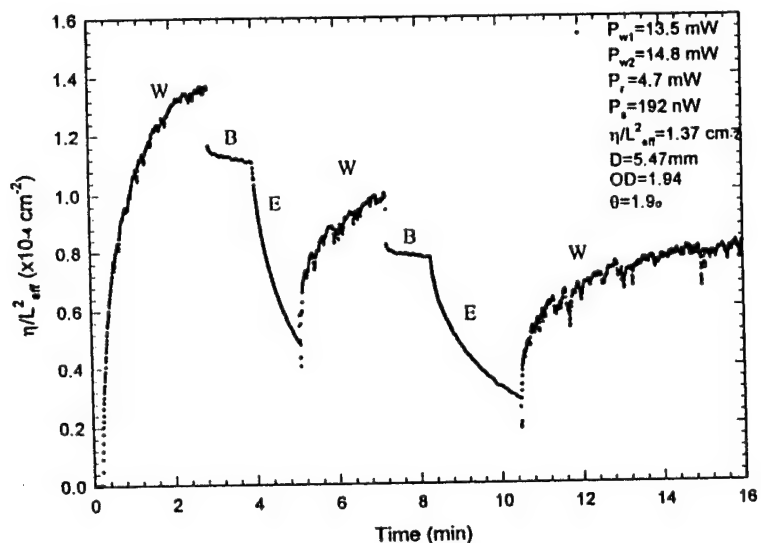


**Figure 31.** Temporal dependence in the grating signal intensity from a base host composition enriched with 5.0 mol% soda and doped with 2.5 mol%  $\text{Eu}_2\text{O}_3$  during cycled write/block/erase exposures.

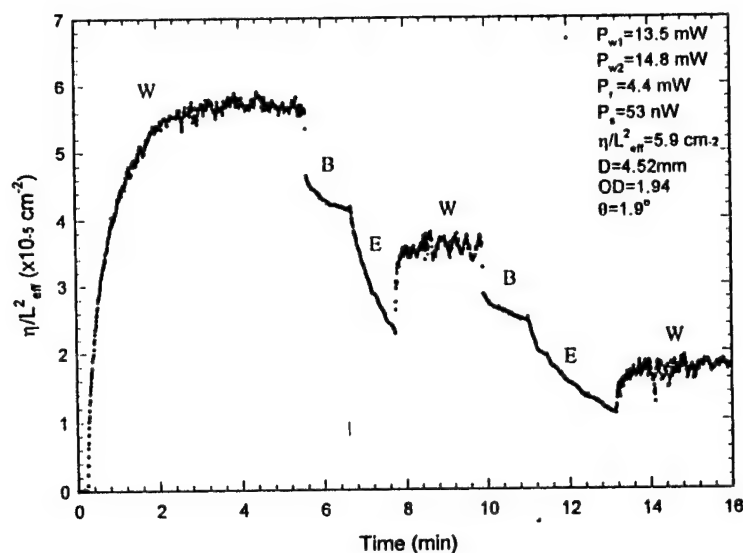


**Figure 32.** Temporal dependence in the grating signal intensity from a base host composition enriched with 10.0 mol% soda and doped with 2.5 mol%  $\text{Eu}_2\text{O}_3$  during cycled write/block/erase exposures.

### ***The Effect of Transition-metal Doping on FWM Scattering Efficiencies***

Only a weak signal could be observed after prolonged write times in bulk samples of the base host composition modified with 0.25 mol%  $\text{V}_2\text{O}_3$  and 0.25 mol%  $\text{V}_2\text{O}_5$ , each subsequently doped with 5.0 mol%  $\text{Eu}_2\text{O}_3$ . Due to the strong absorption at write-beam and read-beam wavelengths in the glass, the crude first-order approximation (based on a pure phase gratings constructed from plane-waves used to calculate scattering efficiencies) could not applied to these results. In order to truly ascertain FWM scattering efficiencies in these compositions, they should be evaluated using thin film specimens rather than bulk samples in order to reduce the interference of the strong transition-metal ion absorption and both write and read wavelengths.

### ***The Effect of Write-Beam Power and Crossing Angle on FWM Scattering Efficiency***

The base host glass enriched with 5.0 mol% silica and doped with 2.5 mol%  $\text{Eu}_2\text{O}_3$  produced gratings with the strongest FWM signals. Interference pattern power-dependencies were evaluated in this sample by altering write-beam power at a series of fixed write-beam crossing angles and then monitoring the relative rates of grating formation and grating erasure. Rates of grating formation and erasure were evaluated using to-

tal write-beam power settings of 8, 18, 28, 44, and 60 mW, at crossing angles (reported as  $\theta$  not  $2\theta$ ) of  $1.9^\circ$ ,  $2.5^\circ$ , and  $3.25^\circ$ . The rates of grating formation and erasure was observed to increase with write-beam power and decrease with the crossing angle. **Figures 33 and 34** show the relative decay in the grating signals at crossing angles of  $3.25^\circ$  and  $1.9^\circ$ , respectively, for different erase powers. **Figure 35** shows the relative decay in the grating signals for the different crossing angles at an erase-beam power of 28 mW.

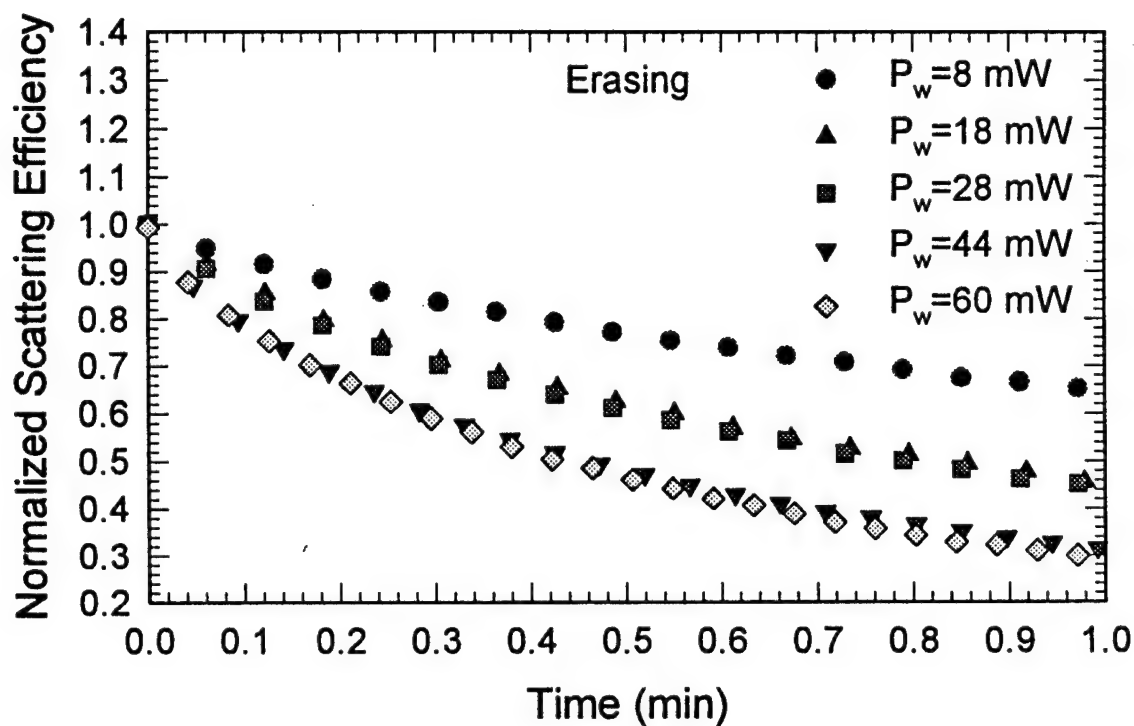


**Figure 33.** Temporal dependence in the grating signal formed with write-beams at a crossing angle of  $3.25^\circ$  in a base host composition enriched with 5.0 mol% silica and doped with 2.5 mol%  $\text{Eu}_2\text{O}_3$  as it is erased by a write-beams with powers of 8, 18, 28, 44, and 60 mW.

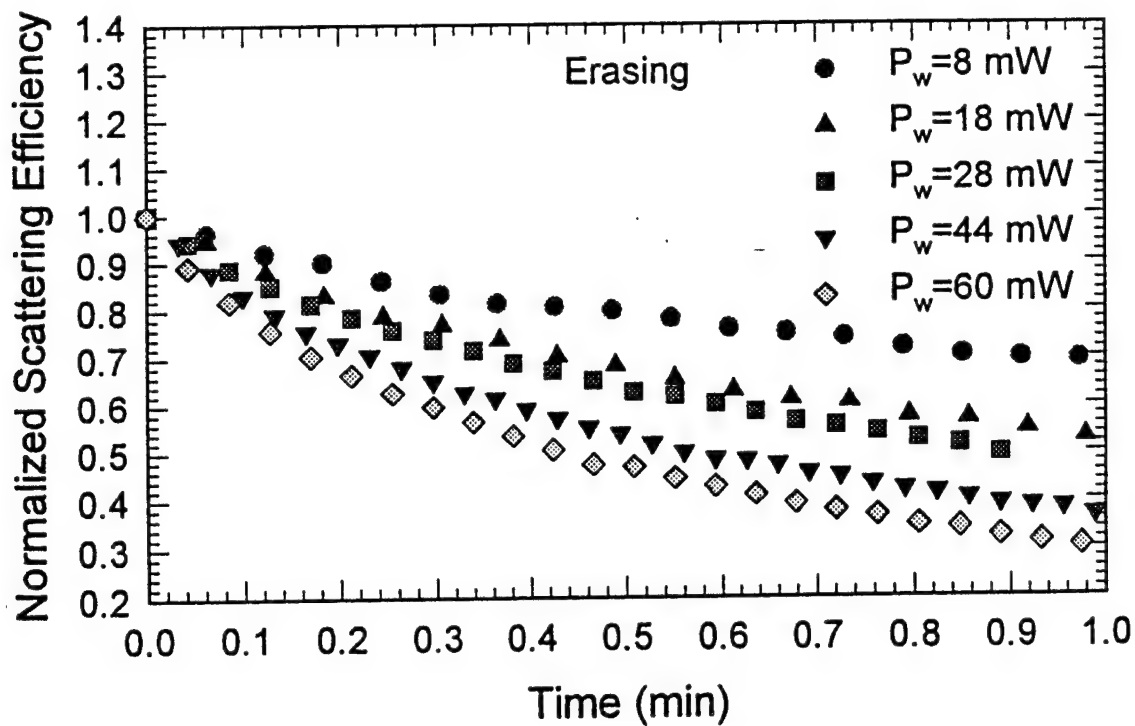


**Figure 34.** Temporal dependence in the grating signal formed with write-beams at a crossing angle of  $1.9^\circ$  in a base host composition enriched with 5.0 mol% silica and doped with 2.5 mol%  $\text{Eu}_2\text{O}_3$  as it is erased by a write-beams with powers of 8, 18, 28, 44, and 60 mW.

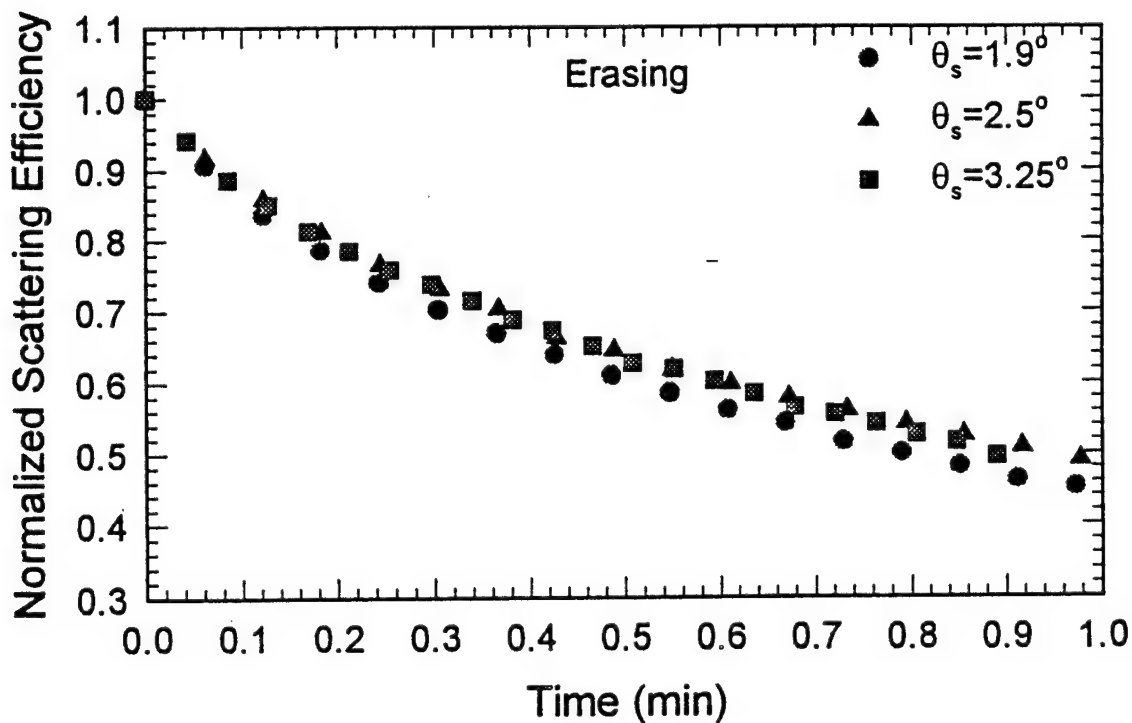


**Figure 35.** Temporal dependence in the grating signal formed with write-beams at crossing angles of  $1.9^\circ$ ,  $2.5^\circ$ , and  $3.25^\circ$  in a base host composition enriched with 5.0 mol% silica and doped with 2.5 mol%  $\text{Eu}_2\text{O}_3$  as it is erased by a 28 mW write-beam.

### *The Transient Decay of FWM Scattering Efficiency in $\text{Eu}_2\text{O}_3$ -doped Glass*

All grating signals appeared to undergo a transient decay immediately after the write-beams were turned off. The magnitude of this transient decay was found to vary from sample to sample and may be due to hyperpolarized ligands in the immediate vicinity of a fluorescing rare-earth ion. As shown in **Figure 36**, the measured transient decay time, 2.2 ms, was found to be independent of write-beam power in these samples.

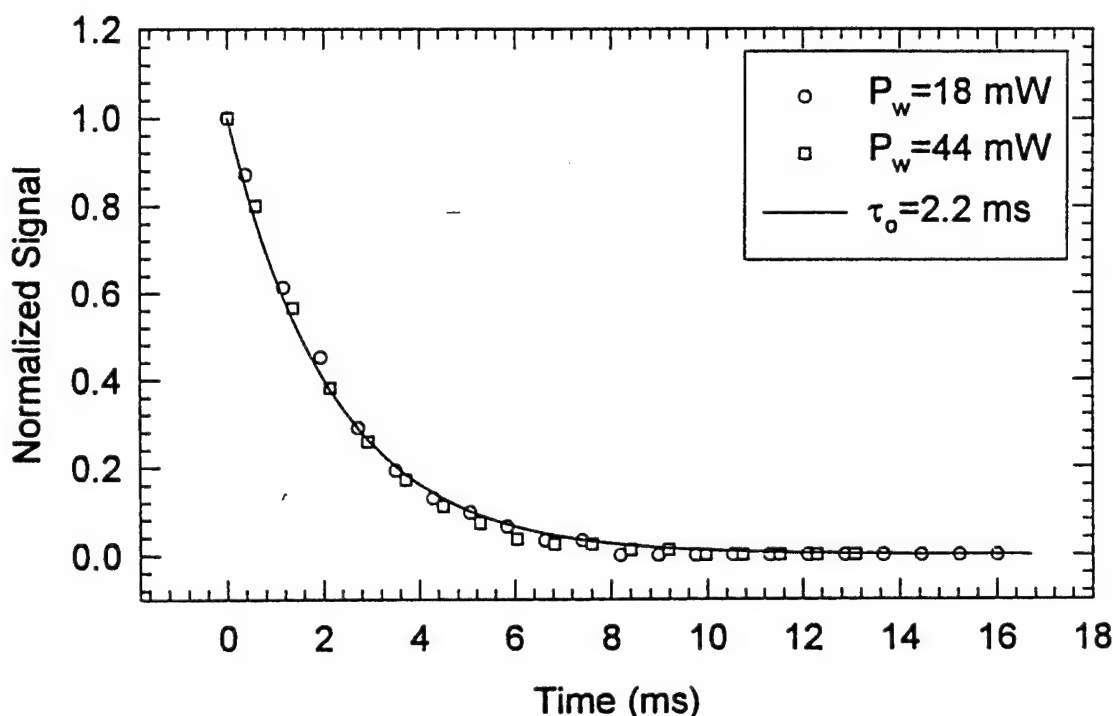


**Figure 36.** Decay in the transient grating signal observed immediately after both write-beams are turned off in a grating formed in a base host composition enriched with 5.0 mol% silica and doped with 2.5 mol%  $\text{Eu}_2\text{O}_3$  using write-beams with powers of 18 and 44 mW.

### **Three-Wave Mixing Measurements**

Three-wave mixing measurements in rare earth-doped glasses required an argon laser to write the grating and the 1.06 micron line of a  $\text{Nd}^{3+}$ :YAG laser to probe the grating. Unfortunately, the start of the Phase II program was delayed by nearly one year due to government budget problems. As a result of this setback, laboratory resource allocations at the Oklahoma State University, Center for Laser Research, Stillwater, OK, were changed and contract collaborators at the Laser Center lost access to a laboratory configuration that would have allowed a  $\text{Nd}^{3+}$ :YAG laser to be placed in an optical table adjacent to the optical table supporting the argon laser. Measurements were attempted by recording the grating with the argon laser and then physically moving the sample to another

laboratory in which the sample could be probed by the YAG laser. Unfortunately, second harmonic generation (SHG) measurements require very stable and precise alignments between the write-beam and probe-beam optics, so phase-matching conditions could not be established in this manner.

### Raman Scattering Measurements

Raman scattering measurements were conducted on all glass samples to determine the density of states profile  $\rho(\omega)$  of localized phonons in the glass network. These measurements were made using off-resonant (514.5 nm) and nearly-resonant (457.9 nm and 472.7 nm) probes  $\text{Eu}_2\text{O}_3$ -doped glasses. An off-resonant probe of 488.0 nm and a resonant probe of 465.8 nm was also used on  $\text{Pr}_2\text{O}_3$ -doped glasses.

It is now well characterized that gratings in rare-earth doped glasses, and probably all glasses, are formed when the energy from an interfering optical pump beam stimulates optical phonons whose populations are distributed in phase with the interference pattern. This is observed in rare-earth doped glasses, since gratings only form when the write-beams populate excited states of the rare-earth ion that decay strongly through a non-radiative branch. Pumping excited states that decay predominantly through a radiative transition will not record a grating. Gratings are also observed in non-rare-earth doped optical fiber by directly pumping ultraviolet absorption bands, or by using a multi-photon pump. Photo-dissociation of a silicon-germanium oxygen-vacancy defect bond or a phosphorous double-bond, both which produce uv-absorption bands at 244 nm, will stimulate intense optical phonon populations.

Grating  $\chi^{(3)}$  and  $\chi^{(3)}$  properties show that a state-defining charge carrier, an electron in the case of pure silica glass, an alkali ion in the case of alkali-modified glasses, is displaced from regions of constructive write-beam optical interference to regions of destructive optical interference. The notion of electron conduction bands is inappropriate for glass. Electrons will travel with ballistic energy in glass when photo-ionized by sufficiently high energy radiation, or will migrate as small polarons, electrons dressed by phonons. It is well known that phonon interactions are responsible for alkali-ion diffusion and migration in glass.

This phenomenology is consistent with the grating process. In regions of constructive write-beam interference, where stimulated optical phonon densities are high, isotropic charge carrier migration and diffusion will be highly activated. In regions of destructive write-beam interference and low optical phonon populations, charge carrier migration and diffusion will be less active. Under these non-equilibrium conditions, charge carriers will migrate out of the more highly activated regions and collect in the less activated regions. As is shown in the linear optical spectra, increasing the content of alkali



ions will alter optical properties. Regions in the glass that have become alkali-rich will have ultraviolet absorption that is shifted to longer wavelengths. These absorption shifts will locally alter dispersion.

Given these considerations, it is of paramount importance to engineer a glass in which phonon energy can activate the migration of a charge carrier across distances great enough to allow it to diffuse out of a region of constructive interference and into a region of destructive interference. Glass is a highly disordered medium (vibrational resonances are highly localized and plane-wave phonons cannot properly exist). To displace charge a significant distances, it becomes necessary to propagate the energy of localized phonons. Localized phonons do not propagate, but under the thermally activated hopping (TAH) model, the energy of a localized phonon at one site (the donor mode) may be passed onto a localized mode at another site (the acceptor mode). Because extended-range phonons have access to the entire sample, they are the most likely candidates for the low-frequency phonons that are emitted and absorbed in the energy transfer between localized donor and acceptor phonons.

Extended-range phonons are likely to facilitate the energy "hopping" between localized donor and acceptor modes, since very few neighboring localized modes are likely to have exactly the same frequency. However, it does become necessary for localized modes at stimulated  $\text{Eu}^{3+}$ -sites to have frequencies similar to the "lattice" localized modes not located at  $\text{Eu}^{3+}$ -sites.

Resonant Raman spectroscopy (using probes at 465.8 nm for  $\text{Eu}^{3+}$ -doped specimens, and 465.8 and 488 nm for  $\text{Pr}^{3+}$ -doped specimens), and nearly-resonant Raman spectroscopy (using probes of 472.7 and 457.9 nm on  $\text{Eu}^{3+}$ -doped specimens) were used to measure the density-of-states profiles  $\mathcal{D}_{\text{RE}}(\omega)$  of localized modes in the immediate environment of a rare-earth ion that was optically stimulated to an excited state by a write-beam. Off-resonant Raman spectroscopy (using a 514.5 nm probe) was used to measure  $\mathcal{D}_{\text{lattice}}(\omega)$ , the density-of-states profile of localized "lattice" modes not found in the immediate environment of the rare-earth ions.

The significance of measuring frequency-coupling between lattice-localized modes and modes localized around {write-beam stimulated rare-earth ions} is shown in the Phase I results. These results distinguished between suitable host glass compositions and glass host compositions in which gratings could be easily recorded. **Figure 38** compares the  $\mathcal{D}_{\text{lattice}}(\omega)$  with  $\mathcal{D}_{\text{RE}}(\omega)$  in a phosphate glass in which gratings could not be recorded. It clearly shows that the write process generates localized modes at stimulated rare-earth ion sites with a frequency distribution that only minimally overlaps the frequency distribution of localized modes that will be "carried" by the lattice. **Figure 39** shows that there is near-"perfect" overlap in the localized-mode frequencies stimulated at  $\text{Eu}^{3+}$ -sites during

the write process with the frequencies of localized modes that can be carried by the lattice.

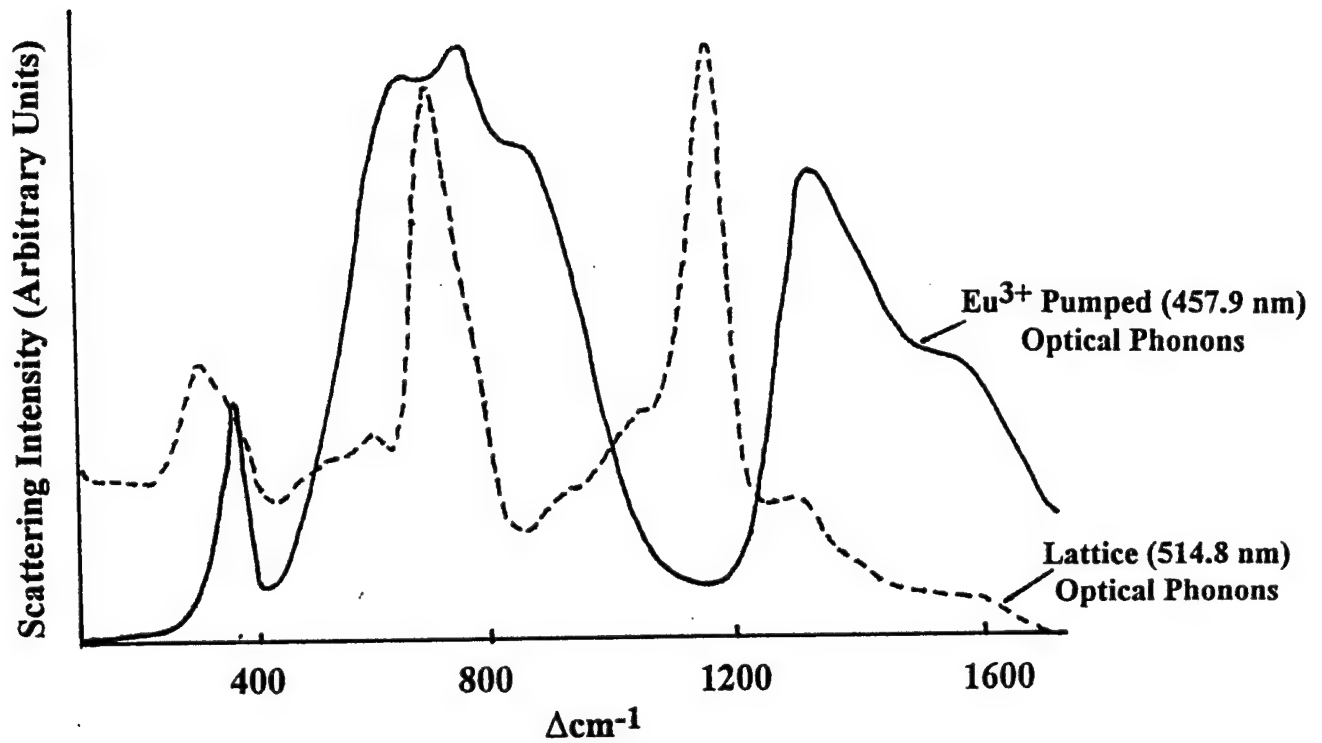


**Figure 38.** Distribution profiles of lattice localized-mode phonons and modes localized at a write-beam-excited Eu<sup>3+</sup>-sites in a phosphate glass that did not produce gratings.

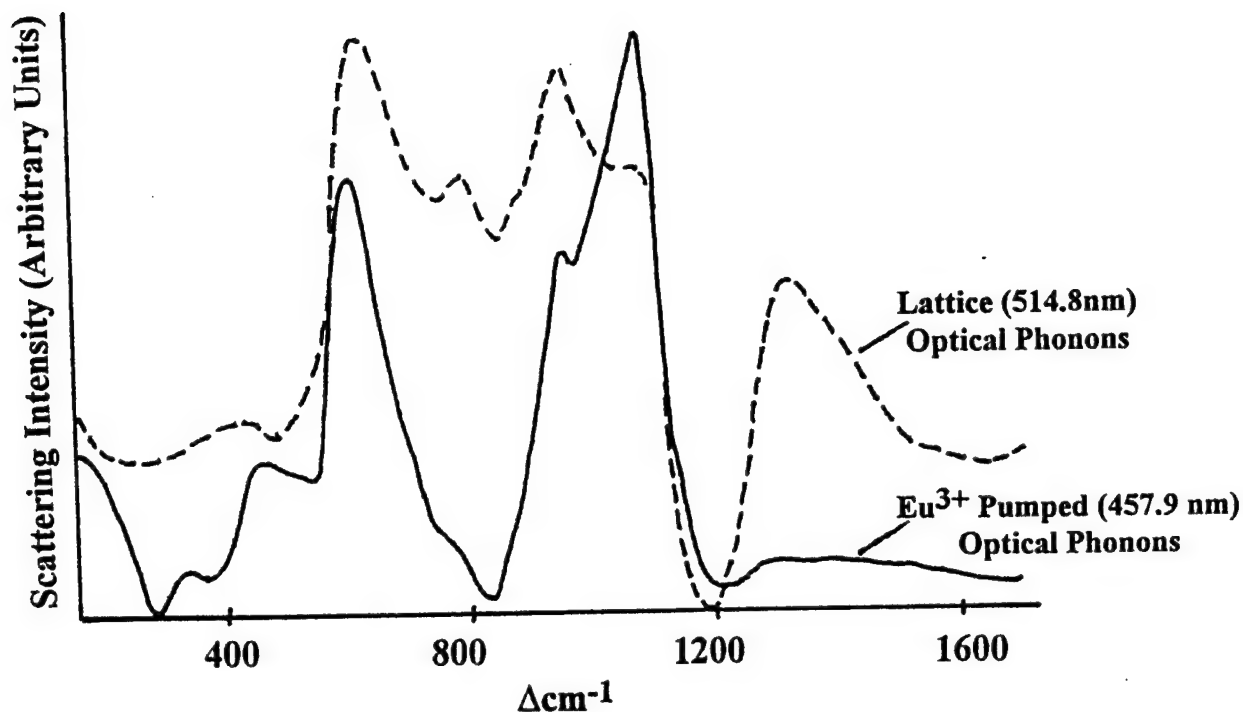


**Figure 39.** Distribution profiles of lattice localized-mode phonons and modes localized at write-beam-excited  $\text{Eu}^{3+}$ -sites in the base host glass composition that easily produced gratings.

### *The Effect of Rare-Earth Ion Doping on Raman Spectra*

**Figure 40** shows the changes in the distribution profiles of lattice-localized modes when europium oxide ( $\text{Eu}_2\text{O}_3$ ) was added to the base host network. An interesting observation of the Raman structure seen at off-resonance (514.5 nm) is the ratio between the peaks at  $949\text{ cm}^{-1}$  and those at  $1086\text{--}1095\text{ cm}^{-1}$ . Comparing the Bragg-1-4 sample (5.0 mol%  $\text{Eu}^{3+}$ ), Bragg-9-1 (2.5 mol%  $\text{Eu}^{3+}$ ), Bragg-8-1 (1.0 mol%  $\text{Eu}^{3+}$ ), Bragg-7-1 (0.5 mol%  $\text{Eu}^{3+}$ ), and Bragg-5-1 (no europium doping) specimens reveals that the peak at  $949\text{ cm}^{-1}$  decreased relative to the peak in the range between  $1086\text{--}1095\text{ cm}^{-1}$  as the europium concentration was reduced. Yet, near-resonance spectra (472.7 nm) of these same specimens show this ratio to be the same for all four of the samples that were doped with europium, where the peak in the range  $1086\text{--}1095\text{ cm}^{-1}$  was dominant. A second comparison has been noted for peaks in the range  $575\text{--}620\text{ cm}^{-1}$  and  $433\text{--}470\text{ cm}^{-1}$ . The ratio of the former peak range to the latter decreased as the europium concentration decreased. Finally, structure at  $1305\text{ cm}^{-1}$  was observed to decrease as the europium concentration decreased, and completely disappeared when europium oxide was not present within the glass sample.

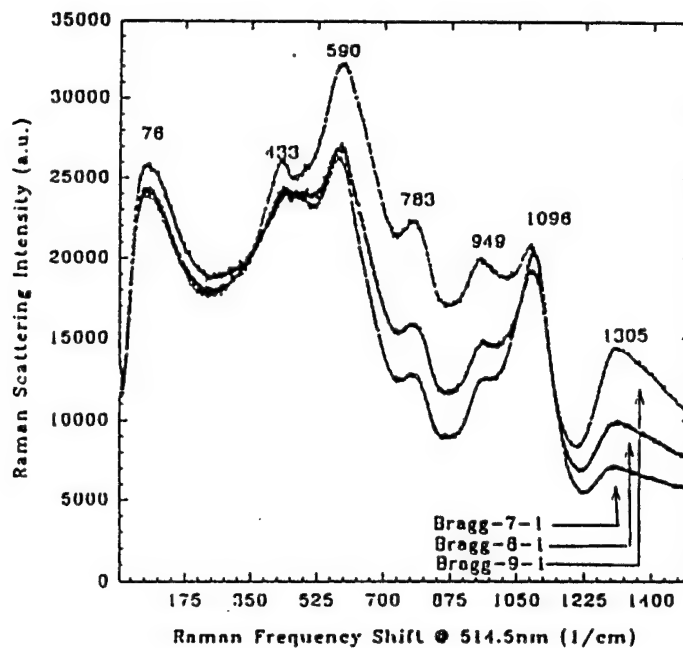


**Figure 40.** The effect gradually increases in the concentration of  $\text{Eu}^{3+}$  in the base aluminosilicate host composition has on the off-resonant (“lattice”) optical phonon frequency distribution profile.

$\text{Pr}_2\text{O}_3$ -doped glasses exhibited significantly different Raman spectra. Rates of grating formation and grating scattering intensity were expected to be greater in the praseodymium-doped glasses compared to europium-doped glasses due to the greatly increased write-beam absorption. These presumptions were proven not to be the case. (Compare **Figures 18** and **20**). An explanation for the counter-intuitive results can be inferred from the Raman spectra presented in **Figure 41**. The lattice-localized modes have a broad-band frequency distribution ranging from  $75\text{ cm}^{-1}$  and  $700\text{ cm}^{-1}$ , with a narrower band between  $900\text{ cm}^{-1}$  and  $1150\text{ cm}^{-1}$ . A  $465.8\text{ nm}$  write-beam excites  $\text{Pr}^{3+}$ -localized frequencies with a broad-band  $600\text{ cm}^{-1}$  and  $1600\text{ cm}^{-1}$ . While there is some frequency overlap it is not substantial. Gratings may form because a larger amount of optical energy is converted to lattice energy. However, rates of grating formation may be slowed substantially by the poor frequency overlap in lattice-localized and the  $\text{Pr}^{3+}$ -localized modes induced by  $465.8\text{ nm}$  write-beams.  $488\text{ nm}$  write-beams stimulate  $\text{Pr}^{3+}$ -localized modes at frequencies with nearly perfect frequency-overlap with the lattice-localized modes. (See **Figure 42**). Conclusive experimental confirmation for this interpretation can be derived by comparing grating formation rates observed using write-beams with equal powers at  $488\text{ nm}$  and  $465.8\text{ nm}$  in  $\text{Pr}^{3+}$ -doped glasses.

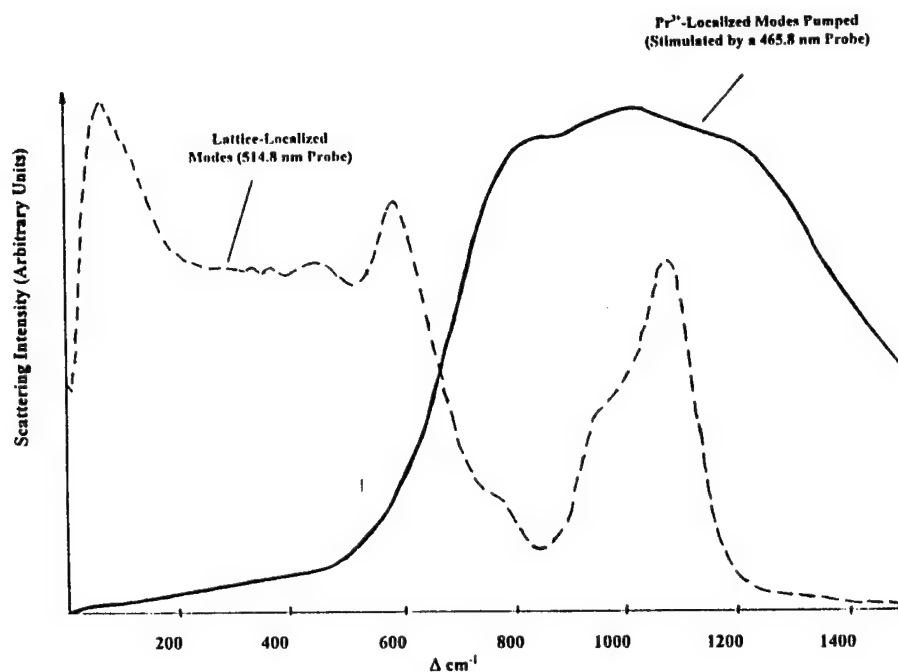


**Figure 41.** Distribution profiles of lattice localized-mode phonons and modes localized at  $\text{Pr}^{3+}$ -sites stimulated by 465.8 nm write-beams in the base host glass composition doped with 2.5 mol%  $\text{Pr}_2\text{O}_3$ .

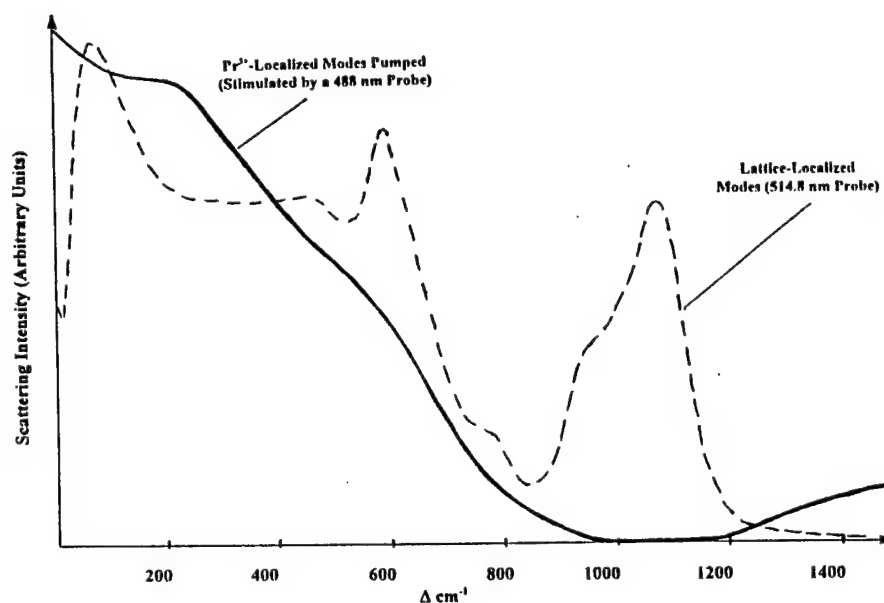


**Figure 42.** Distribution profiles of lattice localized-mode phonons and modes localized at  $\text{Pr}^{3+}$ -sites stimulated by a 488 nm resonant probe in the base host glass composition doped with 2.5 mol%  $\text{Pr}_2\text{O}_3$ .

### *The Effect of Mixed Alkali-Substitutions on Raman Spectra*

Mixed alkali-substitutions ( $\text{Li}_2\text{O}$  and  $\text{K}_2\text{O}$  for 50%  $\text{Na}_2\text{O}$ ) did not significantly alter the off-resonant and nearly resonant Raman spectra in the base host glass. Changes in grating formation/erasure rates are more likely due changes in the extended-range phonon characteristics. There was substantial overlap in the  $\mathcal{D}_{\text{lattice}}(\omega)$  with  $\mathcal{D}_{\text{RE}}(\omega)$  profiles in this series of glasses.

### *The Effect of Mixed-Alkaline Earth Substitutions on Raman Spectra*

Increasing the average mixed-alkaline mass in the base host composition narrowed peak widths at frequencies below  $600\text{ cm}^{-1}$ , and increased peak amplitudes at frequencies above  $600\text{ cm}^{-1}$  in the off-resonant spectra in 2.5 mol%  $\text{Eu}_2\text{O}_3$ -doped glasses. (See **Figure 43**). Mixed-alkaline earth substitutions did not significantly alter the nearly-resonant Raman spectra in the base host glass. There was substantial overlap in the  $\mathcal{D}_{\text{lattice}}(\omega)$  with  $\mathcal{D}_{\text{RE}}(\omega)$  profiles in this series of glasses. Changes in grating formation/erasure rates are more likely due changes in the extended-range phonon characteristics.

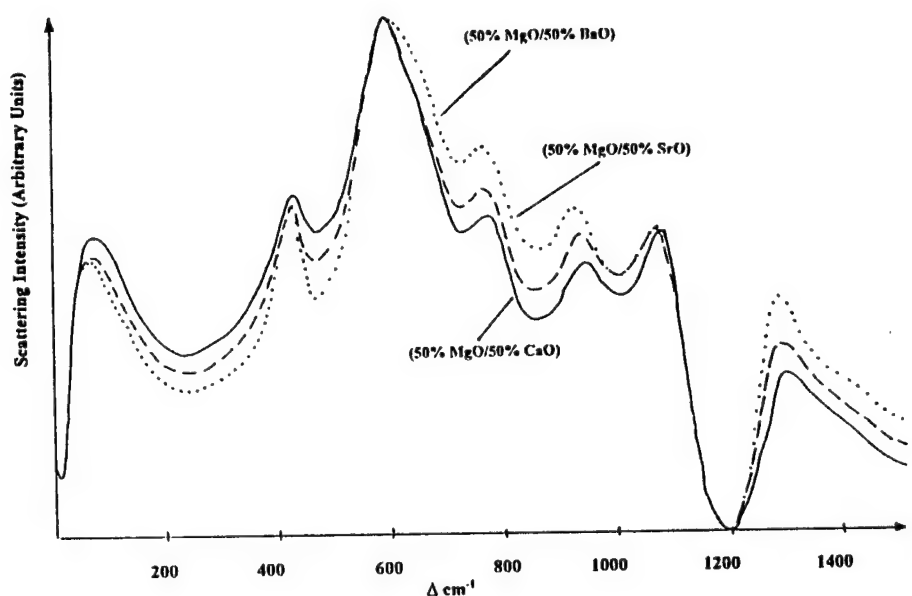


**Figure 43.** Changes in the distribution profiles of lattice localized-mode in the base host glass composition doped with 2.5 mol%  $\text{Eu}_2\text{O}_3$  as 50 mol% of the  $\text{MgO}$  is substituted for  $\text{CaO}$ ,  $\text{SrO}$ , and  $\text{BaO}$ .

### *The Effect of Silica-Enrichment on the Raman Spectra*

Enriching the base host network with 2.5 and 5.0 mol% silica did not significantly alter the off-resonant and nearly resonant Raman spectra in the base host glass. There was substantial overlap in the  $\mathcal{D}_{\text{lattice}}(\omega)$  with  $\mathcal{D}_{\text{RE}}(\omega)$  profiles in this series of glasses.

### *The Effect of Soda-Enrichment on the Raman Spectra*

Enriching the base host network with 5.0 and 10.0 mol%  $\text{Na}_2\text{O}$  altered the Raman spectra in a manner similar to increasing the average alkaline earth mass. Scattering peaks for the lattice-localized phonon spectra at frequencies below  $600\text{ cm}^{-1}$  decreased in intensity, while peaks at frequencies above  $600\text{ cm}^{-1}$  increased in intensity. (See **Figure 44**). Soda-enrichment did not noticeably alter the nearly-resonant Raman spectra in the base host glass. There was substantial overlap in the  $\mathcal{D}_{\text{lattice}}(\omega)$  with  $\mathcal{D}_{\text{RE}}(\omega)$  profiles in this series of glasses.

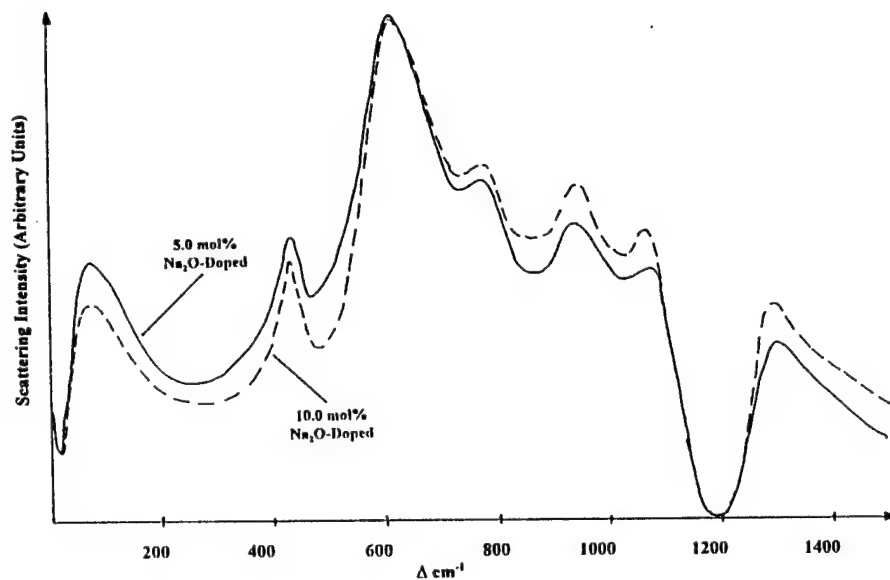


**Figure 44.** Changes in the distribution profiles of lattice localized-mode in the base host glass composition doped with 2.5 mol%  $\text{Eu}_2\text{O}_3$  after it is enriched with 5.0 and 10.0 mol%  $\text{Na}_2\text{O}$ .

## The Effect of Transition-metal Doping on the Raman Spectra

Transition-metal doping introduces dramatic changes in both the nearly-resonant and off-resonant Raman spectra. **Figure 45** shows the nearly-resonant and off-resonant spectra for a base host composition that has been doped with 0.25 mol%  $V^{(III)}_2O_3$  and  $V^{(V)}_2O_5$ , each. The transition-metal doped host was then doped with 5.0 mol%  $Eu_2O_3$ . In both cases, the relative intensity of lower frequency components (75-85  $cm^{-1}$ ) was significantly enhanced over spectra present in samples that had not been transition-metal doped. There is also a strong enhancement in the peaks at 930  $cm^{-1}$  and 1060  $cm^{-1}$ . There was substantial overlap in the  $\beta_{lattice}(\omega)$  with  $\beta_{RE}(\omega)$  profiles in this glass, suggesting that it should be possible to record gratings. Gratings were observed in this sample, but the signals were weak and slow to develop. The lower quality signals were more likely to be due to the fact that the sample was so strongly absorbing, and the 465.8 nm write-beam only penetrates the shoulder of the  $^7F_0 \rightarrow ^5D_2$  excited state transition. Stronger scattering efficiencies and faster grating formation rates should be observed by writing gratings with a 488 nm laser that pumps  $Pr^{3+}$  ions in a transition-metal doped host.

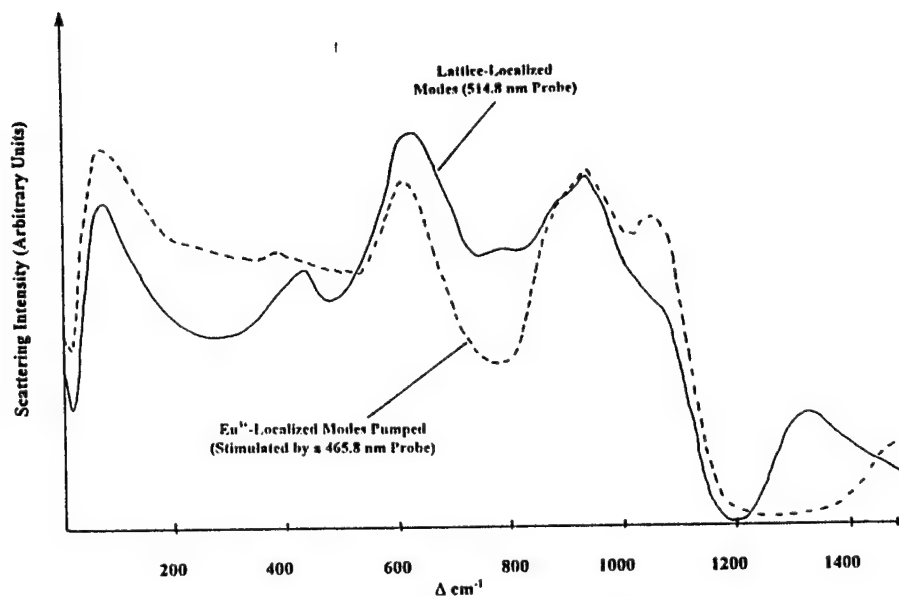


**Figure 45.** Distribution profiles of lattice localized-mode and  $Eu^{3+}$ -localized modes in the base host glass composition doped with 2.5 mol%  $Eu_2O_3$  after 0.25 mol%  $V^{(III)}_2O_3$  and  $V^{(V)}_2O_5$  was added to the network.



## Brillouin Scattering Measurements

Backscattered measurements were made on two base host glass compositions (Bragg-5-1 and Bragg-5-2), which were cooled at a slow and a fast rate, respectively. (See Figure 46). Furthermore, Bragg-5-2 was batched with cullet, whereas Bragg-5-1 was prepared directly from precursor powders. No discernible differences were observed in the two samples. Both samples revealed identical frequency-shifts in the Brillouin spectra. Furthermore, the measured spectra were also the same as the Brillouin scattered shifted spectra for fused silica. The narrow line widths of the peaks indicate that low-frequency extended-range phonons are present in the glass.

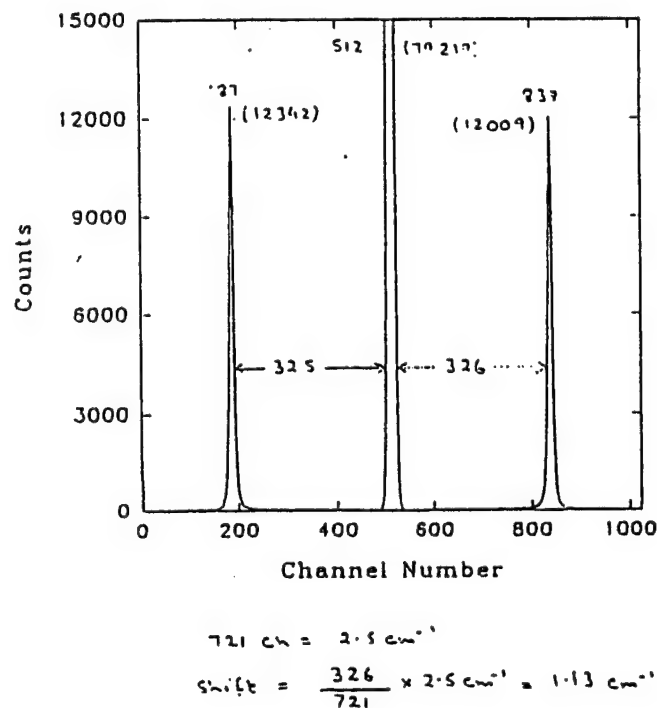


**Figure 46.** Backscattered Brillouin scattering spectra used to determine the longitudinal acoustic phonon spectra in the base host glass composition to which doping modifications were made  $[0.70 \bullet \text{SiO}_2 - 0.03 \bullet \text{Al}_2\text{O}_3 - 0.12 \bullet \text{MgO} - 0.15 \bullet \text{Na}_2\text{O}]$ .

## Fiber-optic Optical Properties

Due to an administrative setback in the Air Force contract procurement office, this contract was without dedicated funding for two months, with six months remaining on the contract. This was at a critical juncture in the contract. Rutgers University, the sub-

contractor who prepared the optical fiber, was about to begin fabrication of the optical fiber. Without the obligated funding, Rutgers could not proceed with fiber preparation. By the time obligated funds had been restored to the contract, machine time at Rutgers was no longer available until January 1996. The Oklahoma State University Center for Laser Research, which characterized the non-linear properties of materials under the contract, had facilities dedicated for the contract until September 1995. As a result of the administrative setback, non-linear optical properties of fiber-optic materials prepared under the contract could not be characterized as planned. Without this characterization, a laser diode could not be fitted with a fiber-optic Bragg-filter.

### *Fiber-optic Index Profiles*

Figure 47 is the step index profile of the preform used to prepare  $\text{Cr}^{2+}/\text{Eu}^{3+}$  doped fiber. The step index change,  $\Delta n$ , between the core and the clad in the fibers prepared under this contract varied between 0.022 for the  $\text{Cr}^{2+}/\text{Eu}^{3+}$  doped fiber and 0.015 for the  $\text{Cr}^{2+}$ -doped fiber.

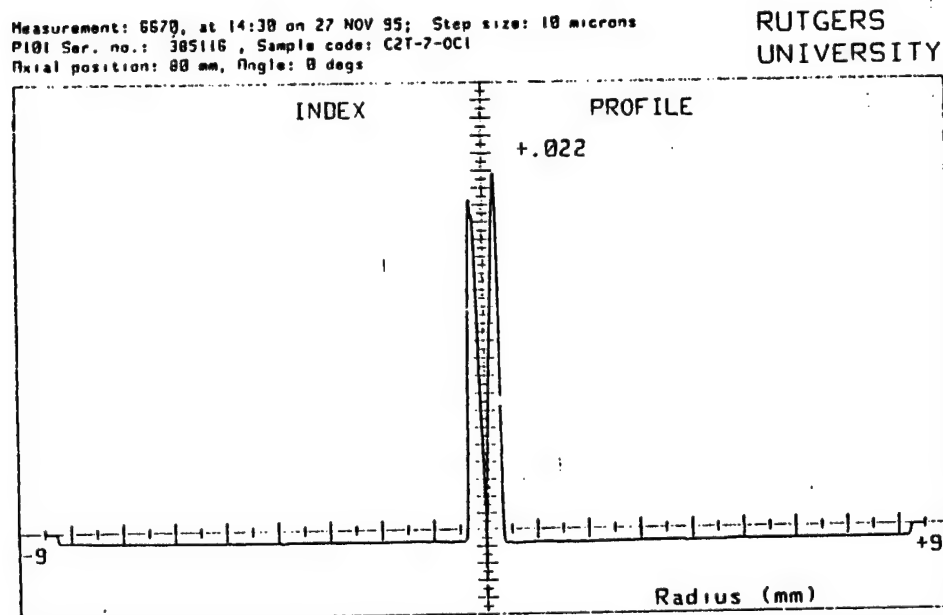


**Figure 47.** Index profile of the preform used to prepare  $\text{Cr}^{2+}/\text{Eu}^{3+}$  doped fiber.

### Fiber Loss Profiles

Optical loss in these fibers were measured by cutback-OTDR. **Figure 48** shows the optical attenuation (loss) in the  $\text{Cr}^{2+}/\text{Eu}^{3+}$  doped fiber. **Figure 49** shows the optical at-

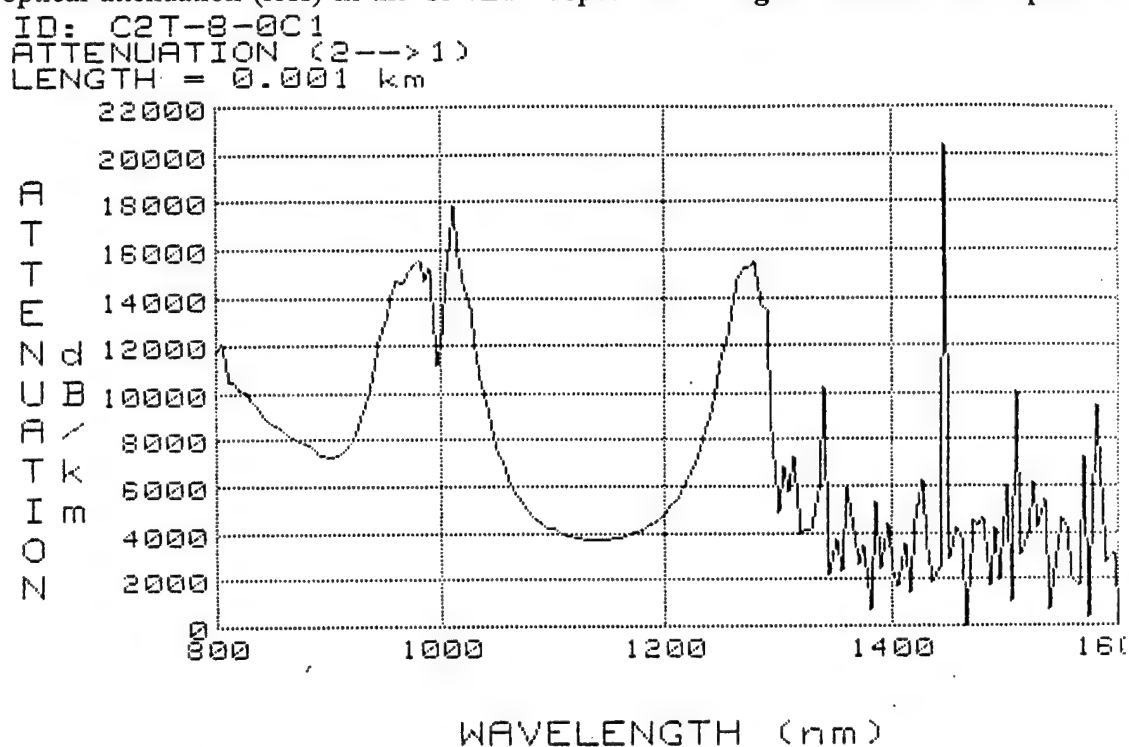


**Figure 48.** Optical attenuation in the  $\text{Cr}^{2+}/\text{Eu}^{3+}$  doped fiber.

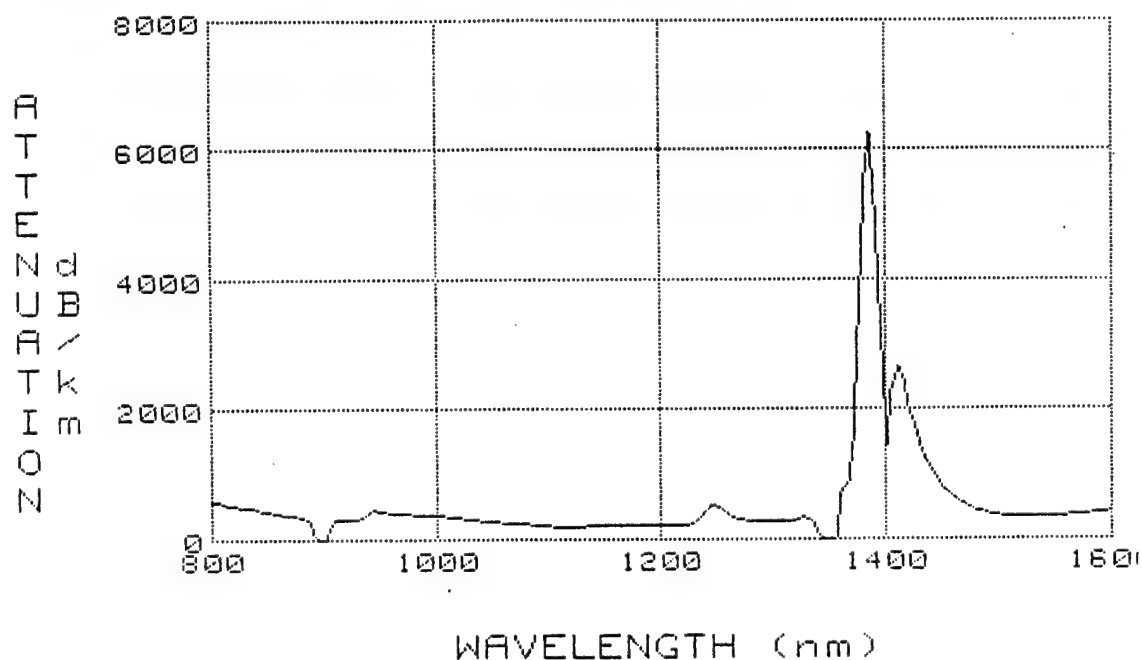


**Figure 49.** Optical attenuation in the  $\text{Cr}^{2+}/\text{Pr}^{3+}$  doped fiber.

## VI. Conclusions and Suggestions for Future Research

This Phase II research studied phenomena associated with optically-prepared gratings in glass. Optically-prepared gratings were recorded in rare earth-doped oxide glass using write-beams tuned to an excited-state transition of the rare earth ion that has a strong decay branch through non-radiative multiphonon emission processes. The properties of superimposed transient and permanent were evaluated. The lifetime of transient gratings (2.2 ms) in europium-doped glass was found to be independent of write beam power, and to be identical to the fluorescence lifetime of the excited state of the rare earth ion. This suggests that transient gratings are related to the hyperpolarizability of ligands in the immediate vicinity of the rare earth ion. Permanent gratings were found to depend on glass composition and to be strongly dependent on the vibrational characteristics of the glass. Since the fluorescence (and transient grating) lifetime(s) were not observed change as a result of the write-process, permanent gratings are attributed to a structural change of the glass close to, but not in the nearest neighbor environment of the rare earth ions.

Resonant and nearly-resonant Raman spectroscopy was used to probe the frequency-dependence in the density of states profiles of optical phonons localized to the rare earth ions and optical phonons localized to the network lattice away from the rare earth ion. Thermal diffusivity measurements were used to examine the strength of extended-range phonons that can be used to couple the photostimulated vibrational energy generated at a rare earth ion site to vibrational modes resonant with the rest of the network. Empirical results suggest that is necessary to use a host glass in which there is a strong frequency overlap between the lattice-localized modes and the write-beam-excited modes at rare earth ion sites to record laser-induced gratings. It is equally important that the host glass contain extended-range phonons to couple these two types of localized modes in the glass.

These results suggest that it is important to engineer host compositions that have vibrational modes localized to the lattice that are connected, through extended-range phonons, with the modes localized at the optically stimulated rare earth ion sites; but, more importantly, the lattice-localized modes must resonate substantially over the same frequencies that the rare earth ion-localized modes resonate. (See **Figure 50**). These findings give credence to the model that assumes the extended-range phonons provides a channel through which the vibrational energy of localized-modes can hop to activate other localized modes. Since these mechanisms allow phonons to "diffuse" through the glass network, alkali-ions, which are known to have phonon-activated diffusion, are the particles that structurally alter the network during the grating formation process.

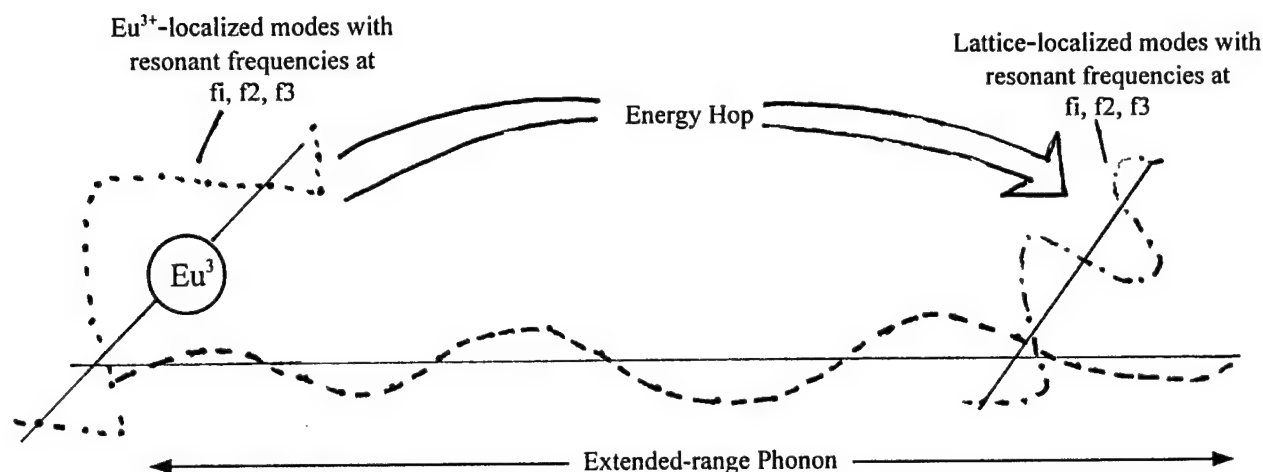


**Figure 50.** Extended-mode phonons couple optically-stimulated localized-modes to lattice-localized modes at similar vibrational frequencies to allow the lattice energy to hop through the network.

The program specifically examined the compositional basis for preparing photosensitive glass with improved scattering efficiencies and faster recording times. This was accomplished by performing doping studies on a suitable magnesium-soda-aluminosilicate base-host composition. The absolute scattering efficiency of the base host composition was compared versus changes in rare earth ion concentration, changes in average alkali-modifier mass, changes in average alkaline earth-modifier mass, changes in network former content, and changes alkali-modifier content. The strongest scattering intensities were observed in systems that contained the highest concentrations of network formers and rare earth ions ( $\eta_{\text{peak}} = 1.55 \times 10^{-3} \text{ cm}^{-2}$ ). However, increasing the network former ( $\text{SiO}_2$ ) concentration by a mere 2% increased the absolute scattering efficiency to a greater degree (120% increase in scattering efficiency per percentage increase in silica mol%) than increasing the rare earth ion concentration by 100% (7.8% increase in scattering efficiency per percentage increase in europium oxide mol%). Increasing the alkali-modifier concentration decreased the absolute scattering efficiency. Higher network former concentrations will increase order in the glass, while higher alkali-modifier concentrations will increase network disorder, even though increases in alkali-modifier concentrations increase the density of state-defining charged-particles available to the network. The results suggest that it is more important to engineer a host that has an ordered network, than it is to increase the glass's sensitivity to the write beam.

Changes in the average mass of alkaline-earth modifiers did not significantly alter the frequency profiles of rare earth-localized and lattice-localized modes in the magnesium-soda-aluminosilicate glass. However, increasing the average mass of alkaline-earth modifiers, by fractionally substituting CaO, SrO, or BaO for MgO, reduced four-wave mixing (FWM) scattering efficiencies. It is conjectured at this time, that these substitutions may have reduced extended-range phonon mean-free-paths, or inhibited the coupling of extended-range phonons to localized-mode phonons. Thermal diffusivity measurements on these glass compositions, currently underway, will conclusively resolve this interpretation.

Mixed-alkali glass compositions, containing 50% Li<sub>2</sub>O and 50% Na<sub>2</sub>O, or 50% K<sub>2</sub>O and Na<sub>2</sub>O with a total alkali-mol% equal to the Na<sub>2</sub>O-mol% in the base host composition, were observed to have weaker peak FWM scattering efficiencies and slower rates of grating formation than in the base host. Alkali cationic diffusion rates are known to be higher in mixed alkali-glasses, than in single-alkali glasses containing equal total alkali-cation concentrations. It was expected that the higher diffusion rates would increase the rates at which gratings could be formed and erased. Mixed-alkali glasses had peak FWM scattering efficiencies that were weaker by an order of magnitude: Na<sup>+</sup>-only scattering efficiency =  $1.76 \times 10^{-4} \text{ cm}^{-2}$ ; Na<sup>+</sup>/Li<sup>+</sup>-mixed scattering efficiency =  $3.3 \times 10^{-5} \text{ cm}^{-2}$ ; Na<sup>+</sup>/K<sup>+</sup>-mixed scattering efficiency =  $4.2 \times 10^{-5} \text{ cm}^{-2}$ . These counter-intuitive results may, in fact, point out that higher cationic diffusivities could be detrimental to the grating process because they facilitate the back-diffusion of alkali-cations out of regions of destructive write-beam optical interference and into the photo-activated regions of constructive write-beam interference. A greater understanding of these results will be gained once thermal diffusivity measurements are completed on these samples and correlated with the other glass compositions.

The program evaluated europium (Eu<sup>3+</sup>) and praseodymium (Pr<sup>3+</sup>) as rare earth ion photosensitizers for the network. Both ions can be pumped by the 465.8 nm line of an argon laser. The fact that praseodymium is more strongly absorbing than europium at 465.8 nm suggests that stronger gratings should be recorded at much fast rates in the base host glass doped with Pr<sup>3+</sup> since the stronger optical attenuation should stimulate stronger lattice excitations. Gratings recorded with 465.8 nm write-beams in praseodymium-doped glasses developed much more slowly, reaching peak scattering efficiencies in 20 minutes compared to 2 minutes in the europium-doped glass. Peak scattering efficiencies were nearly equivalent in the Eu<sup>3+</sup>-doped and Pr<sup>3+</sup>-doped glasses, ( $\eta = 1.76 \times 10^{-4} \text{ cm}^{-2}$ , and  $3.81 \times 10^{-4} \text{ cm}^{-2}$ , respectively).

Raman spectroscopy revealed a relatively poor frequency-overlap in the density of states of Pr<sup>3+</sup>-localized modes stimulated by 465.8 nm write-beams with lattice-localized modes. The poor frequency-matching in the localized-phonon density of state profiles in

$\text{Pr}^{3+}$ -doped glasses pumped by 465.8 nm write-beams is being attributed for the poorer response times. A much greater frequency overlap between  $\text{Pr}^{3+}$ -localized modes and lattice-localized modes is observed when praseodymium is pumped by 488 nm write-beams. This research suggests that even stronger scattering efficiencies, and faster recording rates, should be possible in  $\text{Pr}^{3+}$ -doped glasses when write-beams at 488 nm are used to record the grating.

The program also evaluated transition-metal-doping as a means to increase absolute scattering efficiency. Transition-metal doped glasses were found to be suitable photosensitive glasses; however, the strong absorption of the transition-metal interfered with write-beam power needed to record a grating. More conclusive results will probably be derived using transition-metal-doped thin film glasses containing  $\text{Pr}^{3+}$  ions, and 488 nm write-beams to record the grating.

Future research on gratings in rare earth-doped glasses should correlate thermal diffusivity with grating performance. More work can be done to identify excited states of rare earth ions that have greater absorption to write-beams that stimulate rare earth ion-localized modes at frequencies that strongly overlap the frequency distribution of lattice-localized modes. This research can also be continued by investigating the effect of higher pulse-powered write-beams on grating dynamics.

## References

- Alexander, S., Laermans, C., Orbach, R., and Rosenberg, H.M., Phys. Rev. B 28, 4865 (1983).
- Alexander, S., Entin-Wohlman, O., and Orbach, R., Phys. Rev. B 34, 2726 (1986).
- Anderson, P.W., Halperin, P.J., and Varma, C.M., Philos. Mag. 25, 1, (1972).
- Behrens, E.G., Durville, F.M., and Powell, R.C., Phys. Rev. B, 39(9), 6076 (1989).
- Bell, R.J., Rep. Prog. Phys. 35, 1315 (1972).
- Buchanau, U., Prager, M., Nucker, N., Dianoux, A.J., Ahmad, N., and Phillips, W.A., Phys. Rev. B, 34, 5665 (1986).
- Buchanau, U., Philos. Mag. B, 65(2), 303 (1992).
- Buchanau, U., Galperin, Yu M., Gurevich, V.L., Parshin, D.A., Ramos, M.A., and Schober, H.R., Phys. Rev. B 46(5), 2798 (1992).
- Cahill, D.G., and Pohl, R.O., Solid State Commun. 70, 927 (1989).
- Dean, P. Rev. Mod. Phys. 44, 127 (1972).
- Dixon, G.S., Gault, B.D., Shi, S-y, Watson, P.A., and Wicksted, J.P., to be published.
- Durville, F.M., Behrens, E.G., and Powell, R.C., Phys. Rev. B, 35(8), 4109 (1987).
- Galperin, Yu. M., Karpov, V.G., Kozub, V.I., Adv. Physics, 38, 679.
- Jagganathan, A., O. Entin-Wohlman, and Orbach, R., Phys. Rev. B 39, 13465 (1989).
- Karpov, V.G., Klinger, M.I., Ignatiev, F.N., Soviet Phys. JETP, 57, 43 (1983).
- Meltz, G., Morey, W.W., Glenn, W.H., Opt. Lett., 14(15), 823 (1989).
- Phillips, W.A., J. Low Temp. Phys. 7, 351 (1972).



***MISSION  
OF  
ROME LABORATORY***

**Mission.** The mission of Rome Laboratory is to advance the science and technologies of command, control, communications and intelligence and to transition them into systems to meet customer needs. To achieve this, Rome Lab:

- a. Conducts vigorous research, development and test programs in all applicable technologies;
- b. Transitions technology to current and future systems to improve operational capability, readiness, and supportability;
- c. Provides a full range of technical support to Air Force Materiel Command product centers and other Air Force organizations;
- d. Promotes transfer of technology to the private sector;
- e. Maintains leading edge technological expertise in the areas of surveillance, communications, command and control, intelligence, reliability science, electro-magnetic technology, photonics, signal processing, and computational science.

The thrust areas of technical competence include: Surveillance, Communications, Command and Control, Intelligence, Signal Processing, Computer Science and Technology, Electromagnetic Technology, Photonics and Reliability Sciences.